Universidade de Aveiro
Departamento de Electrónica, Telecomunicações e Informática
2015

David
Pedro Breda

Simulação de um Inversor Ressonante
Simulation of a Resonant Inverter

"Strive for perfection in everything you do. Take the best that exists and make it better. When it does not exist, design it." - Sir Henry Royce

David
Pedro Breda

Simulação de um Inversor Ressonante
Simulation of a Resonant Inverter

Dissertação apresentada à Universidade de Aveiro para cumprimento dos requisitos necessários à obtenção do grau de Mestre em Engenharia Electrónica e Telecomunicações, realizada sob a orientação científica de Rui Manuel Escadas Ramos Martins e co-orientação de Alexandre Manuel Moutela Nunes da Mota, Professores do Departamento Electrónica e Telecomunicações da Universidade de Aveiro.

o júri / the jury

presidente / president	**Professor Doutor Telmo Reis Cunha** Professor Auxiliar, Universidade de Aveiro
vogais / examiners committee	**Professor Doutor José António Barros Vieira** Professor Adjunto, Instituto Politécnico de Castelo Branco
	Professor Doutor Rui Manuel Escadas Ramos Martins Professor Auxiliar, Universidade de Aveiro

agradecimentos / acknowledgements

É com grande gratidão que me dirijo a todos aqueles que me ajudaram ao longo do meu percurso académico.

Aos meus orientadores, Professor Rui Escadas Martins e Professor Alexandre Mota, bem como ao Engenheiro Rómulo Antão, pela disponibilidade, formação e apoio que sempre demonstraram.

À minha família, amigos e namorada pela compreensão e incentivo em todos os momentos.

Muito obrigado.

Resumo

Desenvolvida maioritariamente a partir da Revolução Industrial, a automatização dos sistemas e equipamentos que nos rodeiam é responsável por um progresso tecnológico e crescimento económico sem precedentes, mas também por uma incessante dependência energética. Atualmente, combustíveis fósseis ainda tendem a surgir com principal fonte de energia, mesmo em países desenvolvidos, devido à facilidade na sua extração e domínio da tecnologia necessária à sua utilização. No entanto, a perceção quer da sua findável disponibilidade, quer do impacto ambiental desta prática, tem levado a uma crescente produção de energia proveniente de fontes renováveis.

A sua fácil manutenção, aliada ao facto de serem praticamente inesgotáveis, faz das energias solar e eólica uma solução muito promissora. Neste contexto, esta dissertação propõe facilitar a produção de energia proveniente destas fontes.

Assim, neste trabalho são estudados os inversores de potência, equipamentos responsáveis por converter energia DC disponibilizada por uma fonte solar ou eólica em energia AC tradicional. Seguidamente é discutida e projetada uma nova arquitetura que, para além de conseguir um alto rendimento energético, tem também a capacidade de se adaptar face ao tipo de conversão pretendida pelo utilizador, caso este queira vender energia à rede elétrica, ser independente desta ou apostar num sistema de auto consumo.

Para alcançar o alto rendimento energético prometido, o inversor projetado faz uso de um conversor DC-DC ressonante, cuja arquitetura diminui consideravelmente a energia dissipada na conversão, permitindo assim uma maior densidade de potência.

A versatilidade do equipamento é disponibilizada por um algoritmo de controlo adaptativo, responsável por avaliar o comportamento deste a cada iteração e fazer as alterações necessárias para alcançar a máxima estabilidade ao longo de todo o processo.

Para uma avaliação do funcionamento da arquitetura proposta, apresenta-se a simulação da mesma utilizando o software de simulação PLECS.

Abstract

Mostly developed since the Industrial Revolution, the automation of systems and equipment around us is responsible for a technological progress and economic growth without precedents, but also by a relentless energy dependence.

Currently, fossil fuels still tend to come as the main energy source, even in developed countries, due to the ease in its extraction and the mastery of the technology needed for its use. However, the perception of its ending availability, as well as the environmental impact of this practice has led to a growing energy production originated from renewable sources.

Easy maintenance, coupled with the fact that they are virtually inexhaustible, makes the solar and wind energy very promising solutions. In this context, this work proposes to facilitate energy production from these sources.

To this end, in this work the power inverter is studied, which is an equipment responsible for converting DC power available by solar or wind power in traditional AC power. Then it is discussed and designed a new architecture which, in addition to achieve a high energy efficiency, has also the ability to adapt to the type of conversion desired by the user, namely if he wants to sell electricity to the power grid, be independent of it or bet on a self consumption system.

In order to achieve the promised energy efficiency, the projected inverter uses a resonant DC-DC converter, whose architecture significantly decreases the energy dissipated in the conversion, allowing a higher power density.

The adaptability of the equipment is provided by an adaptive control algorithm, responsible for assessing its behavior on every iteration and making the necessary changes to achieve maximum stability throughout the process.

To evaluate the functioning of the proposed architecture, a simulation is presented using the PLECS simulation software.

Contents

Contents i

List of Figures v

List of Tables ix

Acronyms xi

1 Introduction 1
- 1.1 Motivation . . . 1
- 1.2 Objectives . . . 2
- 1.3 Organization . . . 3

2 Background Technologies 5
- 2.1 Introduction . . . 5
- 2.2 Renewable Energy Sources . . . 6
  - 2.2.1 PV Modules . . . 6
    - 2.2.1.1 Maximum Power Point of a PV Module . . . 8
  - 2.2.2 Wind Turbines . . . 9
    - 2.2.2.1 Maximum Power Point of a Wind Turbine . . . 9
- 2.3 Power Inverters . . . 10
  - 2.3.1 Inverter Block Diagram . . . 11
  - 2.3.2 DC-DC Converters . . . 12
    - 2.3.2.1 Linear Converters . . . 12
    - 2.3.2.2 Switching Converters . . . 12
  - 2.3.3 DC-AC Converter . . . 19
  - 2.3.4 Output Filter . . . 21
  - 2.3.5 Controller . . . 22
- 2.4 Commercial Products . . . 24
  - 2.4.1 SMA Solar Technology AG . . . 24
  - 2.4.2 SolarEdge . . . 25
  - 2.4.3 Products Comparison . . . 26

3 Hardware Architecture **27**
3.1 Introduction . . . 27
3.2 LLC Converter . . . 28
3.2.1 Principle of Operation . . . 28
3.2.2 Resonant Tank Design . . . 32
3.2.3 Galvanic Isolation . . . 38
3.2.3.1 Core Selection . . . 39
3.2.3.2 Winding . . . 42
3.2.4 Rectification . . . 46
3.3 H-Bridge Converter . . . 47
3.4 Output Filter . . . 48

4 Control System Design **51**
4.1 Introduction . . . 51
4.2 FreeRTOS . . . 52
4.2.1 Task Creation and Deletion . . . 52
4.2.2 Scheduling . . . 52
4.3 Control Algorithms . . . 53
4.3.1 MPPT Controller . . . 54
4.3.1.1 MPPT Algorithm Design . . . 54
4.3.2 PID Controller . . . 55
4.3.2.1 LLC Converter Controller Design . . . 56
4.3.3 RST Controller . . . 60
4.3.3.1 Recursive Least Squares (RLS) . . . 63
4.3.3.2 Design of the H-Bridge Controller . . . 66

5 Inverter Operation Modes **69**
5.1 Introduction . . . 69
5.2 Production Mode . . . 70
5.3 Standalone Mode . . . 71
5.4 Self-Consumption Mode . . . 73

6 Simulation **75**
6.1 Introduction . . . 75
6.2 Plexim® PLECS . . . 76
6.3 LLC Converter . . . 78
6.3.1 PLECS Schematic . . . 78
6.3.2 Simulation Results . . . 84
6.4 H-Bridge Converter . . . 87
6.4.1 PLECS Schematic . . . 87
6.4.2 Simulation Results . . . 90
6.5 Proposed Inverter . . . 93
6.5.1 Standalone Mode . . . 94

6.5.2 Production Mode 99
6.5.3 Self-Consumption Mode 103

7 Conclusions and Future Work **107**
7.1 Conclusions 107
7.2 Future Work 108

Appendices **109**

A Circuit Assembly **110**
A.1 Introduction 110
A.2 Components 110
A.2.1 LLC Converter 111
A.2.2 H-Bridge Converter 112
A.2.3 Control System 112
A.3 PCB 113
A.4 Results 113

Bibliography **117**

List of Figures

2.1 Photovoltaic Effect 6
2.2 Solar Panel 6
2.3 PV Production by Technology [8] 7
2.4 Market Share of Thin-Film Technologies [8] 8
2.5 Typical I/V MPPT Curve 8
2.6 Typical P/V MPPT Curve 8
2.7 Horizontal-Axis Wind Turbine 9
2.8 Vertical-Axis Wind Turbine 9
2.9 Typical P/V Wind Generator Curve 10
2.10 Inverter Topologies 10
2.11 Synchronized Waveforms 11
2.12 Inverter Block Diagram 11
2.13 Buck Converter Current Flow Over Time 13
2.14 Boost Converter Current Flow Over Time 14
2.15 Buck-Boost Converter Schematic 14
2.16 Voltage and Current Waveforms on a Transistor 15
2.17 Typical Resonant Converter 15
2.18 Half Bridge Circuit 16
2.19 Full Bridge Circuit 16
2.20 Series, Parallel, LCC and LLC Resonant Tanks 17
2.21 Charge distributions in a diode [17] 18
2.22 Diodes Reverse Recovery Comparison [20] 19
2.23 Inverter Output Possible Waveforms 19
2.24 Sine Wave Generator 20
2.25 PWM to Sine Wave 20
2.26 Filter response by order of attenuation 21
2.27 Passive Filters 22
2.28 Microcontroller Sales Forecast [21] 23
2.29 Digital Control Loop [22] 23
2.30 SMA Flexible Solution [25] 25
2.31 SolarEdge Feed-in Limitation Schematic [27] 25

3.1 Inverter Hardware Block Diagram 27

3.2 Typical LLC Converter Circuit . . . 28
3.3 LLC Tank Transfer Function - [28] . . . 30
3.4 LLC Circuit Signals . . . 31
3.5 LLC Design Flowchart . . . 33
3.6 Different Q values . . . 36
3.7 Different m values . . . 37
3.8 Designed LLC Tank Voltage Gain . . . 38
3.9 Transformer Core Shapes . . . 41
3.10 Flux Levels for MAGNETICS "P" ferrite material necessary to maintain constant $100mW/cm^3$ core losses at various frequencies [34] . . . 43
3.11 Skin Effect Examples at LLC Resonant Frequency, 100kHz . . . 45
3.12 GeneSiC® GB50SLT12-247 Conduction Losses . . . 46
3.13 Transistor Losses . . . 47
3.14 Q-Factor Examples . . . 49
3.15 Designed LC Filter Bode Diagram . . . 50

4.1 Task Change in FreeRTOS . . . 53
4.2 Task Life Cycle in FreeRTOS . . . 53
4.3 Negative Feedback Closed Loop Control . . . 53
4.4 MPPT Algorithm . . . 55
4.5 Feedback loop with PID control [43] . . . 56
4.6 LLC Converter Electrical Circuit . . . 57
4.7 V_{bus} Filtering . . . 58
4.8 RST Controller Block Diagram . . . 60
4.9 RST with RLS Controller Diagram . . . 65
4.10 H-Bridge Converter Electrical Circuit . . . 66
4.11 H-Bridge Converter Step Response . . . 66

5.1 Inverter Modes Diagram . . . 69
5.2 Grid Tie Mode Diagram . . . 71
5.3 Household Electricity Consumption in kWh/year [50] . . . 72
5.4 Trojan Battery Bank Simulator [51] . . . 72
5.5 Domestic Power Consumption vs PV Array Power Production [27] . . . 73

6.1 PLECS User Interface . . . 76
6.2 PLECS Servo Drive Demo [54] . . . 77
6.3 Voltage Source Controlled - PLECS Component . . . 78
6.4 Signal From - PLECS Component . . . 79
6.5 Signal Goto - PLECS Component . . . 79
6.6 Mosfet with Limited di/dt - PLECS Component . . . 79
6.7 Diode - PLECS Component . . . 79
6.8 Capacitor - PLECS Component . . . 79
6.9 Inductor - PLECS Component . . . 80

6.10 Ideal Transformer - PLECS Component 80
6.11 Diode with Reverse Recovery - PLECS Component 80
6.12 Resistor - PLECS Component 81
6.13 LLC Converter - PLECS Schematic 81
6.14 C-Script - PLECS Component 82
6.15 C-Script Window - PLECS Component 82
6.16 Logical Operator - PLECS Component 83
6.17 Turn On Delay - PLECS Component 83
6.18 Relay - PLECS Component 83
6.19 LLC Controller - PLECS Schematic 84
6.20 Ammeter - PLECS Component 84
6.21 Voltmeter - PLECS Component 84
6.22 LLC Converter Energy Efficiency 85
6.23 LLC Converter Simulation Results 86
6.24 Voltage Source DC - PLECS Component 87
6.25 H-Bridge Converter - PLECS Schematic 88
6.26 Symmetrical PWM - PLECS Component 89
6.27 H-Bridge Controller - PLECS Schematic 89
6.28 Voltage Source AC - PLECS Component 90
6.29 H-Bridge Converter Simulation Results 91
6.30 H-Brigbe - RLS Identification Method Estimated Parameters 92
6.31 Inverter Electrical Schematic in PLECS® 93
6.32 Primary Power Source V/I Curves 93
6.33 Possible Loads for the Proposed Inverter 94
6.34 Standalone Mode - Variables over time 96
6.35 Standalone Mode - Variables over time (2) 97
6.36 Standalone Mode - RLS Estimated Parameters 98
6.37 Production Mode - Variables over time 100
6.38 Production Mode - Variables over time (2) 101
6.39 Production Mode - RLS Estimated Parameters 102
6.40 Self-Consumption Mode - Variables over time 104
6.41 Self-Consumption Mode - Variables over time (2) 105
6.42 Self-Consumption Mode - RLS Estimated Parameters 106

A.1 ARM-Cortex Development Board 113
A.2 Schematic View - CadSoft® Eagle 114
A.3 Board View - CadSoft® Eagle 114
A.4 Resonant Inverter Fabricated PCB 115

List of Tables

3.1 MPRIME 250W PV Module Specifications 34
3.2 20kW PV Array Specifications 35
3.3 Part of the Typical Power Handling Chart, by Magnetics [32] 40
3.4 U Shapes Datasheet 42
3.5 Ferrite Power Materials Summary, by Magnetics [34] 42
3.6 AWG Sizes and Current Limits [35] 45

4.1 PID Controller Gains Influence on Output [44] 56
4.2 LLC Converter Parameter Identification 59

6.1 CREE® C2M0025120D Electrical Characteristics 79
6.2 CREE® C2M0025120D Built-in SiC Body Diode Characteristics 80
6.3 GeneSiC® GB50SLT12-247 Silicon Carbide Power Schottky Diode [38] . . 81

A.1 Fairchild FDP054N10 Electrical Characteristics 111
A.2 IXYS DPG10I300PA Electrical Characteristics 111

Acronyms

AC	Alternated Current
ADC	Analog to Digital Converter
AWG	American Wire Gauge
CPU	Central Processing Unit
CSV	Comma Separated Values
DAC	Digital to Analog Converter
DC	Direct Current
EMI	Electromagnetic Interference
ESR	Equivalent Series Resistor
GPIO	General-Purpose Input/Output
GUI	Graphical User Interface
HF	High Frequency
IC	Integrated Circuit
IO	Input/Output
LS	Least Squares
MIPS	Microprocessor without Interlocked Pipeline Stages
MPP	Maximum Power Point
MPPT	Maximum Power Point Tracking
PCB	Printed Circuit Board
PDF	Portable Document Format
PFM	Pulse Frequency Modulation

PID	Proportional Integrative Derivative
PLECS	Piecewise Linear Electrical Circuit Simulation
PO	Percentage Overshoot
PRC	Parallel Resonant Converter
PV	Photovoltaic
PWM	Pulse Width Modulation
RLS	Recursive Least Squares
RMS	Root Mean Square
RTOS	Real-Time Operating System
SPRC	Series Parallel Resonant Converter
SRC	Series Resonant Converter
THD	Total Harmonic Distortion
TRIAC	Triode for Alternating Current
UPS	Uninterruptible Power Supply
ZCS	Zero Current Switching
ZVS	Zero Voltage Switching

Chapter 1

Introduction

1.1 Motivation

Nowadays, more than half the world's electricity is produced in power plants that use fossil fuels as main energy source [1], however, the increasing number of forecasts that predict a declining in oil production [2], as well as the rising awareness of the environmental impact caused by this, are demanding for better alternatives than nuclear energy.

Renewable energy sources are expected to be the fastest-growing energy sector over the next two decades [3], surpassing now 200 billion US dollars in worldwide investment [4]. Portugal is a fine example for this trend, where since October 20th 2014 it is legal for each house to produce its own electricity using solar systems [5].

These systems will change the way people look at electrical energy, from something that it is bought from a big corporation into something that can be produced on a rooftop. They are usually composed by a renewable power source and an inverter which converts the power provided by the source into regular Alternated Current (AC) power.

There are two types of commercial inverters: the "on-grid" which injects into the utility grid the power delivered by the renewable source; and the "off-grid" which can only power isolated circuits. Each one of these approaches requires a specific inverter, despite the similar hardware used in both scenarios.

Since renewable energy systems are being more and more encouraged, this dissertation proposes to develop an equipment that merges the two types of inverters available today, in order to achieve an intelligent and adaptive solution.

This will create a device capable of running in any topology and hopefully facilitate the production of energy using clean energy sources.

1.2 Objectives

At this point, renewable energy solutions are starting to reach the everyday energy consumer and equipment manufacturers are becoming aware of that. The market is absorbing this products at a rate never seen before, and even governments are encouraging people to produce their own energy at home.

Since the inverters offered in these energy solutions do not provide any interoperability between off-grid and on-grid scenarios, the goal of this dissertation is to design an inverter with an efficiency that can compete with commercial products, but most importantly, design it with an intelligent control system. This control system will decide, as required by the user, if the energy produced by the renewable source and converted by the inverter, will be:

- totally injected into the utility grid in a scenario where the user sells its energy to the utility company.
- partially injected into the utility grid in a self consumption scenario.
- powering an isolated electric circuit.

In order to achieve this, the following objectives must be fulfilled:

- Evaluate the technologies that can maximize the energy efficiency of a power inverter.
- Design the electronic circuit of the power inverter.
- Design an adaptive control system that allows the inverter to work in both off-grid and on-grid scenarios.
- Simulate the behavior of the proposed inverter while operating at these scenarios.

1.3 Organization

This dissertation is divided into seven chapters organized as follows:

- **Chapter 1** exposed the motivation, contextualization and objectives of the presented dissertation.
- **Chapter 2** introduces some of the most important background technologies in power conversion and digital control.
- **Chapter 3** describes the design of the hardware architecture.
- **Chapter 4** presents the design of the inverter control system.
- **Chapter 5** describes the proposed operation modes for the resonant inverter.
- **Chapter 6** evaluates the simulation results of the proposed inverter.
- **Chapter 7** summarizes the achievements of this dissertation and possible future improvements.

Chapter 2

Background Technologies

2.1 Introduction

To understand an electronic circuit design and its functionality, it is necessary to understand the scientific knowledge in which that circuit is based.

This chapter introduces some of the most important technologies in the history of renewable power sources and power conversion, while discussing the upsides, downsides and technical information behind each design.

All the concepts here discussed will be essential later, when designing the architecture of the power inverter proposed in this dissertation.

The organization of this chapter is as follows:

- **Section 2.2** introduces the two most used renewable energy sources, solar panels and wind turbines.
- **Section 2.3** describes the power inverters and splits them into smaller subsystems for better understanding.
- **Section 2.4** shows some of the most advanced systems for renewable energies on the market today.

2.2 Renewable Energy Sources

Long before coal or other non renewable energy sources, people used traditional biomass to light fires, wind to grind seeds at windmills or even animal power in agriculture [6].

After the industrial revolution, around the 1860's, the fear of running out of coal made engineers start looking for an alternative. Today, wind generators, solar farms, geothermal plants, among many others, are a reality and provide megawatts of power each day keeping the planet, already so polluted by fossil fuels, a "greener" place.

2.2.1 PV Modules

Edmond Becquerel discovered the photovoltaic effect in 1839 but, due to its inefficiency the process was only used to measure light.

This effect can be explained by a silicon structure doped with different elements creating a p-n junction. When photons (light) hit the material, a great amount of carriers (electrons and holes) are separated from its atoms, generating an electric field across the junction. Placing a conductor between its terminals creates a current proportional to the incident light, as illustrated by figure 2.1.

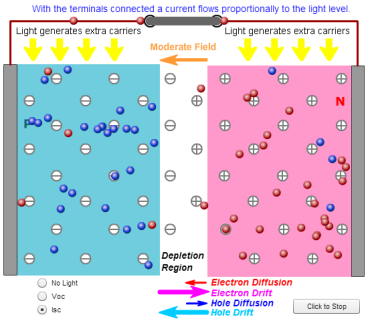

Figure 2.1: Photovoltaic Effect

Figure 2.2: Solar Panel

Most of solar cells are built from silicon [7] connected to make modules, which are also connected to form a solar panel whose final form is illustrated in figure 2.2.

The technology and the purity of the material used to make a solar cell will directly affect its power efficiency and price. As it is possible to see in figure 2.3, the most common technologies used in the present time are: monocrystalline silicon, polycrystalline silicon and thin film.

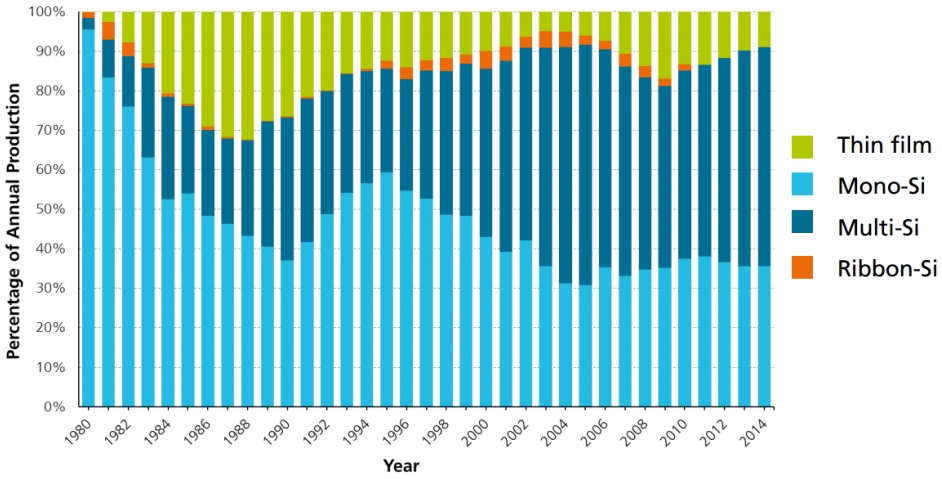

Figure 2.3: PV Production by Technology [8]

- **Monocrystalline Silicon Solar Cells**

Their uniform coloring and look, indicate a high purity silicon. This type of solar cells is made of silicon ingots, that due to their cylindrical shape, present a non-rectangular geometry.

The high purity materials used make monocrystalline solar cells have the highest efficiency rates, typically 15-20%, which makes them the most space efficient too. A longer material lifetime can also be expected, with most manufacturers giving a 25-year warranty certificate on this type of equipment [9].

- **Polycrystalline Silicon Solar Cells**

In this case, in a cheaper process, raw silicon is melted and poured into square molds, giving the cell a perfect square shape. Due to the inferior purity of the materials used, polycrystalline solar cells have a speckled blue color and an inferior efficiency, around 13-16%. Today, this type of cells are around 25% less expensive than monocrystalline solar cells [10].

- **Thin Film Solar Cells**

Thin film solar cells are produced using various semi-conducting materials (including silicon) layered on top of one another creating a series of thin films. Compared to crystalline-based modules, this technology is cheaper and easier to mass produce.

Due to the various substances used in the process, such as amorphous silicon (a-Si), cadmium telluride (Cd-Te), copper indium gallium selenide (CI(G)s), this type of cells have less of a negative impact in terms of high temperatures and shading.

The major disadvantages of this technology are: its typical efficiency, around 10%, and its long-term durability which is often questioned [11].

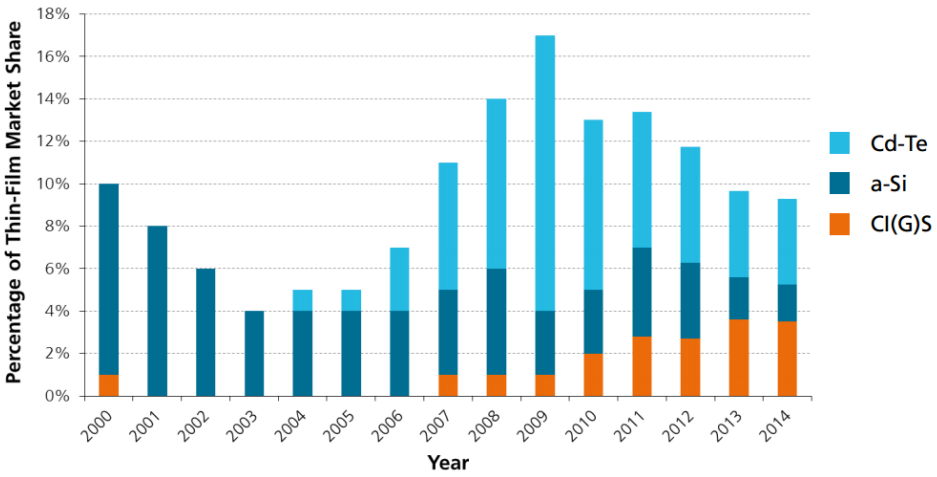

Figure 2.4: Market Share of Thin-Film Technologies [8]

2.2.1.1 Maximum Power Point of a PV Module

The materials used and the internal design of a Photovoltaic (PV) module causes its output current to be inversely proportional to its output voltage. As illustrated in figure 2.5, at lower output voltages the module has the behavior of a current source, however, at its maximum output voltage (V_{oc}) the current flowing through its terminals drops to zero.

Thus, when powering a very light or very heavy load, the power obtained from the PV source it will only be a fraction of its potential output power due to its low current and high voltage, and high current and low voltage, respectively.

This means that there is a point between these two situations where the PV output power is maximum. This point is called Maximum Power Point (MPP), which can be traced by an Maximum Power Point Tracking (MPPT) controller (explained later in this dissertation).

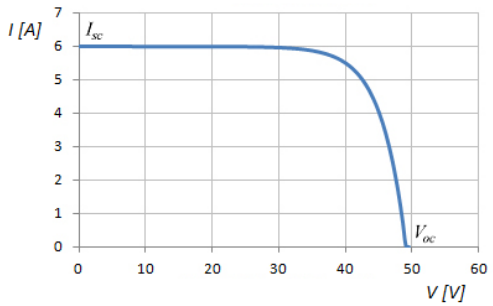

Figure 2.5: Typical I/V MPPT Curve

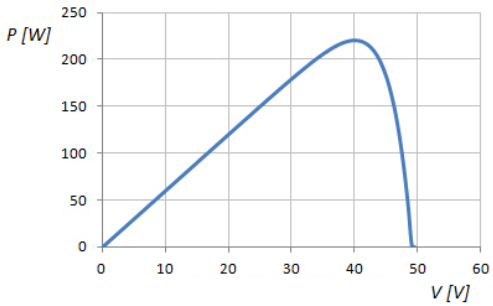

Figure 2.6: Typical P/V MPPT Curve

2.2.2 Wind Turbines

The earliest known design of a wind powered device comes from Persia, around 500-900 A.D., to automate grain-grinding and water-pumping [12]. Since then windmills have been used for similar purposes all across the world.

A wind turbine is a device similar to a windmill, that converts kinetic energy from the wind into electrical power.

Today, wind turbines are designed to produce megawatts of power and most of them are horizontal-axis, as illustrated in figure 2.7.

Figure 2.7: Horizontal-Axis Wind Turbine

Figure 2.8: Vertical-Axis Wind Turbine

Since wind is much more unpredictable than the sun, a complex control system must be implemented in every turbine in order to keep a stable power output, even with variable wind speed and direction. Its goal is, through sensors like anemometers and wind vanes, control actuators like the gearbox or blade pitch, to keep the rotation speed of the generator constant over time, preventing voltage or current peaks. To prevent failure in case of excessive wind speed, due to natural phenomenons, an emergency brake must also be implemented in all turbines.

Wind turbines under 100 kilowatts cost around €3000 to €8000 per kilowatt of capacity [13]. This value is almost the same of a solar system [14], however, due to the mechanical parts that compose the generator, a higher maintenance cost can be expected. On the other hand, the noise produced by the blades and the air flow rate needed to generate electricity makes this type of device more suitable for rural environments.

2.2.2.1 Maximum Power Point of a Wind Turbine

Not very different from solar panels, it is possible to see in figure 2.9 that wind turbines also have a MPP.

The major difference between these two sources stands in the fact that wind is constantly changing, which requires a more complex MPPT. Besides the clouds movement during the day, the position of the sun changes very slowly, making the MPP in solar modules change very slowly too.

In wind turbines the MPPT algorithm has to run faster in order to keep up with wind variations.

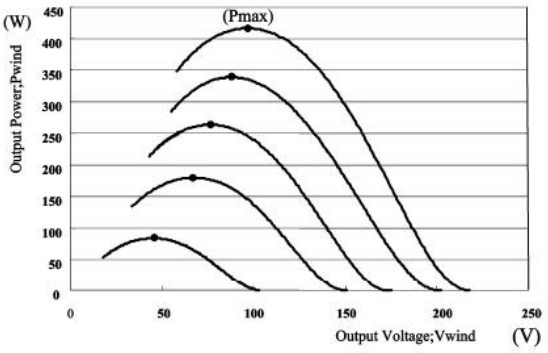

Figure 2.9: Typical P/V Wind Generator Curve

PV modules and wind turbines are just two of the many renewable power sources available today, however, their cost, increasing power efficiency and low maintenance make them the most relevant in terms of domestic renewable power sources.

2.3 Power Inverters

A power inverter, or just inverter, is an electronic circuit/equipment that converts Direct Current (DC) to AC with a controlled frequency and a precise voltage/current waveform and magnitude. This sort of converters can be found in Uninterruptible Power Supply (UPS)'s, electric motor speed control, renewable energy systems, induction heating, among many other applications that require power conversion.

There are two major categories when defining power inverters: standalone or off-grid and grid connected or grid-tie inverters. As illustrated in figure 2.10, the difference between them lies in the fact that grid-tie inverters are connected to the public utility grid, providing power to it, and standalone inverters are used in isolated environments.

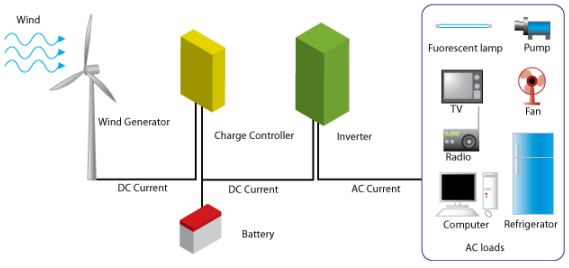

(a) Off-Grid

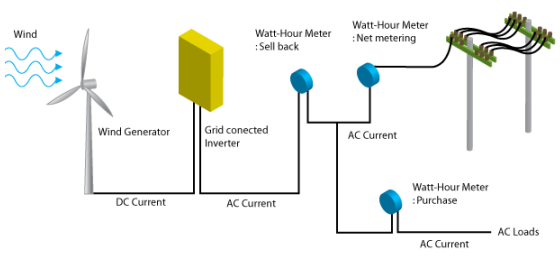

(b) On-Grid

Figure 2.10: Inverter Topologies

Due to the AC waveform of the public utility grid, inverters that deliver power to it must synchronize its output waveform, as illustrated in figure 2.11, in order to minimize differences in frequency and amplitude. If synchronization fails, an electric potential tension is created between the inverter and the grid, causing a current across the inverter that may damage its electronic components.

Grid connected inverters must also turn themselves off automatically when the public utility power fails, in order to not injure any workers that might be handling electrical cables, in a condition called "islanding".

Standalone inverters do not need to have these features since they are used to power isolated circuits that are not connected to other power sources. This makes them simpler and cheaper even when presenting a nominal output voltage similar to the grid.

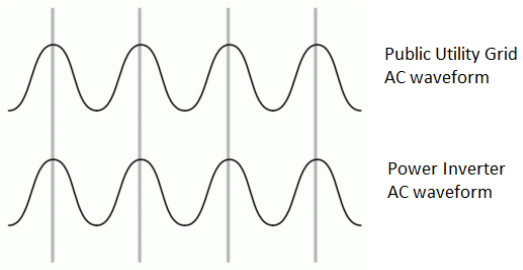

Figure 2.11: Synchronized Waveforms

2.3.1 Inverter Block Diagram

Usually, a power inverter can be separated into blocks, as shown in the figure 2.12:

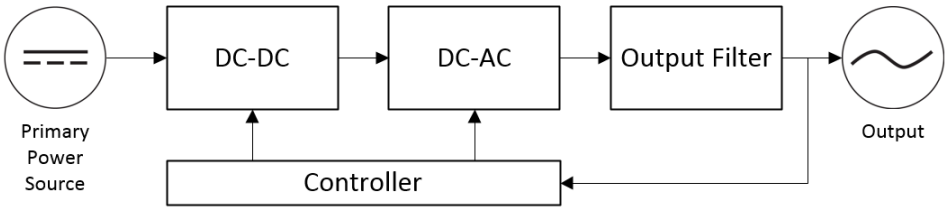

Figure 2.12: Inverter Block Diagram

1. **The Primary Power Source** generates the DC electrical energy, in some cases obtained by rectification and filtering.

2. **The DC-DC Converter**, that connects to the primary power source, is responsible for converting an input voltage level to another.

3. **The DC-AC Converter** shapes the DC voltage, previously elevated or lowered, into an AC waveform.

4. **The Output Filter** removes most of the unwanted frequencies and smooths the output waveform.

5. **The Controller** manages all the control signals based on voltage or current sensors.

As technology evolves, all these previous blocks keep changing in order to achieve less conversion losses. The next sections will try to fully explain their technical specifications and progress over time.

2.3.2 DC-DC Converters

Several methods can be used to achieve DC-DC conversion. Each method has its own advantages and disadvantages, however, all have the same goal: to change a voltage level to another, spending as little power as possible in the conversion.

2.3.2.1 Linear Converters

This type of converters act like a variable resistor which varies in accordance with the load. In a series configuration, this allows the converter to deliver a stable output voltage, dissipating the excess power as heat.

This architecture can only provide an output voltage lower than its input along with an average energy efficiency of 40% [15], however, the availability of compact and cheap parts, along with the fact they are easy to implement and inherently low-noise, make this type of converters very popular in low power applications.

2.3.2.2 Switching Converters

A switching converter is an electronic circuit that makes use of transistors, inductors, capacitors and rectifiers to transfer energy from input to output. The transistors used in this type of circuits change state at a certain frequency, usually denoted as "switching frequency".

High switching frequencies make possible to achieve smaller, cheaper and lighter circuits, since for equal peak-to-peak output ripple current and for equal output ripple voltage, the values of the inductors and capacitors used, respectively, are inversely proportional to the switching frequency [16].

These converters have an typical energy efficiency of 85% [15], which makes them very efficient when compared to linear converters.

In a very simple approach, the next circuits will help explain how basic electronic components can be arranged in order to form a step-up converter, a step-down converter or both.

The Buck Converter is a step down voltage regulator/converter, which means that the output voltage is lower than the input voltage.

At its charging cycle, shown in figure 2.13-a), the transistor in "on" and the diode is in reverse mode. At this point, the inductor and capacitor are being charged by the input and the voltage across the load is given by the voltage across the capacitor, which is charged by the current rate allowed by the inductor.

When the transistor changes its state to "off", the current that flows through the inductor cannot be discontinued, so the rectifier starts conducting. At the same time, the current through the inductor starts decreasing and the capacitor starts discharging towards the load.

On a very simple explanation, the output voltage is roughly proportional to the duty cycle of the control signal used to drive the transistor. With a duty cycle of 100%, the inductor becomes a shunt and the capacitor will charge until it reaches the input voltage of the circuit, having the voltage across the load, the same value. Using a duty cycle of 0%, the transistor will never connect the capacitor to the input and it will never charge, which means that the voltage across the load will be 0 at all times.

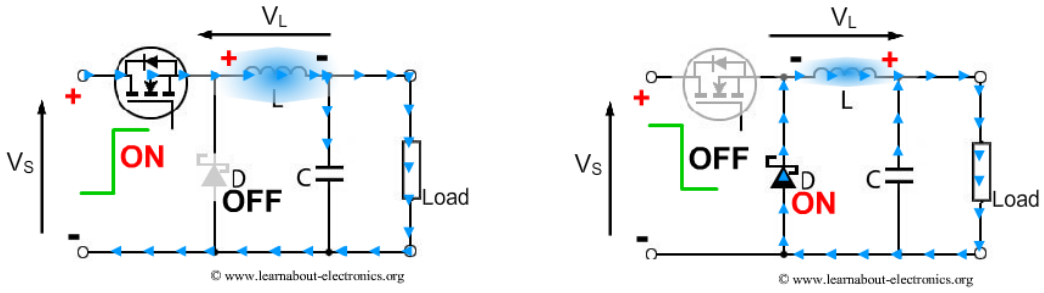

(a) Charging Cycle (b) Discharging Cycle

Figure 2.13: Buck Converter Current Flow Over Time

The Boost Converter is a step-up voltage regulator, which means it has an output voltage higher than its input voltage.

As it is shown in figure 2.14, when the transistor turns "on", the inductor makes a connection between the positive and the negative input terminals. This generates a current that charges the inductor, creating a voltage across its terminals.

When the transistor turns "off", the inductor discharges its stored energy towards the capacitor and the load. At this point, the voltage across the load is equal to the input voltage of the circuit plus the voltage across the inductor.

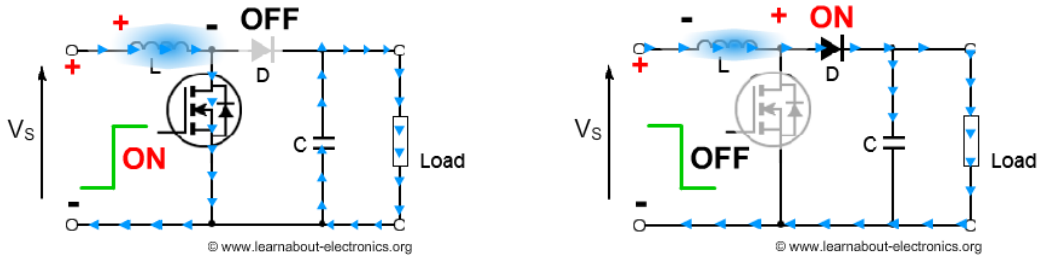

(a) Charging Cycle (b) Discharging Cycle

Figure 2.14: Boost Converter Current Flow Over Time

The Buck-Boost Converter is simply the combination of the previous circuits, allowing the output voltage level to be higher or lower than the input.

Observing figure 2.15, if the output voltage level required is higher than the input, then the circuit has to behave like a Boost Converter. In order to do that, the control system has to change the state of the transistor $Tr1$ to "on" at all moments, while the transistor $Tr2$ changes state at a certain switching frequency. The circuit now behaves as a Boost Converter.

If the output voltage level required is lower than the input voltage, the system has to behave like a Buck Converter. To achieve this, the control system has to turn "off" the transistor $Tr2$ while the transistor $Tr1$ changes state at a certain switching frequency.

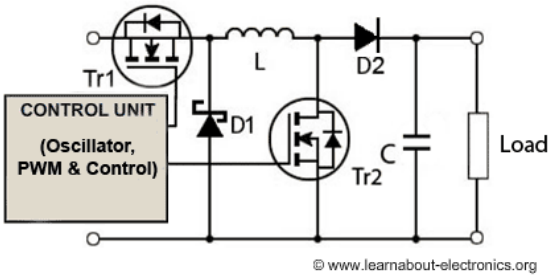

Figure 2.15: Buck-Boost Converter Schematic

- **Resonant Converters**

Being much more efficient than linear converters, the switching methodology presented in the previous circuits can still be improved in order to achieve a lower power dissipation. This is based on the fact that when the transistors change state, the current and voltage across them lead to some switching losses.

This power dissipation lasts nanoseconds, typically a fraction of a power transistor rise/fall time, as illustrated in figure 2.16, but considering that the transistors switch state

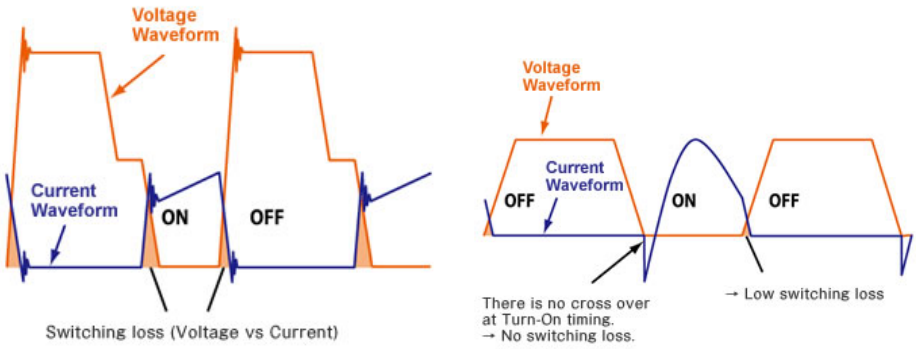

(a) Boost Converter (b) Resonant Converter

Figure 2.16: Voltage and Current Waveforms on a Transistor

at a rate of hundreds kHz or even MHz, the impact of these losses becomes noticeable on the energy efficiency of the converter.

Since switching losses on switching converters are impossible to neutralize, the next step is to minimize them using a resonant circuit topology. To understand how this can be achieved, it is also necessary to understand the circuit of a typical resonant inverter, illustrated in figure 2.17.

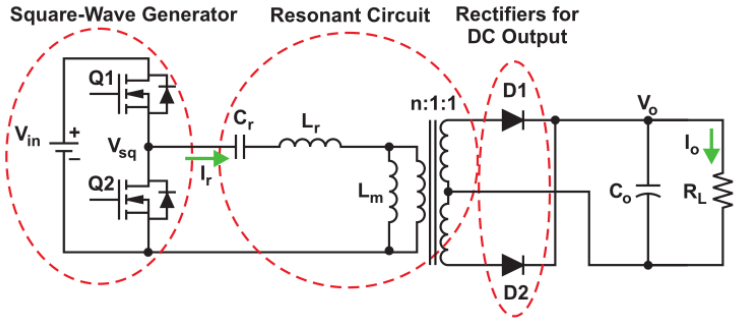

Figure 2.17: Typical Resonant Converter

The main blocks that compose a resonant converter are the following:

The Square-Wave Generator can be a half-bridge, figure 2.18, or a full-bridge, figure 2.19, depending on the electronic circuit, as it will be explained later.

A half-brige has an upper and lower transistor, in a cascode arrangement, which are turned "on" and "off" complementary to each other with a non-overlapping dead-time. This prevents short-circuits, which can lead to the total destruction of the transistors. The output voltage of this circuit will alternate between the supply voltage, V_{in}, and ground, or zero.

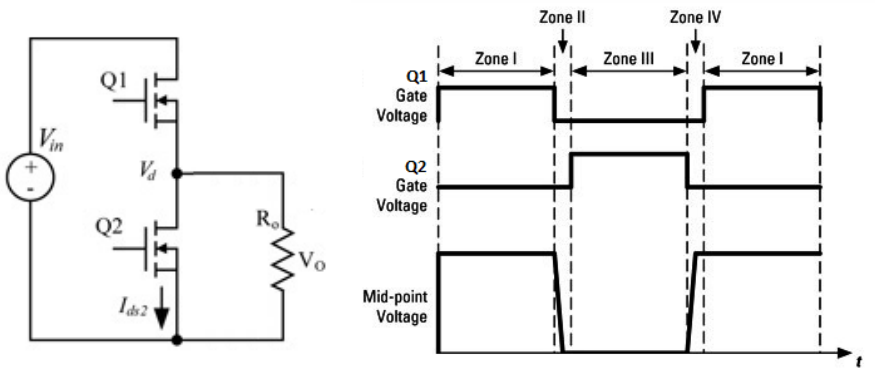

(a) Circuit (b) Signals

Figure 2.18: Half Bridge Circuit

A full-bridge, or h-bridge, adds two transistors to the circuit but makes use of the same control signals as the half-bridge. This can be arranged simply by connecting the gate of the transistor $Q1$ to the gate of the transistor $Q4$, and the gate of $Q2$ to $Q3$, illustrated on figure 2.19. The output voltage level now alternates from the supply voltage, V_{in}, to its inverted, or negative value, $-V_{in}$.

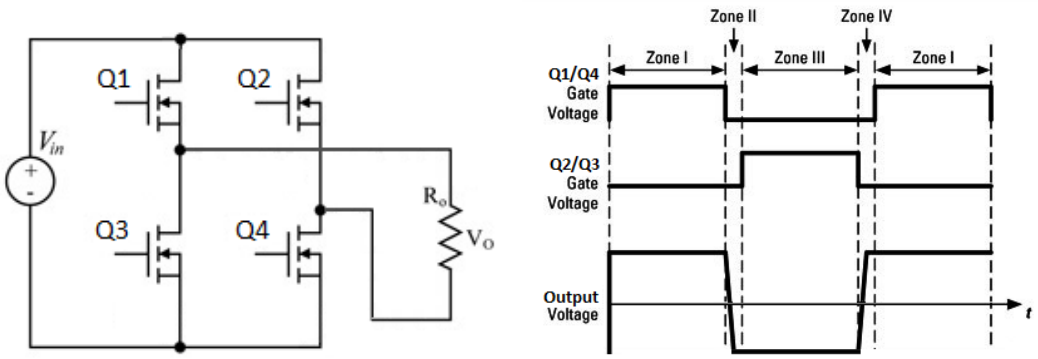

(a) Circuit (b) Signals

Figure 2.19: Full Bridge Circuit

The difference between these two designs stands in the fact that, in isolated circuits like the one illustrated in figure 2.17, which require a transformer, a half-bridge uses two times more secondary winding turns for the same voltage gain. Thus, twice the secondary winding resistance can be expected, increasing conduction losses compared to the full-bridge. Due to this fact, in electronic circuits with high primary currents it is recommended to use a full-bridge in order to maximize energy efficiency.

The Resonant Circuit is composed by the resonant tank (and the high frequency

transformer in case of an isolated topology). The tank can have three different topologies: Series, Parallel and Series-Parallel. In a resumed and simple way, each one will be explained according to what is most important for the inverter prototype purposed in this dissertation.

The Series Resonant Converter (SRC), as the name implies, has a capacitor and an inductor in series, creating a tank that it is also in series with the load. Because of that it acts like a voltage divider, presenting a maximum voltage gain of 1. This happens when the switching frequency applied to the square-wave generator matches the resonant frequency of the tank and its impedance becomes very small. As a consequence of this design, under light-load conditions, the impedance of the load becomes very large comparing to the impedance of the resonant tank making difficult to regulate the output voltage, and almost impossible at a no-load situation.

The Parallel Resonant Converter (PRC), takes the capacitor in series with the inductor and puts it in parallel with the load. This topology fixes the output voltage regulation issue, but also requires large circulating currents in order to magnetize the tank. This makes it less efficient when working with larger currents, but unlike the SRC, it is possible to have a voltage gain larger than 1.

In order to merge the advantages and solve the issues of the above topologies, both can be combined forming a Series Parallel Resonant Converter (SPRC). This can be a LLC (two inductors and a capacitor) or a LCC (one inductor and two capacitors).

Since capacitors with low Equivalent Series Resistor (ESR), required to accommodate large currents with less losses, can be very expensive, its preferable to use a LLC topology. The advantage of this lies in the fact that in isolated circuits it is possible to manipulate the winding of the transformer and create a series inductance L_r and a magnetizing inductance L_m as parasite inductors. Using a LCC topology, two physical capacitors must be used in the tank circuit.

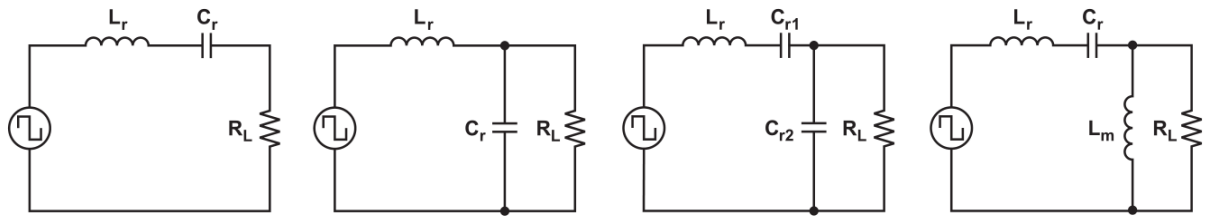

Figure 2.20: Series, Parallel, LCC and LLC Resonant Tanks

The Rectifiers cause conduction losses that are proportional to the forward voltage drop of the diode. To decrease those losses it is important to choose rectifiers with a small forward voltage drop, like Schottky diodes.

Apart from conduction losses, diodes also cause switching losses when used at high frequencies. These take place when the transistors that compose the "square-wave generator" switch state and consequently invert the charge of the p-n junction of the diode, which forces the rearrangement of the carriers, as illustrated in figure 2.21. From the moment that the transistor changes state to the complete rearrangement of the carriers, the diode temporarily conducts in the reverse direction. To this short period of time is called Reverse Recovery Time.

Thus, diodes with a short reverse recovery time are crucial to design a converter with low switching losses.

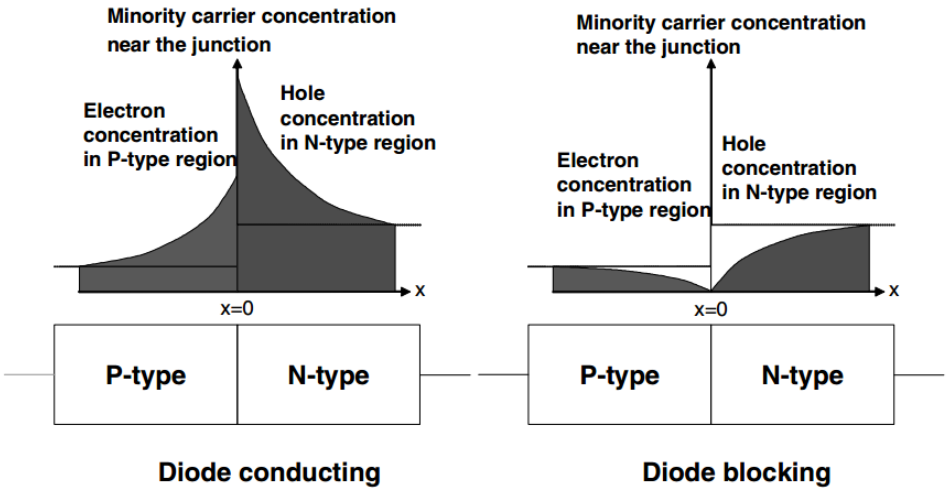

Figure 2.21: Charge distributions in a diode [17]

As silicon components approach their theoretical limits, new technologies based on compound materials, such as Silicon Carbide, or just SiC due to chemical representation, are capable to dramatically improve component capabilities [18]. Figure 2.22 shows SiC diodes recovering much faster than any other rectifiers, which can be translated into much lower switching losses and therefore, higher power efficiency.

Besides the fast recovery, SiC technology provides reduced forward voltages, high operation temperatures and low leakage currents [19].

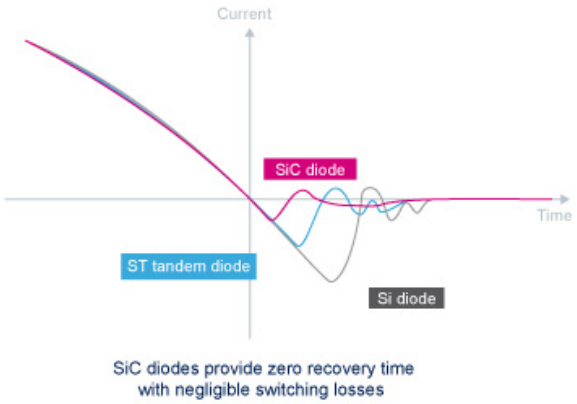

Figure 2.22: Diodes Reverse Recovery Comparison [20]

2.3.3 DC-AC Converter

This block, present in any inverter, has the task to shape a DC voltage into an AC waveform, using an electronic circuit.

Most of the inverters sold today have an output waveform that can be described as a "Sinewave", "Modified Sinewave" or "Squarewave", as represented in figure 2.23.

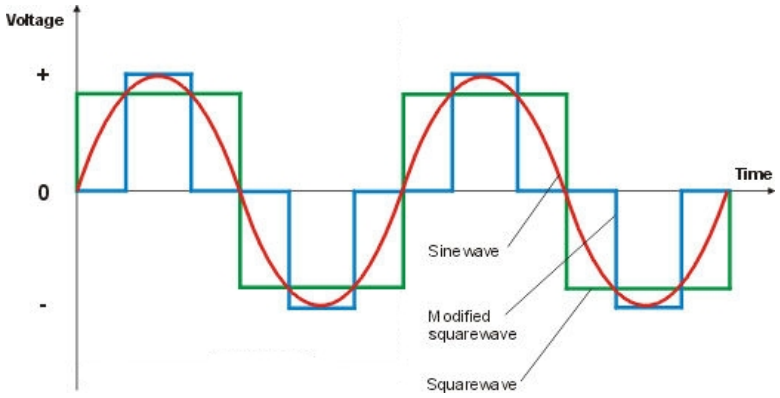

Figure 2.23: Inverter Output Possible Waveforms

A **Squarewave** can be found on the cheapest inverters, due to the low cost components in the circuit needed to create this waveform. This type of waveform is composed by three different voltage levels: zero, a positive and a symmetrical negative value. The high Total Harmonic Distortion (THD) present in this signal forces capacitors and inductors, present in non-resistive loads, to handle very high currents and voltages, which can lead to equipment failure.

A Sinewave is the waveform present in the public utility grid, as a result of the rotative movement of AC generators installed in power plants.

Since all the domestic appliances are designed to operate with this kind of waveform, an inverter with this output waveform will guarantee that the equipment that it is powering will operate at its full potential.

The presence of other frequencies in public utility grid, that not the usual 50 or 60 Hz AC, reduces the amount of real power capacity of a power supply and also increases the losses by thermal dissipation in the transmission cables due to skin effect.

The added complexity necessary to produce this type of waveform, in terms of electronic components and filters, makes products with this type of output more expensive. Most designs often use a full-bridge followed by a low pass filter.

In a simple explanation, and looking at figure 2.24, when the transistors $Q1$ and $Q4$ are "on" and $Q2$ and $Q3$ are off, the voltage across the load rises towards V_{dc}. When the transistors $Q2$ and $Q3$ are "on", $Q1$ and $Q4$ are "off", the voltage across the load drops towards $-V_{dc}$.

Thus, using a microcontroller with a Pulse Width Modulation (PWM) signal, it is possible to control the inverter output voltage, as shown in figure 2.25.

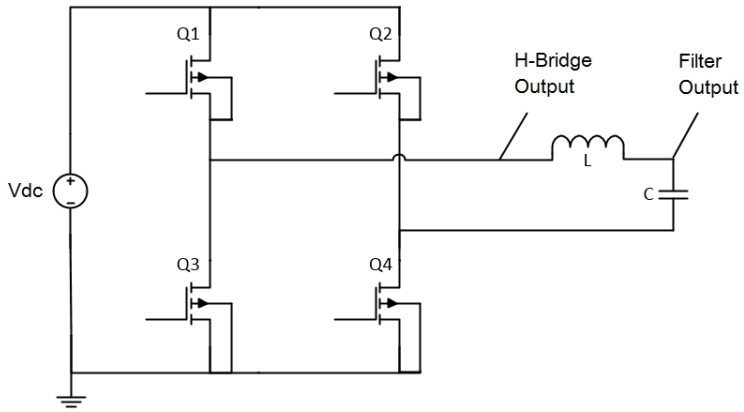

Figure 2.24: Sine Wave Generator

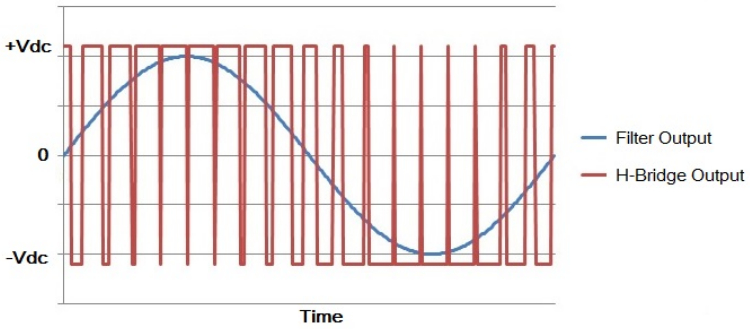

Figure 2.25: PWM to Sine Wave

A Modified Squarewave offers an "almost sinewave" and it is the most cost-effective waveform. While requiring a fairly simple electronic circuit to produce it, this type of signal can perfectly power typical resistive loads such as incandescent or halogen lights and most of domestic appliances.

Due to its moderate THD, non-resistive electronics such as televisions or radios can present a faulty behavior, which can lead device malfunction after some time. Thus, the use of this waveform to power this type of electronics is heavily discouraged.

2.3.4 Output Filter

Filtering, in electronics, is the process of removing unwanted frequencies from a certain signal. In terms of cut-off frequencies there are low-pass, band-pass and high-pass filters.

Since the output voltage from the DC-AC Converter is corrupted with the PWM carrier frequency and other harmonics, it is necessary to clean the signal in order to achieve a sine wave with the lowest THD as possible.

Due to the low frequency of the utility grid, a low-pass filter is commonly used in these situations. The order of the filter will set its attenuation factor beyond the cut-off frequency.

As figure 2.26 illustrates, a filter with a certain cut-off frequency presents an attenuation that varies with its order. In this case, five orders of attenuation are illustrated and it is possible to see that each one adds -20dB's per decade on the transition band of the filter.

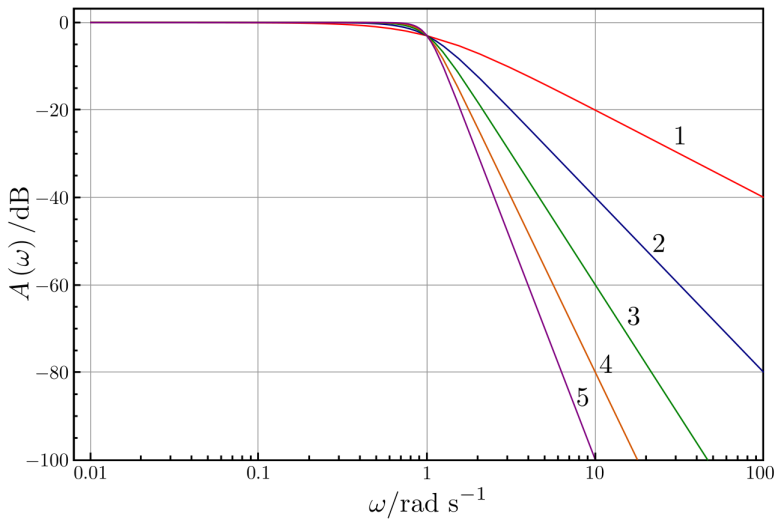

Figure 2.26: Filter response by order of attenuation

In order to achieve a "clean" signal, taking into account the cost of the filter, the PWM frequency should be as high as possible, allowing the low-pass filter to have a higher

cutoff frequency, which translates into smaller and cheaper inductors and capacitors. This associated to the fact that commutation losses in the transistors of the DC-AC converter increase with frequency, creates a compromise between equipment cost and performance.

Power electronic circuits demand passive filters as shown in figure 2.27, in order to accommodate the high currents and voltages.

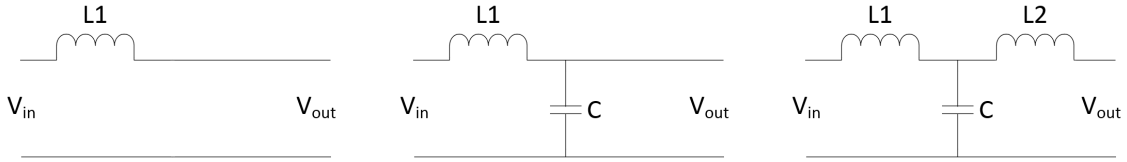

(a) L Filter (b) LC Filter (c) LCL Filter

Figure 2.27: Passive Filters

A L filter, the simplest passive filter, consists of one inductor in series with the output. Built by only one component, it is a first order filter with an attenuation of -20dB's per decade.

A LC filter adds a capacitor in parallel with the output, becoming a second order filter with an attenuation of -40 dB's per decade.

A LCL filter is a LC filter with a second inductor in series with the load, forming a T shape. It is a third order filter and has an attenuation of -60 dB's per decade.

It is possible to increase the order of the filter by adding inductors and capacitors, which would provide a greater attenuation. However, since each order of attenuation adds a certain delay to the filtered signal, this would make necessary to increase the complexity of the controller in order to achieve stability.

2.3.5 Controller

A controller is a device that, through a comparison between a predetermined reference and an input signal from a measured process variable, calculates an output signal required by the process being controlled in order to provide corrective action within a control loop.

Today, a wide range of microprocessors is available, offering memory, peripherals and a Central Processing Unit (CPU), all in the same chip. As technology evolves, the cost/performance of these devices has been dropping day after day, which associated to the programmability, ruggedness and speed, makes them a very attractive solution when it comes to control system design.

As illustrated in figure 2.28, 8-bit and 16-bit microcontrollers have more than half of the market share today, however, their performance can be questionable when applied in

switching converters. In order to solve this problem, it is necessary to choose chips with faster clocks and greater computational power.

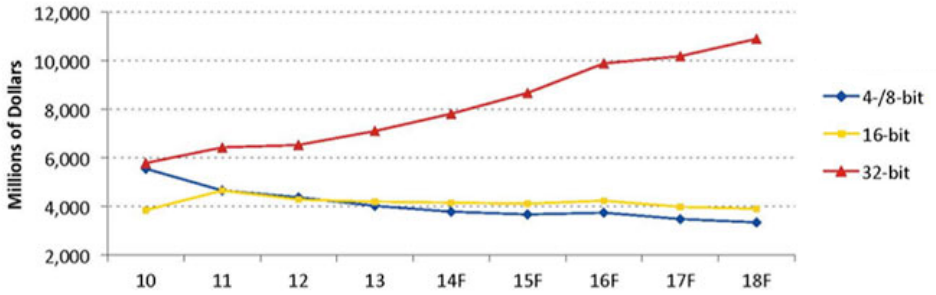

Figure 2.28: Microcontroller Sales Forecast [21]

Benchmark tools such as CoreMark can be used to measures the performance of CPU's used in embedded systems. Similar to the out-of-date Dhrystone benchmark, it gives the user an idea of the processing capability of the microprocessor.

In a typical digital feedback system, illustrated in figure 2.29, microprocessors read the reference signal $r(t)$ and the output signal $\hat{y}(t)$ using Analog to Digital Converter (ADC)s, then calculate the control signal using a control algorithm, and apply that signal to the controlling process using a digital or analog output signal.

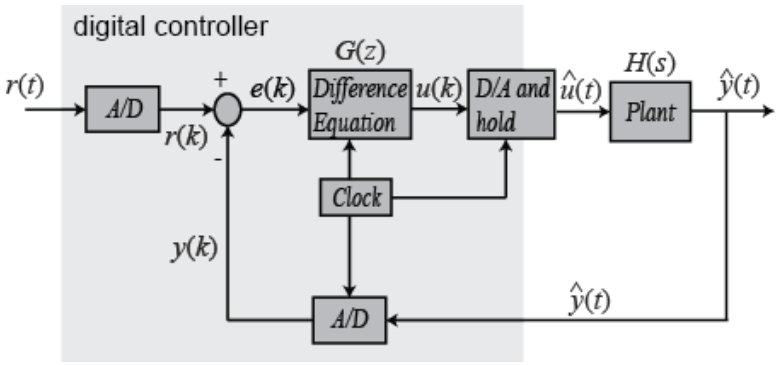

Figure 2.29: Digital Control Loop [22]

As explained in section 2.3, off-grid inverters generate their own output signal, however, on-grid inverters need to synchronize their output signal with the public utility grid. Both systems, even if using a different reference signal, need a control system to keep their output waveforms stable in order not to damage any appliances connected to them, or cause a short circuit between the inverter and the grid, in case of grid-connected inverters.

Later in this dissertation, algorithms to design a control system for the proposed inverter will be discussed.

2.4 Commercial Products

The concept of power inverter was born to fulfill industrial needs on motor control, however, nowadays, due to development of renewable energies solutions, this equipment can be found in an ordinary household. With or without government incentives, everyday more and more people are investing in clean energy solutions and companies tend to follow that trend. To understand the basic features of commercial products available today, inverters produced by two of the most influential companies will be analyzed next. Due to the objectives of this dissertation, the main characteristics described will be: electrical specifications such as maximum/minimum input and output voltages, energy yield, and output power; as well as interoperability between off-grid, on-grid and self-consumption scenarios.

2.4.1 SMA Solar Technology AG

SMA Solar Technology AG stands out for being one of the most awarded company in solar systems development, having a wide range of solutions not just to domestic environments but industrial environments as well.

As a domestic solution, SMA offers the Sunny Boy on-grid inverter which can deliver up to 5250W. This equipment has a maximum DC input voltage of 750V, a maximum efficiency of 97% and a built in MPPT. Its "dedicated power socket" functions as a small off-grid inverter output, which allows the user to power small appliances or charge electronic devices during prolonged utility power outages [23].

For off-grid systems, SMA offers the Sunny Island with DC input voltages from 41 to 63V in order to be powered by battery banks. Capable of a maximum output power of 6000W, and an efficiency of 95%, this represents SMA's offer when it comes to off-grid power inverters [24].

SMA also offers a self-consumption solution where both inverters described above can be used simultaneously to minimize the amount of energy consumed from the utility grid. It was called "SMA Flexible Storage System" and its architecture is illustrated in figure 2.30. Using this scenario, during daylight, a "SMA Energy Meter" senses how much power is being consumed by the house and instructs the grid-connected inverter (Sunny Boy) to produce that exact amount of power, while the excess produced by the PV modules is used to charge the batteries. At night, the off-grid inverter (Sunny Island) delivers power to the house using those same batteries [25].

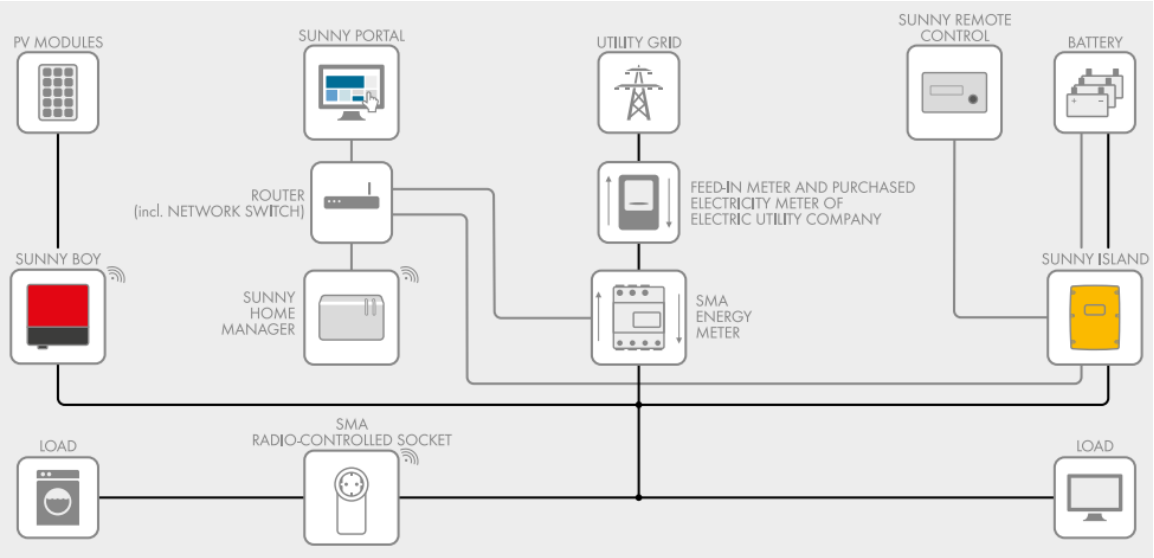

Figure 2.30: SMA Flexible Solution [25]

2.4.2 SolarEdge

Founded in 2006, SolarEdge is a provider of solar inverters, monitoring solutions for photovoltaic arrays and power optimizers [26].

Unlike SMA inverters which have a built in MPPT controller, SolarEdge inverters require an external power optimizer for each solar panel, which constantly and individually track the MPP of its energy source. The only task of the inverter is to convert DC into AC and synchronize its output with the public utility grid. Available from 2.2kW to 17kW, these on-grid inverters have a peak efficiency of 98%, a maximum input voltage of 900V and a self-consumption mode called Feed-in Limitation [27].

In self-consumption mode, an extra meter (SolarEdge Electricity Meter) is used to sense the current consumed by a circuit and instruct the inverter to generate that exact amount of power. Therefore, when the solar PV output is enough to cover the circuit consumption, the power coming from the utility grid is theoretically zero, as illustrated in figure 2.31.

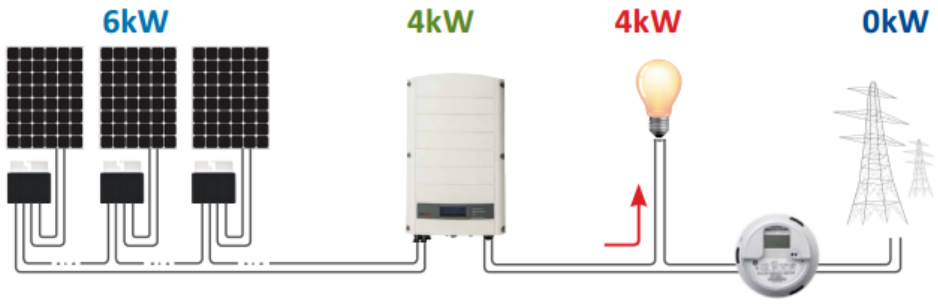

Figure 2.31: SolarEdge Feed-in Limitation Schematic [27]

2.4.3 Products Comparison

The devices and solutions analyzed in this section represent the state of the art when it comes to DC-AC power inversion using renewable energy sources.

- Both on-grid and off-grid inverters presented by SMA hold a high benchmark in terms of power efficiency, however, the need of multiple inverters in the adaptable solution developed increases its cost unnecessarily.
- When comparing to SMA's, SolarEdge offers a much simpler self-consumption solution, however, the lack of a off-grid or battery powered system can be disappointing. The inexistent MPPT controller on SolarEdge inverters makes it necessary to use multiple SolarEdge power optimizers, which increases the cost of the system and reduces interoperability.

Thus, this dissertation will try to design an inverter with an energy yield similar to the commercial products described above, with a built-in MPPT controller without the need of extra power controllers or optimizers.

The proposed inverter must also be capable of operating in off-grid, on-grid and self-consumption scenarios without any hardware modifications needed, unlike the devices presented in this section.

Chapter 3

Hardware Architecture

3.1 Introduction

As seen in the previous chapter, a power inverter can be separated into a small amount of subsystems: the DC-DC Converter, responsible for converting the primary power source voltage to a higher or lower level; the DC-AC Converter, which transforms the V_{BUS} DC voltage into an AC waveform; the output filter that removes most of the unwanted noise from the output signal.

The inverter proposed in this dissertation has a single-phase, sinusoidal, output voltage of $230V$ Root Mean Square (RMS), a maximum output power of 20kW and an input voltage range from $200V$ to $950V$, in order to compete with the commercial devices described before.

In this chapter, all these subsystems will be thoroughly described, designed and connected as illustrated in figure 3.1, in order to achieve the technical specifications just described, with the maximum energy efficiency possible.

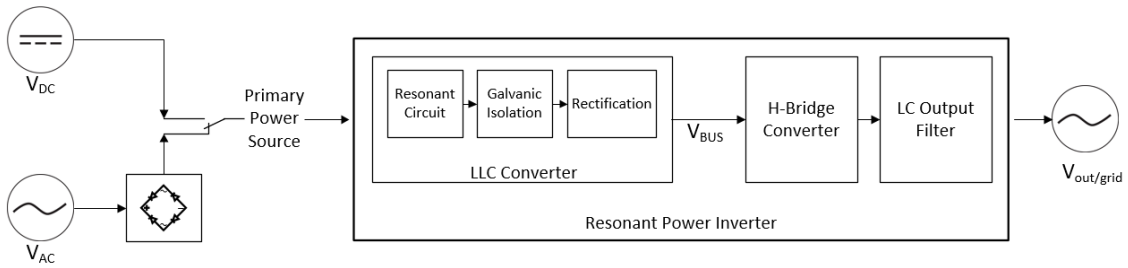

Figure 3.1: Inverter Hardware Block Diagram

The organization of this chapter is as follows:

- In **Section 3.2** the LLC Converter circuit will be explained and designed.
- In **Section 3.3** will be discussed the architecture of the H-Bridge Converter.
- In **Section 3.4** will be designed and discussed output filter of the inverter.

3.2 LLC Converter

Nowadays the most efficient way to achieve DC power conversion is using resonant converters, like the LLC Converter, due to the minimal switching losses achieved by soft-switching.

This circuit, illustrated in figure 3.2, is responsible for converting a voltage level, in this case provided by the DC source, to another, V_{BUS}. In the presence of a control system, fully explained in the next chapter, this LLC Converter will allow a variable input voltage while maintaining its output, V_{BUS}, constant, providing a stable voltage source for the DC-AC Converter. This will allow the proposed power inverter to have a wide input voltage range and a high energy efficiency.

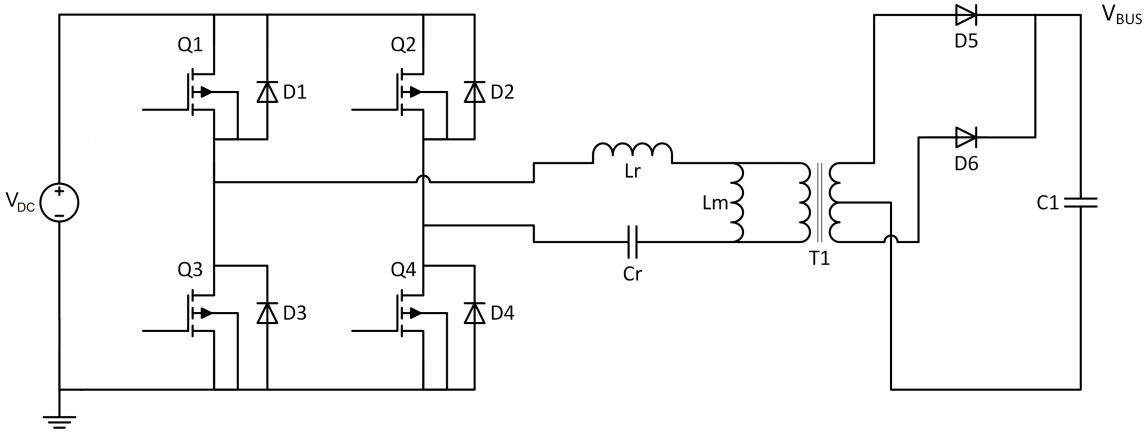

Figure 3.2: Typical LLC Converter Circuit

3.2.1 Principle of Operation

The LLC Converter achieves a very high energy efficiency due to the soft-switching methodology implemented by its resonant architecture. This reduces switching losses, transistor stress, and Electromagnetic Interference (EMI) during power conversion.

Looking at figure 3.2, the transistors $Q1$ to $Q4$ build a full-bridge. As explained in subsection 2.3.2.2, this circuit generates a square wave with an amplitude that alternates between V_{DC} and $-V_{DC}$, in this case, and a frequency equal to the frequency of the control signal that drives the transistors.

Connected to the output of this full-bridge is the resonant tank, which has resonant frequency that can be expressed by:

$$f_{LLC} = \frac{1}{2\pi\sqrt{(L_r + L_m)C_r}} \tag{3.1}$$

When the frequency of the square wave is different from the resonant frequency of the tank, this last one presents a higher impedance. Therefore, the current delivered to the load can be controlled by the impedance of the tank, which depends on the frequency of the generated square wave. In the same way, a variation of the load will force a change in the square wave frequency in order to maintain the output voltage stable.

The LLC resonant tank transfer function can be expressed by [28]:

$$K(Q, m, F_x) = \frac{|V_{out}(s)|}{|V_{in}(s)|} = \frac{F_x^2 \cdot (m-1)}{\sqrt{(m \cdot F_x^2 - 1)^2 + (F_x^2 - 1)^2 \cdot (m-1)^2 \cdot Q^2}} \tag{3.2}$$

Where:

$$Q = \frac{\sqrt{L_r/C_r}}{R_{ac}} \quad \text{Quality factor} \tag{3.3}$$

$$R_{ac} = \frac{8}{\pi^2} \cdot \frac{N_p^2}{N_s^2} \cdot R_0 \quad \text{Reflected load resistance} \tag{3.4}$$

$$F_x = \frac{f_{sw}}{f_r} \quad \text{Normalized switching frequency} \tag{3.5}$$

$$f_r = \frac{1}{2\pi\sqrt{L_r \cdot C_r}} \quad \text{Resonant frequency} \tag{3.6}$$

$$m = \frac{L_r + L_m}{L_r} \quad \text{Ratio of total primary inductance to resonant inductance} \tag{3.7}$$

f_{sw} Switching frequency

N_p Number of turns of the primary coil

N_s Number of turns of the secondary coil

R_o Load connected to the output of the LLC Converter

Thus, as illustrated in figure 3.3, generating a square wave with a frequency lower than the resonant frequency of the tank, will make the LLC Converter act as a step up, or boost converter. Higher frequencies have the opposite effect, making the converter to act as a step down, or buck converter. At the resonant frequency the voltage gain in unitary.

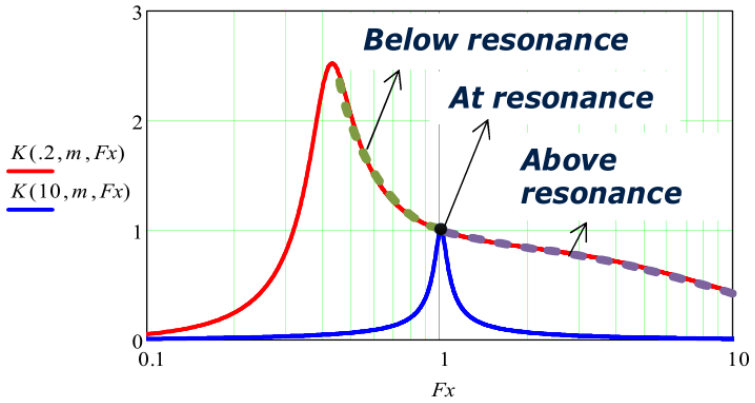

Figure 3.3: LLC Tank Transfer Function - [28]

When simulating the behavior of the tank at these three regions of operation, as figure 3.4 illustrates, for the same output voltage and power, it is possible to see considerable differences on its behavior.

At a switching frequency below the resonant frequency of the tank, the transistors of the full-bridge change state when the current flowing in the tank is almost zero, achieving Zero Current Switching (ZCS). This minimizes switching losses in the transistors but discharges the filtering capacitor for a longer period of time. Consequently, when the capacitor get charged again, the greater voltage difference creates a greater charging current.

Above the resonant frequency, the transistors of the full-bridge change state when the voltage difference between the power source and the tank is almost zero, achieving Zero Voltage Switching (ZVS).

In terms of losses, due to the higher currents, working below the resonant frequency of the tank will result in greater conduction losses, however, working above it will result in greater switching losses due to the higher switching frequencies used. Thus, minimal losses can be expected when the switching frequency equals the resonant frequency of the tank.

Connected to the output of the tank, a High Frequency (HF) transformer, $T1$, is placed to give the design a wider range of possible output DC voltages at V_{BUS}, obtained after standard rectification in $D5$ and $D6$, followed by filtering in $C1$.

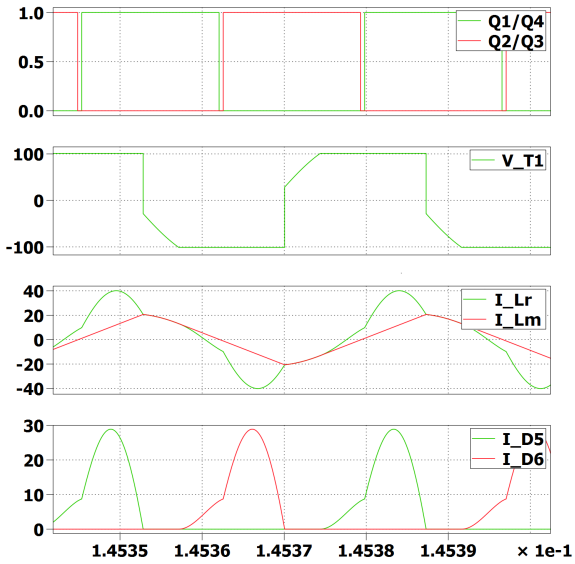

(a) Below Resonant Frequency

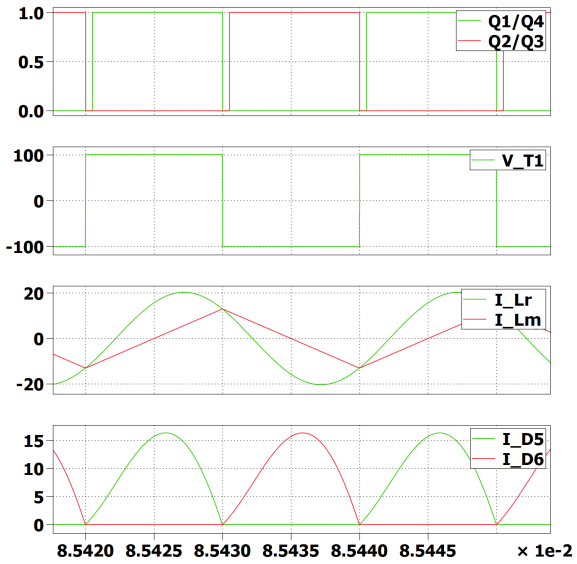

(b) At Resonant Frequency

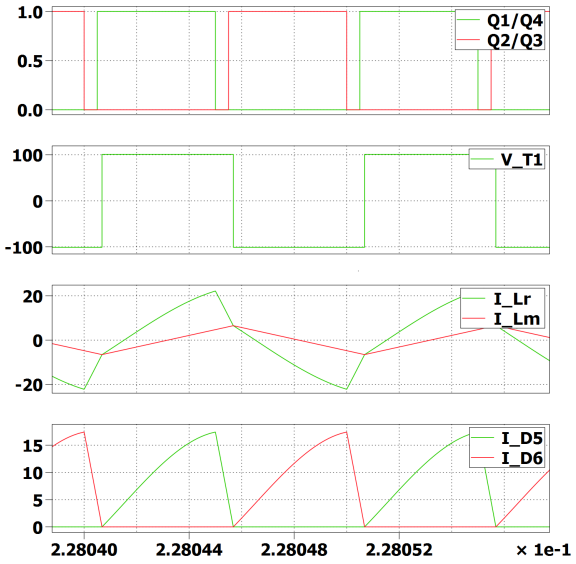

(c) Above Resonant Frequency

Figure 3.4: LLC Circuit Signals

Where V_T1 shows the voltage level at the primary winding of the transformer.

3.2.2 Resonant Tank Design

As seen in the previous section, the LLC resonant tank is responsible for the ZVS and ZCS soft-switching states present in the converter, however this circuit is also responsible for a voltage gain due to its transfer function, illustrated in figure 3.3.

This voltage gain can be greater or lower than 1, and since it depends on the switching frequency of the resonant tank, even with a variable input voltage it is possible to have a stable output voltage, simply by adjusting the switching frequency of the resonant circuit.

In this section, the architecture of the LLC resonant tank will be discussed and implemented following the flowchart illustrated in figure 3.5. This simple approach takes into account the maximum and minimum gain of a LLC circuit, and the two variables that can manipulate those gains, Q (Quality Factor) and m (the ratio of the two inductances used to compose the tank).

The first step will be to determine the turn ratio of the transformer, followed by Q that will be chosen by taking into account the minimum gain required for the LLC converter, and m by the maximum gain.

Having settled values for these variables, it will be possible to create a system of equations and calculate the values of the two inductors and one capacitor that compose the resonant tank.

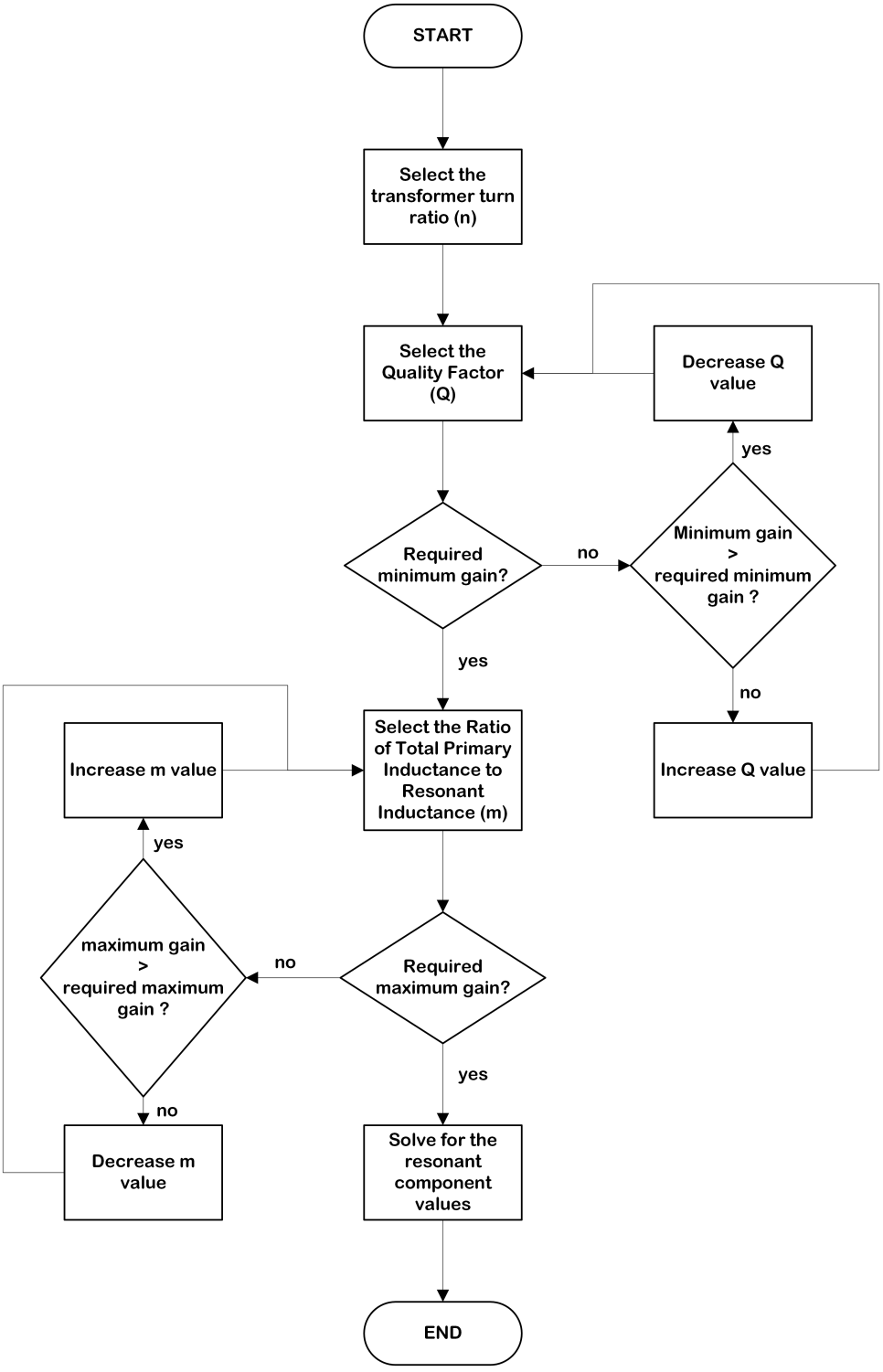

Figure 3.5: LLC Design Flowchart

- **Select the transformer turn ratio (n)**

As stated before, the LLC Converter achieves minimal losses when using a switching frequency equal to its resonant frequency, which makes its gain unitary. Based on that, the transformer turn ratio, n, should be chosen in order to have minimal losses when output power is maximum. This will minimize heat dissipation and thermal stress for all the electronic components.

Since n can be calculated by the ratio between the input of the LLC converter (presented below as an array of solar panels) and its output V_{bus} (that will power the next stages of the circuit) it is appropriate to analyze the electrical specifications of an arrays of solar panels with an output power of 20kW. This type of power source was chosen due to its stable output power, which will make calculations easier.

A standard 250W PV module from MPRIME [29], with the electric specifications presented on table 3.1, will be used to estimate the 20kW PV array specifications.

Nominal Power (W)	250
Positive Power Tolerance	[PNOM-0; PNOM+4.99W]
MPP Current (A)	8.34
MPP Voltage (V)	30.02
Open Circuit Voltage (V)	37.60
Short Circuit Current (A)	8.68
Module Efficiency (%)	15.6
Maximum System Voltage (V)	1000
Maximum Series Fuse Rating (A)	15
NOCT	47.3 ^{o}C
Power Temperature Coefficient:	-0.45%/^{o}C

Table 3.1: MPRIME 250W PV Module Specifications

To build a PV array capable of delivering 20kW of power, with multiple 250W PV modules, it is necessary to connect the modules to form arrays, preferable in series to minimize output current of the array. This configuration leads to less conduction losses in the wires, however, it is imperative not to exceed the maximum system voltage of the module, 1000V.

One of the best configurations is to use 80 PV modules of 250W each, forming 4 rows connected in parallel, made of 20 modules each, connected in series. This array has its electrical specification exhibited in table 3.2.

In order to choose V_{BUS}, a compromise must be made. Its value must be greater than the maximum peak of utility grid voltage ($230V + 10\%$) at all times, so that power can be deliver into it, however, if much higher, the inverter will present greater losses and therefore a lower energy yield.

If too close to the RMS voltage of the grid, in case of a sudden voltage drop at the primary power source, it may cause the inverter control system not to adjust V_{BUS} fast

Nominal Power (W)	20 000
MPP Current (A)	33.36
MPP Voltage (V)	600.4
Open Circuit Voltage (V)	752
Short Circuit Current (A)	34.72

Table 3.2: 20kW PV Array Specifications

enough, clipping the output waveform. If equal or lower, the inverter wont be able to deliver power to it due to the neutral voltage difference.

Utility grid peak voltage: $(230 + 10\%) \cdot \sqrt{2} = 357.8V$
V_{BUS} chosen: $400V$

To achieve minimal losses, when the power output of the PV array is maximum, delivering an MPP voltage of 600.4V, the LLC Converter must operate in a region where its conversion losses are minimized. This happens when the operating frequency of the converter is the same as resonant tank and the voltage gain is unitary. Therefore, the turn ratio of the transformer should be:

$$n = \frac{Np}{Ns} = \frac{600.4}{400} \approx \frac{6}{4} = 1.5$$

- **Select the Quality Factor (Q)**

Looking at equation 3.2, it is possible to see that lowering the value of the Quality Factor (Q) will increase the maximum voltage gain of the resonant tank, but the same result can be obtained by lowering the Ratio of Total Primary Inductance to Resonant Inductance (m). Sometimes this can cause some conflict when tuning the parameters of the converter due to these two variables almost identical behavior. However, the Quality Factor (Q) should not be associated to the maximum voltage gain, since it describes how under-damped the resonator is. Thus, its value has a direct impact on the bandwidth of the resonant tank.

High values of Q will make the tank achieve its minimum gain using a narrower range of switching frequencies, which will make it harder to control. Low values of Q offer a wider range of switching frequencies for the same gain, allowing fine adjustments but presenting higher switching losses.

When establishing the maximum switching frequency first, changing the value of Q will determine the step-down behavior of the LLC converter and consequently the maximum input voltage supported by the circuit.

The maximum input voltage of the inverter was previously settled as 950V, which

demands a minimum voltage gain of:

$$Gain_{min} = \frac{V_{BUS} \cdot n}{Vin_{max}} \approx 0.6$$

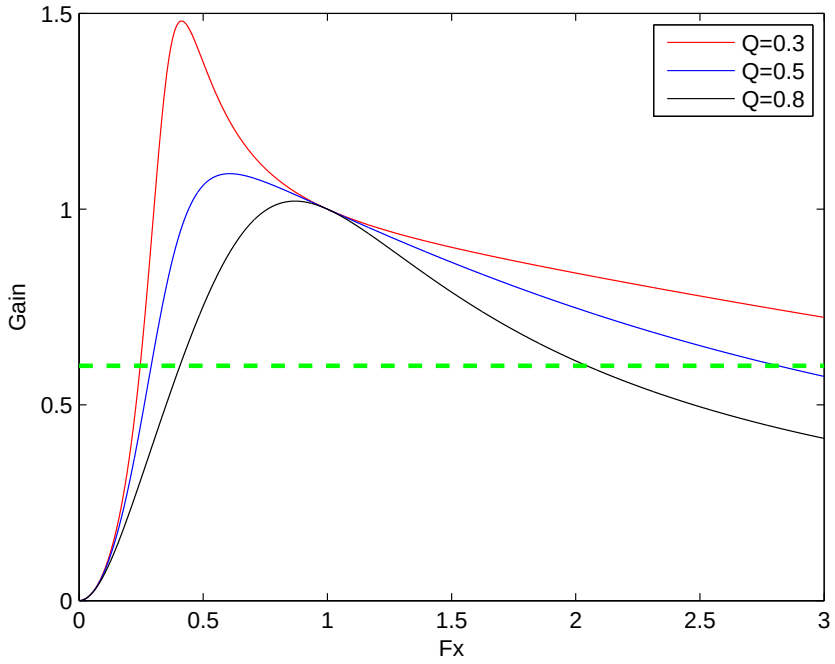

Figure 3.6: Different Q values

As illustrated on figure 3.6, a value around 0.5 should be a good choice for Q, considering a maximum value for the switching frequency of the tank a value around three times its resonant frequency, in order to keep switching losses low.

- **Select the Ratio of Total Primary Inductance to Resonant Inductance (m)**

Analogous to the Quality Factor, which settles the maximum input voltage of the converter, the Ratio of Total Primary Inductance to Resonant Inductance (m) settles its minimum input voltage, determined by the maximum voltage gain of the resonant tank.

A low m value sets a higher gain, as well as a more flexible regulation due to a narrower operating frequency range. A high m value sets a lower gain and a higher magnetizing inductance, which leads to a lower magnetizing current on the tank and, therefore, a more efficient power conversion.

As settled before, a voltage of $200V$ is a good value for the lower input voltage. It can compete with commercial products, giving the user a wide range of setups and power

sources. Calculating the gain:

$$Gain_{max} = \frac{DC_{BUS} \cdot n}{Vin_{min}} = 3$$

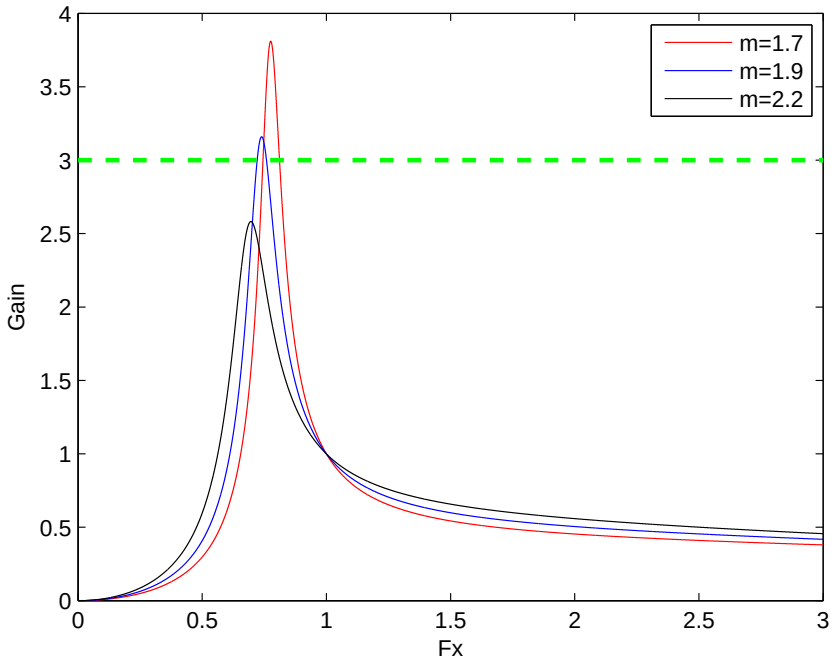

Figure 3.7: Different m values

As illustrated in figure 3.7, a value around 1.9 is a good choice for m.

- **Solve for the resonant component values**

Both values have a direct impact on the voltage gain of the resonant tank, and when choosing the first parameter, Q, the parameter m has to be randomly chosen in order to solve the equation. Thus, at this point, the parameters chosen previously might not offer the promised results.

In order to get the transfer function that delivers the maximum and minimum gains established previously, minor adjustments might be needed in both parameters. Solving the transfer equation of the tank, adjusting the Q and m values for 0.4 and 2.2 respectively, makes it possible to have an LLC Converter with a behavior that suits the electrical characteristics proposed for the resonant inverter, as illustrated by figure 3.8.

To obtain L_m, L_r and C_r solving the equations present in section 3.2.1, it is necessary to consider:

$$R_0 = \frac{230\ V_{RMS}^2}{20000\ W} = 2.645\ \Omega$$

$$fr = 100\ kHz$$

This resonant frequency was chosen due to its good compromise between switching losses and component cost.

Finally, solving the equations for $Q = 0.4$ and $m = 2.2$:

$$\begin{gathered} f_{min} = 68.8321E + 3\ (Hz) \\ L_m = 11.1461E - 6\ (H) \\ L_r = 9.2884E - 6\ (H) \\ C_r = 272.7077E - 9\ (F) \end{gathered}$$

Which result in the following voltage gain:

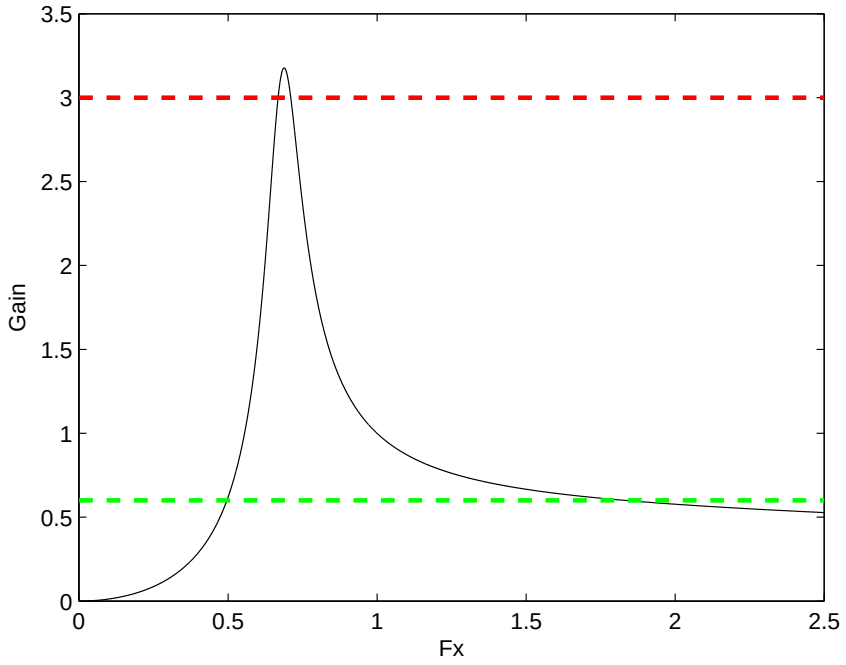

Figure 3.8: Designed LLC Tank Voltage Gain

3.2.3 Galvanic Isolation

Since ungrounded arrays started to become common, galvanic isolation is fading out from inverters, providing better energy yield and lighter equipment. Due to the lack of galvanic isolation on these new inverters, additional protection systems must be installed

in the circuit so that, in case of a malfunction, it interrupts the flowing current preventing a catastrophic event [30].

Since one the objectives of this dissertation is to, as future work, implement the designed inverter in real hardware and prove its conceptualization, in order to provide extra security, galvanic isolation will be added into the design. As a downside, this feature, delivered by the HF transformer T1 illustrated in figure 3.2, will decrease the overall efficiency of the equipment.

3.2.3.1 Core Selection

When designing a transformer, selecting the right core is essential in order to avoid losses and many related malfunctions. Mostly made of ferrite materials, a HF transformer core has many variables as size and material, each recommended for a certain scenario. If under-dimensioned, this part of the transformer may not handle all electromagnetic energy and saturate, causing the inductance of the coil to drop immediately. This event will increase the circulating current on the wiring and eventually damage the transformer and other components due to overheat.

When designing a HF power transformer, there are two methods to choose a ferrite core [31]:

Core Selection by Power Handling Capacity based upon the frequency of operation, circuit topology, flux and power required by the circuit, lists the most appropriated core in the Typical Power Handling Chart, partially presented in table 3.3.

Core Selection by WaAc Product, which can be explained by the power handling capacity of a transformer core by:

$$WaAc = \frac{P_o \cdot D_{cma}}{K_t \cdot B_{max} \cdot f} \tag{3.8}$$

Where:

P_o = Output Power
D_{cma} = Current Density
K_t = Topology Constant
B_{max} = Flux Density
f = Frequency of operation

Examples of topology constants (K_t):

Forward converter = 0.0005
Push-Pull = 0.001
Half-bridge = 0.0014
Full-bridge = 0.0014
Flyback = 0.00033 (single winding)
Flyback = 0.00025 (multiple winding)

Choosing the first method, and looking at the Typical Power Handling Chart, in part illustrated in figure 3.3, makes it possible to see that some of the listed cores can handle 20 kW at a frequency greater than the minimum frequency of operation of the LLC Converter, around 68.8 kHz. The E Core 49928 EE, U Cores 49330 UU, 49332 UU, 49920 UU, 49925 UI, 49925 UU and Toroid Cores 49725 TC and 49740 TC can be used in this inverter.

Power in Watts				Pot, RS, DS	E Cores	RM, PQ, EP	UU, UI, UR	ETD, EER, EC	EFD, Planar	Toroid
20 kHz	50 kHz	100kHz	250 kHz							
2	3	4	7	41811 RS DS PC	41205 EE 41707 EE	41313 EP 41812 RM 41912 RM			42107 EE 41805 EE	40907 TC 41406 TC 41303 TC 41435 TC 41304 TC 41206 TC 41506 TC 41407 TC 41405 TC 41305 TC
5	8	11	21	41814 PC 42311 RS DS HS	41808 EE	41717 EP 42013 RM 42016 PQ 42610 PQ			42019 EFD 42216 EI 43208 EI	41410 TC 41306 TC 41450 TC 41605 TC
...										
2800	4200	6500	12675				49316 UI 49316 UU		49938 EE	47325 TC 48613 TC 48625TC 48626 TC 49715 TC 49718 TC
11700	19000	26500	51500		49928 EE		49330 UU 49332 UU 49920 UU 49925 UI 49925 UU			49725 TC 49740 TC

Ferrite Core selection listed by typical Power Handling Capabilities (Chart is for Power Ferrite Materials, F, P, R, L and T, Push-Pull Square wave operation)

Wattage values shown above are for push-pull converter design. De-rate by a factor of 3 or4 for flyback. De-rate by a factor of 2 for feed-forward converter.
Example: For a feed-forward converter to be used at 300 watts select a core that is rated at 600 watts based on the converter topology.

Note: Assuming Core Loss to be Approximately 100 mW/cm³, B Levels Used in this Chart are:
@ 20 kHz - 200 mT, 2000 gauss; @ 50 kHz - 130 mT, 1300 gauss; @ 100 kHz - 90 mT, 900 gauss; @ 250 kHz - 70 mT, 700 gauss

Table 3.3: Part of the Typical Power Handling Chart, by Magnetics [32]

These results give three possible core shapes: E, U and Toroid. All have specific parameters such as core cost, winding cost, winding flexibility, heat dissipation, among others, that can make a geometry ideal in a certain situation but not so good at others

[33].

Toroids are the most economical core shape to produce. Since no bobbin is required, assembly costs are minimal and accessories are not needed. Shielding is good, not great. The very low stray magnetic fields achieved, small size and light weight make them ideal for constrained space applications.

E Cores have low core cost, low winding cost and a simple assembly process. Heat dissipation is very good but shielding is poor. This geometry is typically used in power applications like telecommunication inductors.

U Cores are excellent for high power transformation in tight spaces. Due to the shape of these cores, low leakage inductance and superior voltage isolation are possible. This along with an economical assembly make this shape ideal for high power density transformer applications.

(a) Toroid Core (b) E Core (c) U Core

Figure 3.9: Transformer Core Shapes

The larger space for winding, provided by the U Core, can make the winding of the transformer fit in a smaller casing, increasing the power density of the inverter, that combined with a better voltage isolation makes this shape a good choice for the prototype.

As listed on table 3.4, the cores, although having the same shape, have different specifications and can be made from multiple ferrite materials.

Looking at table 3.5, it is possible to see that F, P, K and R offer higher saturation flux densities, that associated to low core losses make these materials more suitable for high power/temperature scenarios. J and W, due to higher impedances, are more appropriate for broadband transformers and/or low level transformers.

0P49925UC has, compared to the cores listed, a small volume which can make the proposed resonant inverter smaller and lighter. Due to that, it is considered a good choice.

Part Number	Perm	Material	Shape	AL Inductance nH/T^2	OD / Length mm	ID / Leg Length mm	HT / Height mm	Le Path Length mm	Ae Cross Section mm^2	Ve Volume mm^3	WaAc
0P49330UC	2,500	P	U	7,219	93.0	76.0	30.0	354	840	297,000	
0P49332UC	2,500	P	U	7,700	93.0	76.0	32.0	353	905	319,000	
0P49925UC	2,500	P	U	4,920	102	57.1	25.4	308	645	199,000	975
0R49925UC	2,300	R	U	4,533	102	57.1	25.4	308	645	199,000	975
0P49920UC	2,500	P	U	3,572	126	91.0	20.0	480	560	268,800	221

Table 3.4: U Shapes Datasheet

		F	P	R	K	J	W +
μi(20)gauss)	25°C	3000	2500	2300	1500	5000	10,000
μp(2000 gauss)	100°C	4600	6500	6500	3500	5500	12,000
Saturation	25°C	4900	5000	5000	4600	4300	4300
Flux Density B_m Gauss	100°C	3700	3900	3700	3900	2500	2500
Core Loss (mw/cm³)	25°C	100	125	140			
(Typical)	60°C	180	80*	100			
@100 kHz, 1000 Gauss	100°C	225	125	70			

*@80°C +@10kHz

Table 3.5: Ferrite Power Materials Summary, by Magnetics [34]

3.2.3.2 Winding

The windings of a transformer are basically mutual inductors, and just like in any inductor the number of turns will influence the magnetic field generated and therefore the power delivered. This magnetic field is caused by a alternated current that demands a certain amount of copper in order not to overheat the metallic conductor.

These are two very important parameters when designing a transformer that, when miscalculated can cause the transformer not to work properly due to magnetic and/or conduction losses, core saturation or overheat (it is to take in account that the ferrite properties are temperature dependent).

- **Number of Turns**

With the ferrite core previously chosen, primary and secondary turns can be calculated by [31]:

$$N_p = \frac{V_p \cdot 10^8}{4 \cdot B \cdot A_c \cdot f} = 24.61 \tag{3.9}$$

$$N_s = \frac{V_s}{V_p} \cdot N_p = 16.41 \tag{3.10}$$

Where:

V_p = Primary Voltage ($600V$)
B = Flux level, figure 3.10
A_c = Core Cross Section ($6.45cm^2$)
f = LLC Converter Minimum Frequency of Operation

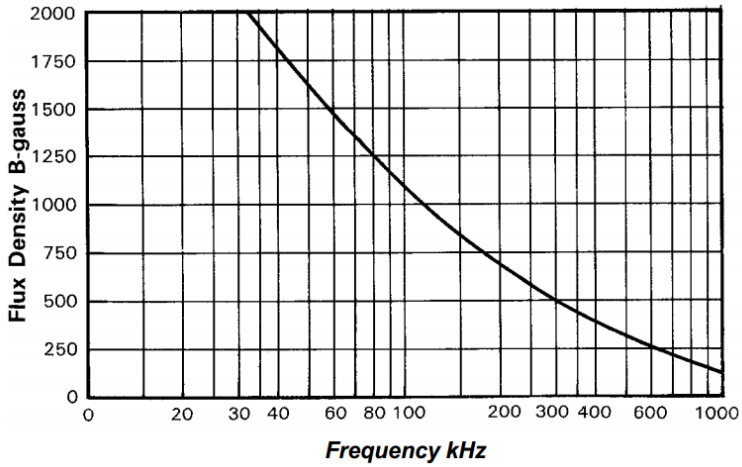

Figure 3.10: Flux Levels for MAGNETICS "P" ferrite material necessary to maintain constant $100mW/cm^3$ core losses at various frequencies [34]

Unlike many other switching converters, the LLC converter has a variable operating frequency. To be sure that the HF transformer can handle the worst case scenario, the number of turns must be calculated using its minimum operating frequency. At this frequency, magnetic flux levels achieve a maximum value and the core must not saturate in order to avoid overheating.

- **Wire Section**

This parameter can be calculated by the winding area of the ferrite core, W_a, divided by the primary and secondary windings, that together fill this space.

$$K \cdot W_a = N_p \cdot A_{wp} + 2 \cdot N_s \cdot A_{ws} \tag{3.11}$$

Where:

K = Filling Factor (around 0.4 for Toroids and 0.6 for E,U,I and Pot Cores)
W_a = Core Winding Area ($31.7mm \cdot 50.8mm = 1610.4mm^2$)
N_p = Primary Number of Turns
A_{wp} = Primary Wire Area
N_s = Secondary Number of Turns
A_{ws} = Secondary Wire Area

In this case the secondary winding is multiplied by a factor of 2 due the center-tapped topology of the transformer. This 1:1+1 configuration makes rectification easier due to the use of half of the diodes of a full-bridge rectifier. On a 1:1 configuration, a full-bridge rectifier would be mandatory.

Solving the equation 3.11:

$$A_{wp} = 20.1mm^2$$
$$A_{ws} = 15.1mm^2$$

Such wire section cannot be accomplished using a single copper wire due to the frequency of operation of the LLC converter. Looking at table 3.6, a wire with a section of these dimensions has a recommended maximum frequency around 700 Hz due to a phenomenon called Skin Effect.

Using Wolfram CDF Player with Skin Effects in Straight Wires [36], it is possible to see that operating at the LLC resonant frequency, most of the section of a 6mm diameter wire would have a current density around zero. All of the current would circulate near its surface, creating huge current density in that area. This would make the wire to overheat causing its isolation to melt, short circuiting the winding.

Looking again at the American Wire Gauge (AWG) table, for an operation frequency of 100kHz, it is recommended the AWG 26 wire, which has a diameter of 0.4mm. When performing the simulation using this wire, the current density appears to be uniform, as expected. Both results are illustrated in figure 3.11.

So, instead of using one wire with a section of $20.1mm^2$ of diameter, multiple wires with smaller wire section can be used in parallel. This is the principle behind Litz wire, which makes it possible to use high currents at high frequencies. Using Litz wire it is possible to achieve less conduction losses and therefore higher power efficiency in the HF [37].

AWG	Diameter [mm]	Area [mm^2]	Resistance [Ohms / km]	Max Current [Amperes]	Max Frequency for 100% skin depth
2	6.54304	33.6	0.512664	94	410 Hz
3	5.82676	26.7	0.64616	75	500 Hz
4	5.18922	21.2	0.81508	60	650 Hz
5	4.62026	16.8	1.027624	47	810 Hz
6	4.1148	13.3	1.295928	37	1100 Hz
24	0.51054	0.205	84.1976	0.577	68 kHz
25	0.45466	0.162	106.1736	0.457	85 kHz
26	0.40386	0.129	133.8568	0.361	107 kHz
27	0.36068	0.102	168.8216	0.288	130 kHz
28	0.32004	0.081	212.872	0.226	170 kHz
29	0.28702	0.0642	268.4024	0.182	210 kHz

Table 3.6: AWG Sizes and Current Limits [35]

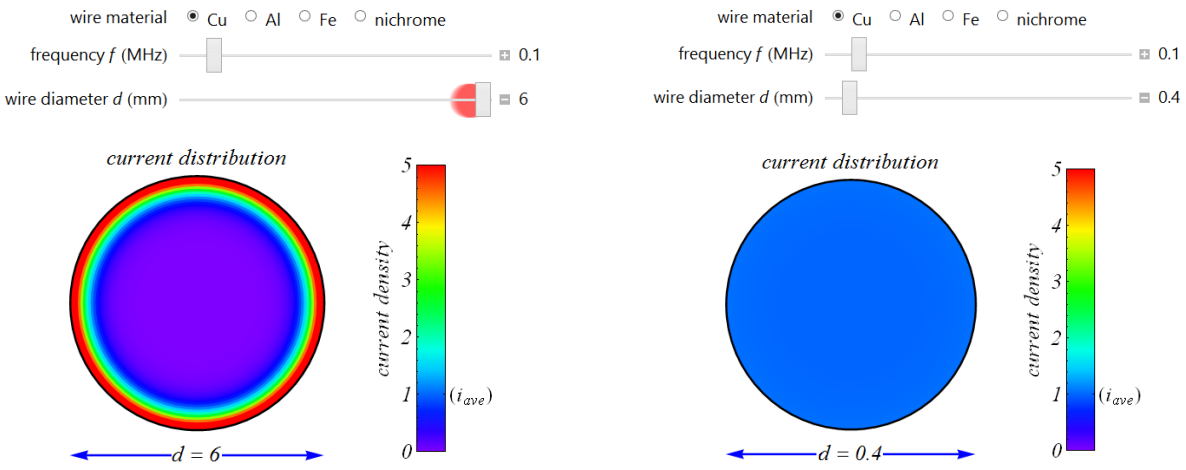

(a) 6mm Diameter Wire

(b) 0.4mm Diameter Wire

Figure 3.11: Skin Effect Examples at LLC Resonant Frequency, 100kHz

3.2.4 Rectification

Connected to the HF transformer, the diodes $D5$ and $D6$ rectify the square wave formed by the full-bridge, charging C1 that will create a DC voltage, V_{BUS}.

These rectifiers operate at the switching frequency of the LLC converter, from around 70kHz to 200kHz, and the current across each component can be calculated as half of the output current of the inverter, plus some losses. In power switching, silicon rectifiers have considerable switching losses due to large reverse recovery time, as illustrated in figure 2.22. In order to solve this problem Silicon Carbide, or SiC, rectifiers can be used in the circuit.

SiC Schottky diodes have almost no reverse recovery time, are a good option when trying to minimize switching losses and are available for the voltage levels proposed in this design. Using GeneSiC® GB50SLT12-247 Silicon Carbide Power Schottky Diode, forward voltages can be as low as $1.5V$ at 25ºC, reaching a maximum value of $3.0V$ at 175ºC [38].

Thus, the conduction losses on the diodes can be expressed by:

$$V_f \cdot I_f = 3.0 \cdot \frac{20000\ W}{230\ V} = 260.9\ W$$

Representing just 1.30% of the output power operating at the worst case scenario (175ºC), the conduction losses on rectification have a very acceptable value.

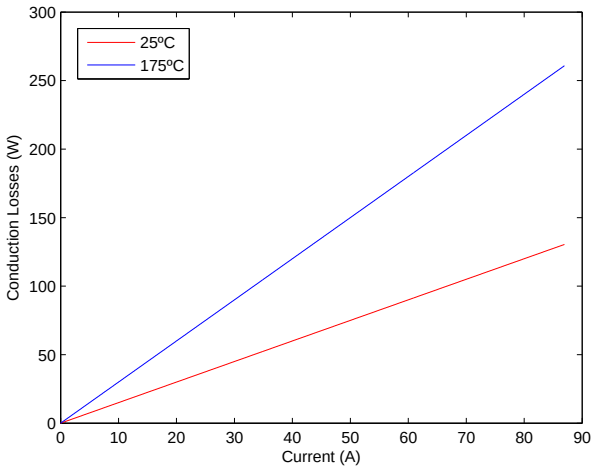

Figure 3.12: GeneSiC® GB50SLT12-247 Conduction Losses

In figure 3.12 it is possible to see a calculation of the GeneSiC® GB50SLT12-247 conduction losses based on its datasheet, where forward voltages are presented for two temperatures of operation.

This diode was chosen due to its electrical specifications, needed to accommodate the high voltages, high currents and high switching frequency that can be found at the DC-DC converter.

3.3 H-Bridge Converter

As stated in section 2.3.3, this H-Bridge Converter shapes the V_{BUS} DC voltage, provided by the DC-DC Converter, into an AC waveform. In the presence of a control system, fully explained in the next chapter, this H-Bridge Converter will give the proposed inverter a stable output waveform, even with load variations or topology variations (off-grid, on-grid or self-comsuption).

In terms of electrical design, this bridge is an exact replica of the bridge used on the LLC Converter, however instead of soft-switching, hard-switching is used here and consequently more switching losses are expected.

These switching losses occur during the rise and fall time of the transistors, where V_{DS} times I_{DS}, the power dissipated by the transistor, is greater than zero, as illustrated in figure 3.13.

It is easy to understand that these peaks of dissipated power are proportional to the switching frequency of the transistor. Thus, a compromise must be established in terms of the frequency of operation:

- If too high the bridge can be very inefficient due to switching losses.
- If too low the output filter must have a low cut-off frequency which will demand larger and more expensive inductors and capacitors.

A value around 30 kHz is acceptable for the switching frequency of this bridge since it is high enough to allow a small output filter, but not so high that causes switching losses to be noticeable. It is also above the audible range, thus no noise is expected to be generated.

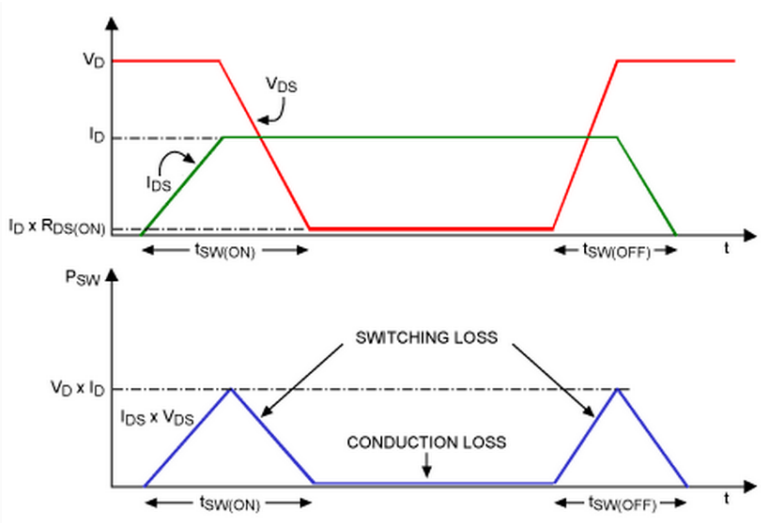

Figure 3.13: Transistor Losses

3.4 Output Filter

The output filter of the proposed inverter attenuates voltage/current ripples caused by the high frequency H-Bridge Converter, smoothing its output voltage/current waveform. Due to the high frequencies used in switching, compared to the AC waveform generated, low pass filters should be used.

As seen in section 2.3.4, the greater the order of the filter, the greater the attenuation provided. However, more complex filters like the LCL filter, can cause steady state and transient problems due to resonance [39], have a greater cost due to the price of the components and require a more complex control system. Therefore, it was decided that the LC filter offers the best price/performance, having its transfer function given by:

$$H(s) = \frac{\frac{1}{LC}}{s^2 + s\frac{1}{R_l C} + \frac{1}{LC}} \tag{3.12}$$

Where:

$$R_l = \frac{230\ V_{rms}^2}{20000\ W}$$

Which can be related to a second order network in the standard form:

$$H(s) = \frac{A}{s^2 + s\frac{\omega_0}{Q} + \omega_0^2} \tag{3.13}$$

Where, knowing the gain of the filter (A), the cutoff frequency (ω_0) and the Q-factor (Q) can be extracted, :

$$\omega_0 = \frac{1}{\sqrt{LC}} \tag{3.14}$$

$$Q = R_l\sqrt{\frac{C}{L}} \tag{3.15}$$

The cut-off frequency of this filter is inversely proportional to its ripple rejection cost, signal delay and consequently control system complexity. A value greater, or equal, than ten times the frequency of utility grid can be considered a good choice [40].

The Q-factor expresses the damping of the LC filter, as illustrated in figure 3.14. If too low, the circuit may have high frequency losses; if too high, peaking can occur. The ideal value for this parameter is 0.707 due to its response, which does not attenuates pass-band frequencies, neither amplifies stop-band frequencies.

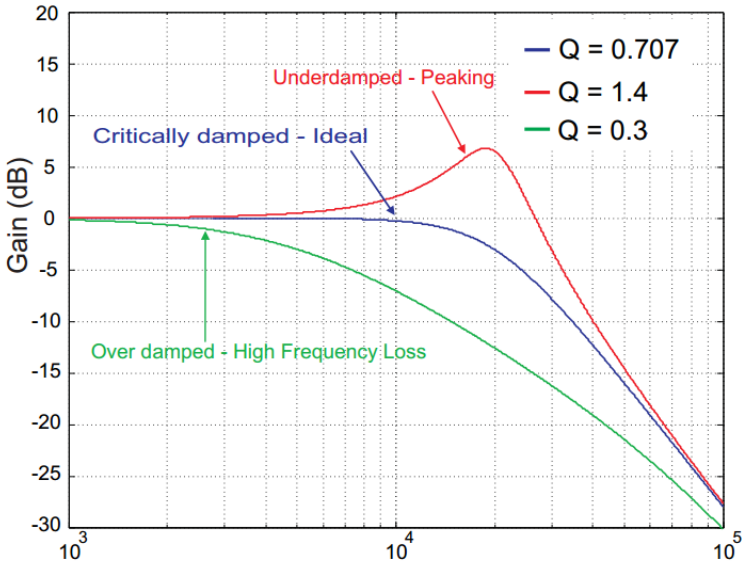

Figure 3.14: Q-Factor Examples

In order to get the values for the L and C components that compose the filter, a system of equations can be built using the two previous parameters:

$$\begin{cases} \dfrac{1}{2\pi\sqrt{LC}} = \dfrac{\omega_0}{2\pi} = 1\ kHz \\ \\ R_l\sqrt{\dfrac{C}{L}} = Q = 0.707 \end{cases}$$

Solving for L and C:

$$\begin{cases} L = 5.9542\ E-04\ (H) \\ \\ C = 4.2542\ E-05\ (F) \end{cases}$$

Using these values it is possible to plot the Bode Diagram of the filter, illustrated in figure 3.15.

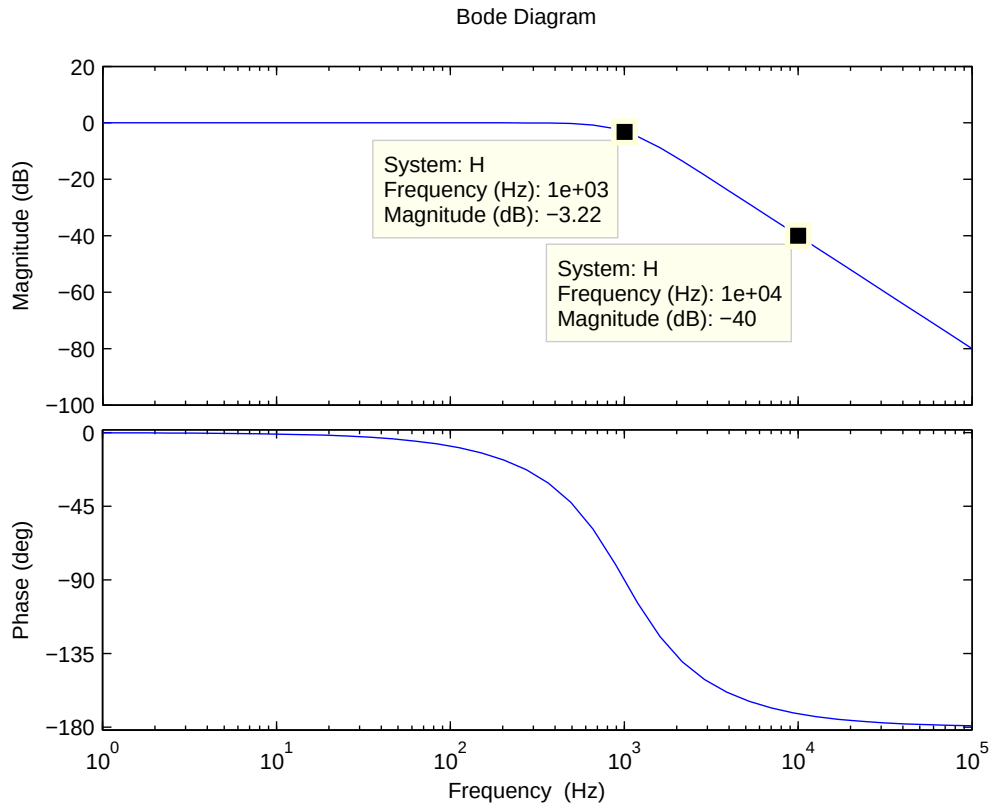

Figure 3.15: Designed LC Filter Bode Diagram

As it is possible to see, the results obtained show a critically damped behavior, a cutoff frequency at 1 kHz and an attenuation of -40 dB's at 10 kHz, all as expected.

Later in this dissertation, the behavior of the output filter will be simulated and evaluated.

Chapter 4

Control System Design

4.1 Introduction

The use of switching converters greatly improves the energy yield and power density of an electronic circuit, however, they often require a more complex system design. Besides the inductors and capacitors, a digital control system is often implemented in order to generate the control signals that drive the transistors, which are responsible for the switching architecture.

In simpler converters, a feedback loop composed by basic electronic components might be sufficient, however, when the hardware used has the complexity level of the circuits designed in the previous chapter, a more complex and robust control system is mandatory.

The proposed power inverter, as seen in chapter 3, has a wide input voltage range in order to allow the use of multiple power sources, each with different electrical specifications. Even so, a variable input voltage or load changes must not affect its output waveform.

Thus, in this chapter will be designed a control system for the proposed inverter using multiple control algorithms and a Real-Time Operating System (RTOS). This will assure a flexible and stable power conversion.

The organization of this chapter is as follows:

- **Section 4.2** introduces a Real Time Operating System (RTOS) for multi threaded control systems.
- **Section 4.3** describes the control system design and the control algorithms used.

4.2 FreeRTOS

When an algorithm is simply uploaded to a microprocessor, its execution may be queued by hardware interrupts, which can occur at any moment. In control systems that require precise time intervals between adjustments, such delays cannot be tolerated. In order to solve this problem FreeRTOS can be used.

FreeRTOS is an open source RTOS, or real-time kernel for embedded systems, allowing a certain number of tasks to be executed as independent threads and different priorities, always meeting their real time requirements. Queues, binary counting semaphores and mutexes can also be implemented [41].

Using a kernel greatly improves code modularity, development or/and testing, maintainability/extensibility, abstraction of timing information, and flexible interrupt handling. A small memory footprint, low overhead, very fast execution and a tick-less option available for low power applications, make FreeRTOS a very popular solution in embedded systems design.

4.2.1 Task Creation and Deletion

A task can be created calling the FreeRTOS function xTaskCreate(). Its input arguments are: a pointer to the function where the task is implemented; the name of the task; length of the stack used; a pointer to the arguments given by the task; a priority value; and a pointer to an identifier that allows to handle the task.

```
BaseType_t xTaskCreate (TaskFunction_t pvTaskCode, const
  ↪ char * const pcName, unsigned short usStackDepth,
  ↪ void *pvParameters, UBaseType_t uxPriority,
  ↪ TaskHandle_t *pvCreatedTask)
```

To delete a task, the function vTaskDelete() can be called using the pointer to it.

```
void vTaskDelete( TaskHandle_t xTask );
```

4.2.2 Scheduling

Once a task is created, it is ready to be executed when the kernel decides so. In order to do this, a constant time spaced events, or ticks, are implemented in FreeRTOS.

When a tick interrupt occurs, the task being executed is suspended, and the kernel chooses, based on a priority system, which task should be resumed. A method to avoid starvation, a phenomenon where a low priority task is never executed, must be implemented by the user, if necessary.

Figures 4.2 and 4.1 clearly illustrate task switching methodology and task life cycle in FreeRTOS, respectively.

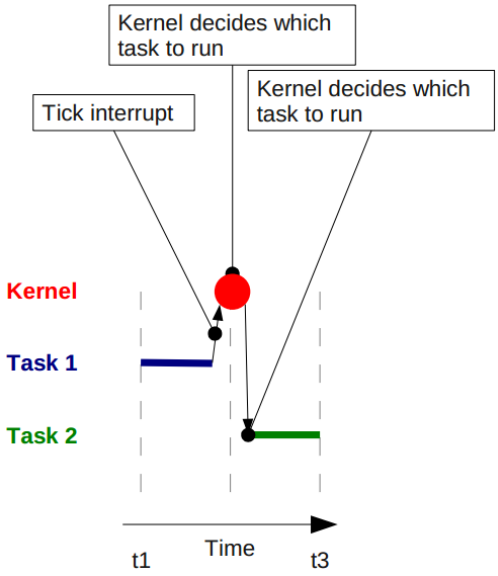

Figure 4.1: Task Change in FreeRTOS

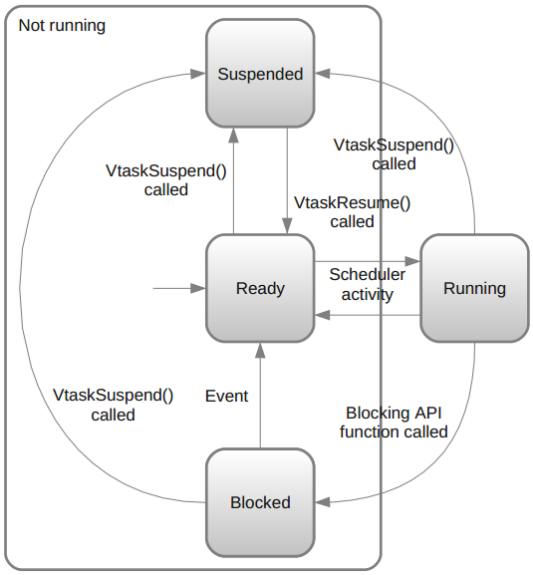

Figure 4.2: Task Life Cycle in FreeRTOS

4.3 Control Algorithms

As important as the hardware, the control algorithms will establish the stability, flexibility and even power efficiency of the proposed inverter.

Control algorithms can be found in many embedded systems and, besides the number of different possible approaches, most can be represented by a closed loop, as figure 4.3 illustrates.

The purpose of a control algorithm is to get a parameter of the physical system, such as voltage, water flow, or power thrust, as close as possible to a reference value. This reference can be given as an input to the controller or it can be computed by it using a mathematical equation.

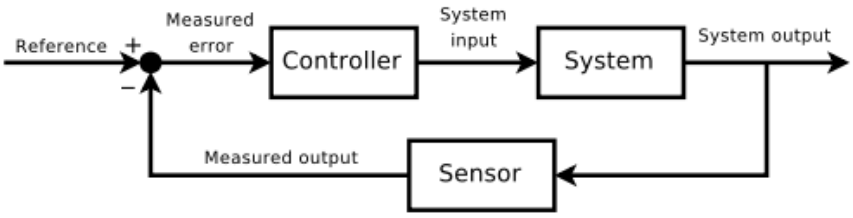

Figure 4.3: Negative Feedback Closed Loop Control

In order to get a stable output waveform from the proposed inverter, even with a variable input voltage and multiple output topologies (fully explained in chapter 5), multiple control threads need to be running at the same time:

- The **MPPT Controller** will be responsible for maximizing power delivered by the primary power source, increasing the energy efficiency of the overall system.
- The **The PID Controller** will control the LLC Converter, designed in section 3.2. This will allow the converter to have a stable output voltage, V_{BUS}, even with a variable input voltage.
- **The RST Controller** will control the H-Bridge Converter, designed in section 3.3. This will allow the proposed inverter to have a stable output waveform.

4.3.1 MPPT Controller

The overall performance of a power inverter can be influenced by its hardware and software. In this section it will be explained how software can make an inverter maximize the power generated by a renewable source. This will increase the output power of the system, making the device more productive and its use more lucrative.

As seen in section 2.2.1.1 and 2.2.2.1, it is possible to track the MPP of a certain power source by adjusting its output current, or in other words, adjusting the load connected to it. Using this concept, a simple MPPT algorithm will be designed in the next section.

4.3.1.1 MPPT Algorithm Design

Remembering the typical I/V curves of the renewable energy sources discussed earlier in this dissertation, it is possible to choose two different starting points for the algorithm: the short-circuit or the open-circuit topology. These two possibilities represent the extremities of the V/I curves.

The hardware of the proposed inverter was designed to tolerate the open-circuit voltage of a typical 20kW PV array, whose electrical specification can be found in table 3.2. Thus, choosing this topology for a starting point will avoid conduction losses caused by large short-circuit currents.

After established the open-circuit starting point, the inverter connected to the power source may start increasing gradually its power production, which will also increase its input current. After some iterations, the power delivered by the source will decrease meaning that the MPP was reached. The inverter should now decrease its output power in order to operate at the MPP of the source, maximizing the power delivered by the system.

Based on this idea, it is possible to design with a simple MPPT algorithm:

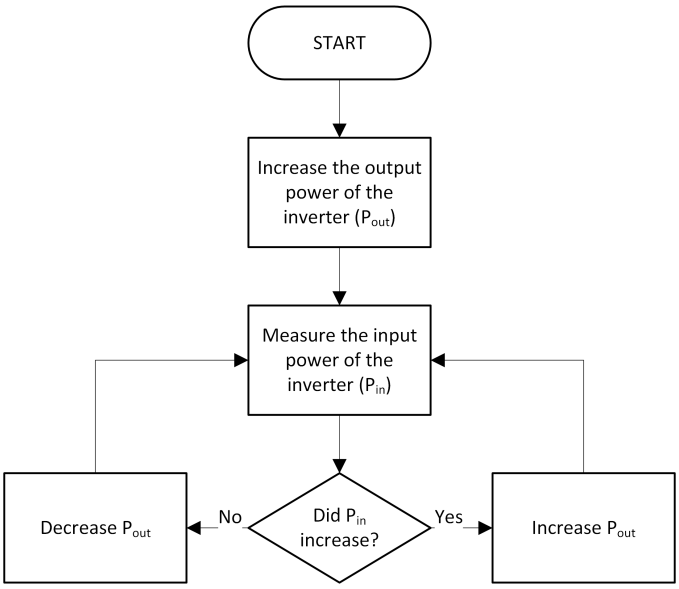

Figure 4.4: MPPT Algorithm

At the end of each control iteration, the output parameter of this algorithm (the output power of the inverter) will be used as a reference value by the RST Controller, which will be explained later.

4.3.2 PID Controller

The Proportional Integrative Derivative (PID) algorithm is one of the most used control algorithms in the world. Due to its performance, simplicity and range of application, it is implemented since it was designed for automatic ship steering [42].

As the name implies, this algorithm consists of minimizing the difference between a system parameter and a theoretical reference using a proportional term, an integral term and a derivative term.

The Proportional Term is simply the result of a constant value, the proportional gain, Kp, multiplied by the error. The higher the constant value, the greater the changes in the control signal.

The Integral Term is given by the integral of the error, multiplied by a gain, Ki. This means that while the error is not zero, the absolute value of the control signal will increase making the steady state error, theoretically, zero.

The Derivative Term is responsible for calculating the slope of error over time and multiplying this value by a gain, Kd. This helps predicting the behavior of the system, however, in systems affected by noise, noise amplification can occur, which will corrupt the control signal. Filters can be used to solve this problem but they will add a delay to the

controller, which can lead to instability. Due to this, many PID controllers are just PI.

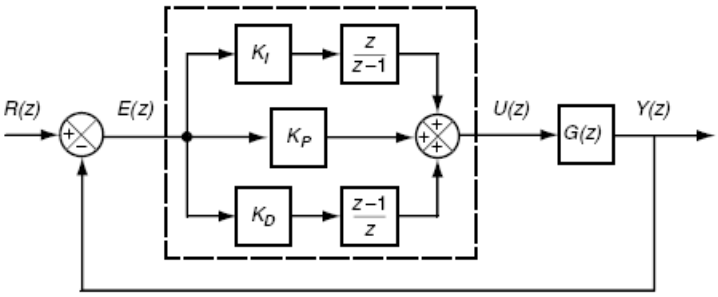

Figure 4.5: Feedback loop with PID control [43]

A low overshoot, fast rise time and fast settling time are the characteristics of a system response when controlled by a well tuned PID algorithm. These attributes are a direct consequence of the values chosen for the three gains of the controller, as shown on table 4.1:

Gain	Rise Time	Overshoot	Settling Time	Steady-State Error
Kp	Decrease	Increase	N/D	Decrease
Ki	Decrease	Increase	Increase	Eliminate
Kd	N/D	Decrease	Decrease	N/D

Table 4.1: PID Controller Gains Influence on Output [44]

In order to choose the right values for these three parameters, a mathematical model of the system must be calculated. After that, multiple tunning methods (Ziegler–Nichols Method, Cohen–Coon Method, Step-Response Method or Manual Tunning Method are a few examples) can be used to tune those parameters.

4.3.2.1 LLC Converter Controller Design

The simple operation principle of the LLC Converter, in which to get an higher output voltage its switching frequency must be lowered, and vice-versa, along with the fact that instant load variations do not affect instantly the converter thanks to its large filtering capacitor, makes a simple control algorithm like the PID good enough for its control system.

The control algorithm will take advantage of the voltage gain provided by the resonant tank and adjust the switching frequency of the converter, making V_{BUS} as stable as possible, even with a fluctuating input voltage.

In order to design the controller it is essential to have a good mathematical model of the LLC Converter. The more accurate the model, the better the controlled system will

behave. In a PID control algorithm the parameters K_p, K_i, K_d and sample frequency (f_s) must be calculated based on this identification process.

Using a simulation software, fully detailed in chapter 6, the LLC Converter circuit, illustrated in figure 4.6 was simulated in order to get its step response.

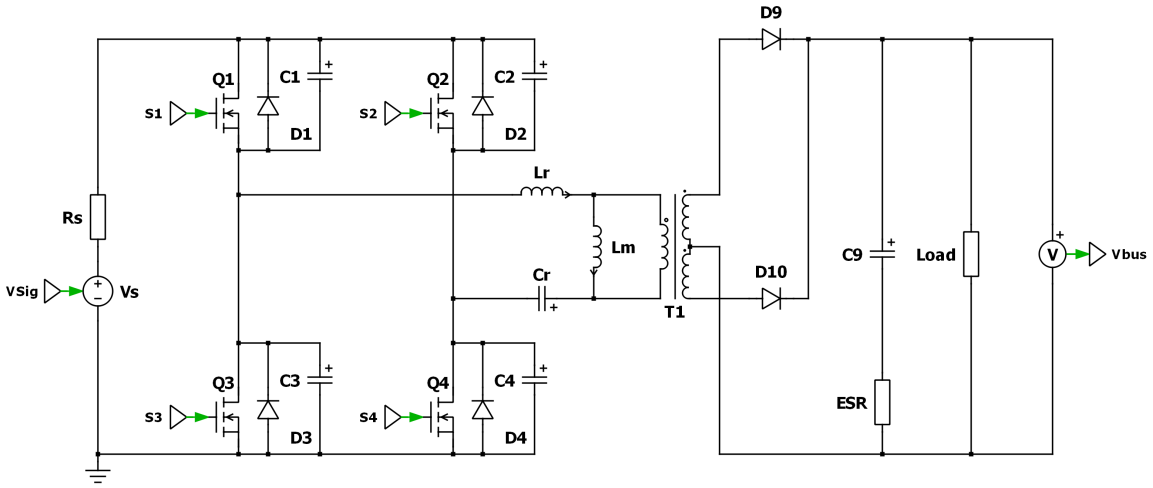

Figure 4.6: LLC Converter Electrical Circuit

The following parameters where used:

$$V_s = 600\ V \qquad \text{Source Voltage}$$

$$f_{sw} = 100\ kHz \qquad \text{Switching Frequency}$$

$$Load = \frac{V_{BUS}^2}{P_{inverter}} = \frac{400^2}{20000} \qquad \text{Load Resistor}$$

The step response of the system is illustrated in figure 4.7-a). As it is possible to see, the transient system output is corrupted with noise, which will certainly compromise the performance of the control system. When analyzing this perturbation in figure 4.7-b) it is clear that its frequency and the switching frequency are the same. Since the output of the purposed control system will be the switching frequency of this circuit, making it a known value to the controller, a filter can be applied.

This can be done by oversampling V_{bus} and applying a mean to the obtained values during a time interval proportional to the tank operating frequency.

After applying this filter in the same simulation software used to get the step response of the converter, a much cleaner V_{bus} signal was achieved. As shown in figure 4.7-c), the simulated system has no overshoot and therefore, can be modeled as a first order system. No dead-time was visible either.

To improve the mathematical model of the system, multiple input signals with the same output power and voltage were applied to the circuit, resulting on table 4.2.

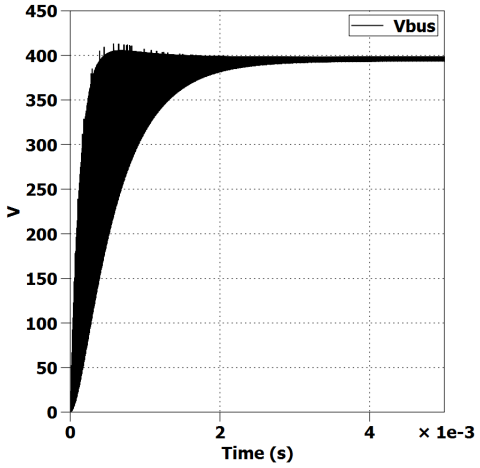

(a) V_{bus}

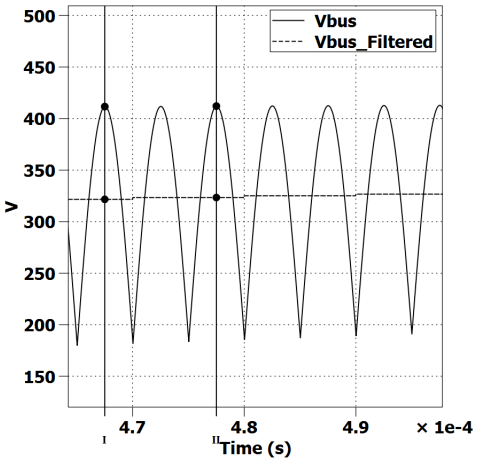

(b) V_{bus} noise frequency

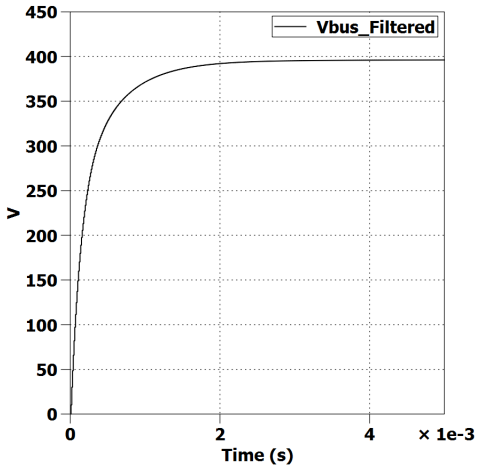

(c) Filtered V_{bus}

Figure 4.7: V_{bus} Filtering

The mathematical model of this first order system can be expressed by the Laplace equation [45]:

$$G(s) = \frac{K}{\tau s + 1} \tag{4.1}$$

Where K is the gain of the system, and τ is the time constant of the system. Finding these parameters makes it possible to automatically set the sample frequency, which can be calculated dividing the minimum rise time (t_r) of the system from 4 to 10 divisions [46]. Choosing 10 divisions:

f_{sw} **(kHz)**	t_r**(s)**	$\tau(s)$
68.83	0.114265	0.049522
85	0.011990	0.007558
100	0.000671	0.000234
125	0.009482	0.004930
150	0.015607	0.008301

Table 4.2: LLC Converter Parameter Identification

$$fs_{PID} = \frac{1}{\frac{0.671\ ms}{10}} = 14.903\ kHz \tag{4.2}$$

At this point, using the equation 4.1 it is possible to create a first order system in MATLAB® with the same behavior as the LLC Converter. The MATLAB® PID tuning algorithm "pidtune" [47] was used to tune the parameters of the PID Controller, which returned:

$$K_p = 0.00763$$
$$K_i = 254.003$$
$$K_d = 1.142\ E-7$$

Using the following control equation makes it possible to have a PID control system for the LLC Converter:

$$u_c(k) = K_p \cdot e(k) + K_i \cdot T_s \cdot \sum_{0}^{k} e(k) + \frac{K_d}{T_s}\left[e(k) - e(k-1)\right] \tag{4.3}$$

Where e is the error of the output signal and T_s is the sample period of the controller.

The value of $u_c(k)$ can now be used to establish the frequency of a square wave control signal which will drive the transistors of the LLC Converter. In the next chapter, the behavior of the PID control algorithm will be discussed and evaluated .

4.3.3 RST Controller

Introduced in 1976 and based on the classic control theory, the purpose of this controller is to obtain a closed loop system with premeditated poles and consequently a premeditated system behavior.

Its control algorithm will control the H-Bridge Converter, designed in section 3.3, which will generate the sinusoidal output waveform of the proposed inverter.

The control function can be represented by [46]:

$$R(q) \cdot u(k) = T(q) \cdot u_c(k) - S(q) \cdot y(k) \tag{4.4}$$

Where:

$y(k)$ = system output
$u(k)$ = control signal
$u_c(k)$ = reference signal
$deg(R(q)) \geq deg(T(q))$ and $deg(R(q)) \geq deg(S(q))$, for causality.

Simplified, the equation can be translated into the block diagram illustrated in figure 4.8. R and S are designed to achieve regulation performance and T to achieve tracking performance. All these are polynomials, which can be described by:

$$R(q) = r_0 \cdot q^{n_r} + r_1 \cdot q^{n_{r-1}} + r_2 \cdot q^{n_{r-2}} + \cdots + r_{n_r} \tag{4.5}$$
$$S(q) = s_0 \cdot q^{n_s} + s_1 \cdot q^{n_{s-1}} + s_2 \cdot q^{n_{s-2}} + \cdots + s_{n_s} \tag{4.6}$$
$$T(q) = t_0 \cdot q^{n_t} + t_1 \cdot q^{n_{t-1}} + t_2 \cdot q^{n_{t-2}} + \cdots + t_{n_t} \tag{4.7}$$

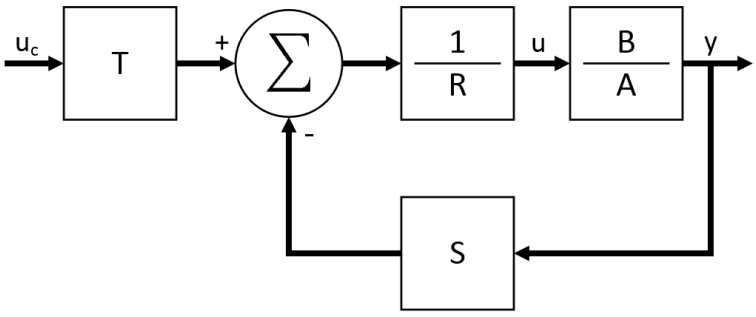

Figure 4.8: RST Controller Block Diagram

This architecture makes the closed loop poles of the system to be the singularities of $AR+BS$ and closed loop zeros to be the singularities of B and T, as expressed in equation 4.8.

$$\frac{BT}{AR + BS} = \frac{B_m}{A_m} \tag{4.8}$$

However, $AR + BS = Am$ may not lead to a single solution due to the polynomials orders. This can be solved by introducing an auxiliary polynomial observer A_{obs} and making:

$$AR + BS = A_{obs} \cdot A_m \tag{4.9}$$

In order to keep the dynamics of the system, T has to be defined by:

$$T = \frac{A_{obs} \cdot B_m}{B} \tag{4.10}$$

What makes:

$$y = \frac{B \cdot T}{A_{obs} \cdot A_m} = \frac{B_m}{A_m} \cdot u_c \tag{4.11}$$

In a situation where the open loop system has some noise associated to it, the following expression can be applied:

$$A \cdot y = B \cdot u + \xi \tag{4.12}$$

Looking at equation 4.4, the output would be:

$$y = \frac{B_m}{A_m} \cdot u_c + \frac{R}{A_{obs} + A_m} \cdot \xi \tag{4.13}$$

What clearly shows that A_{obs} establishes the system response to outside perturbations. This require its dynamics to be faster than A_m, however, if too fast the control signal may oscillate, if too slow the response to noise can be degraded.

Choosing $deg(R) = deg(S) = deg(A)$, the order of A_{obs} can be obtained by:

$$deg(A_{obs}) = 2 \cdot deg(A) - deg(A_m) \tag{4.14}$$

To achieve a null stationary error, it is necessary to introduce an integral term, which in this case is associated to the digital filter R:

$$R = (q - 1) \cdot R_1 \tag{4.15}$$

This modification can be introduced in equation 4.9, that becomes:

$$A \cdot R_1(q-1) + BS = A_{obs} \cdot A_m \tag{4.16}$$

Finally, the coefficients $R(q)$ and $S(q)$, from equation 4.4, can be found by solving equation 4.16, usually called Diophantine Equation.

For a first order system, and knowing the polynomials [46]:

$$\begin{aligned} A &= A(q) = q - a \\ B &= B(q) = b \\ A_m &= A_m(q) = q - a_m \\ A_{obs} &= A_0(q) = q - a_o \\ R &= R(q) = q - 1 \\ S &= S(q) = qs_0 + s_1 \end{aligned}$$

The following Diophantine Equation is obtained:

$$(q-a)(q-1) + b(qs_0 + s_1) = (q - a_m)(q - a_{0)}) \tag{4.17}$$

Solving in order to the last unknown coefficients:

$$s_0 = \frac{1 + a - a_m - a_0}{b} \tag{4.18}$$

$$s_1 = \frac{a_m a_0 - a}{b} \tag{4.19}$$

For a second order system, the approach is the same, except the polynomials are an order greater [46]:

$$r_1 = P_0 - b_1 s_0 \tag{4.20}$$

$$s_0 = -\frac{P_1 + b_1 s_1}{P_2} \tag{4.21}$$

$$s_1 = -\frac{b_1(P_5 P_2 - P_1 a_2 b_1) + b_2 P_6}{b_2(P_4 b_1 - P_2 b_2) - a_2 b_1^3} \tag{4.22}$$

$$s_2 = \frac{P_6 + (P_4 b_1 - P_2 b_2) s_1}{P_2 b_1} \tag{4.23}$$

Where:

$$\begin{aligned}
P_0 &= a_{m1} + a_{obs1} + 1 - a_1 \\
P_1 &= a_2 + a_1 P_0 - a_{m1} - a_{m2} - a_{obs2} - a_{obs1}(1 + a_{m1}) - 1 \\
P_2 &= b_1(1 - a_1) + b_2 \\
P_3 &= a_2(P_0 - 1) - a_1 P_0 - a_{m1} a_{obs2} - a_{m2} a_{obs1} \\
P_4 &= b_1(a_1 - a_2) \\
P_5 &= -a_2 P_0 - a_{m2} a_{obs2} \\
P_6 &= -P_3 P_2 + P_4 P_1
\end{aligned}$$

And where b_1/a_1 and b_2/a_2 are the zeros/poles of the open loop system, b_{m1}/a_{m1} and b_{m2}/a_{m2} are the zeros/poles of the closed loop system and b_{obs1}/a_{obs1} and b_{obs2}/a_{obs2} are the zeros/poles of the observing system.

On the next section, an identification method responsible for estimating b_1/a_1 and b_2/a_2, which most of the times have unknown values, will be discussed.

4.3.3.1 Recursive Least Squares (RLS)

The Recursive Least Squares (RLS) is a system identification method that can be integrated in the RST control algorithm, in order to adjust the mathematical model of the physical system, iteration after iteration. This will allow the controller to adjust its behavior over time, accommodating system variations without loosing accuracy.

In control theory, system identification is one of the most important aspects when designing a good controller. It helps predicting the response of a system when applied a

certain input signal, but more important than that, it is crucial when choosing an appropriate control strategy.

Most of the times, an early system identification is performed to set the parameters of the controller, which remains constant during the control process. However, this analyses can be performed systematically, comparing the output of the mathematical model $\hat{y}$ to the real system output y. The estimation error, ε, can then be used to upgrade the mathematical model.

Invented by Karl Friedrich Gauss, the Least Squares (LS) method represents a linear and noise free system by the following equation:

$$y(k) = \varphi_1(k)\theta_1 + \varphi_2(k)\theta_2 + \cdots + \varphi_n(k)\theta_n \tag{4.24}$$

or:

$$y(k) = \varphi^T(k)\theta \tag{4.25}$$

where vectors $\boldsymbol{\varphi}(k)$ and $\boldsymbol{\theta}$ can be represented as:

$$\boldsymbol{\varphi}(k) = [\varphi_1(k)\ \varphi_2(k)\ \cdots\ \varphi_n(k)]^T \tag{4.26}$$

$$\boldsymbol{\theta} = [\theta_1\ \theta_2\ \cdots\ \theta_n]^T \tag{4.27}$$

where n is the number parameters of the mathematical model, y the observable variable also refereed as output, θ the vector of unknown parameters, and φ the vector of known variables, usually storing delayed input or output signals of the real system.

The main objective is to estimate the vector of parameters $\hat{\boldsymbol{\theta}}$ that minimizes the following cost equation:

$$J = J\left(\hat{\theta}, N\right) = \frac{1}{2}\sum_{i=1}^{N}\varepsilon^2(i) \tag{4.28}$$

where:

$$\varepsilon(i) = y(i) - \hat{y}(i) \tag{4.29}$$

or:

$$\varepsilon(i) = y(i) - \varphi^T\hat{\theta} \tag{4.30}$$

Denoted as the estimation error, ε, is a function of quadratic cost that when put into a vector can be represented by:

$$\mathbf{E} = [\varepsilon(1)\ \varepsilon(2)\ \cdots\varepsilon(N)]^T \tag{4.31}$$

which in the presence of an output vector:

$$\mathbf{Y} = [y(1)\ y(2)\ \cdots\ y(N)]^T \tag{4.32}$$

an estimated output vector:

$$\hat{\mathbf{Y}} = \left[\hat{y(1)}\ \hat{y(2)}\ \cdots\ \hat{y}(N)\right]^T \tag{4.33}$$

a matrix of data:

$$\mathbf{\Phi} = \begin{bmatrix} \varphi^T(1) \\ \varphi^T(2) \\ \cdots \\ \varphi^T(N) \end{bmatrix} \tag{4.34}$$

and assuming the following relations:

$$\mathbf{E} = \mathbf{Y} - \hat{\mathbf{Y}} \tag{4.35}$$

$$\hat{\mathbf{Y}} = \mathbf{\Phi}\hat{\boldsymbol{\theta}} \tag{4.36}$$

$$\mathbf{E} = \mathbf{Y} - \mathbf{\Phi}\hat{\boldsymbol{\theta}} \tag{4.37}$$

makes possible to achieve the estimated parameter vector:

$$\hat{\boldsymbol{\theta}} = \left(\mathbf{\Phi}^T\mathbf{\Phi}\right)^{-1}\mathbf{\Phi}^T\mathbf{\Phi} \tag{4.38}$$

The use of the LS method, just described, at the end of each RST control iteration makes possible to build a recursive implementation of the method.

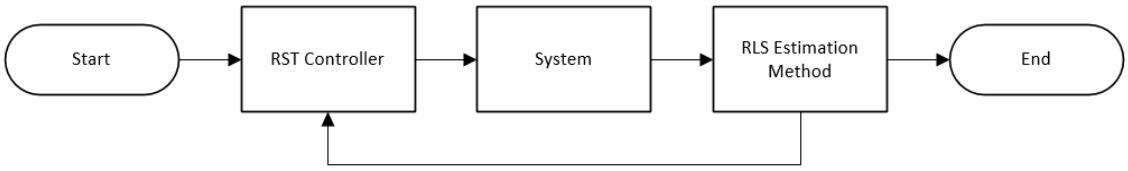

Figure 4.9: RST with RLS Controller Diagram

As seen on figure 4.9, the RLS Estimation Method takes place after the RST control algorithm. This allows to estimate the vector of parameters ($\hat{\boldsymbol{\theta}}$) based on:

- previously estimated parameters ($\hat{\boldsymbol{\theta}}$)
- previous outputs from the system ($\mathbf{\Phi}$)
- the current output from the system (y)

After the estimation of the new parameters of the system, the RST Controller uses those values to improve the closed loop response of the system during the next control iteration.

The next section will be responsible to explain how this is implemented on the proposed inverter.

4.3.3.2 Design of the H-Bridge Controller

In this section it will be designed the controller for the H-Bridge Converter. This controller will be responsible to ensure the sinusoidal output waveform of the proposed inverter.

In order to configure the controller, an early system identification is performed to know its open loop response. Being the RST control algorithm based on pole placement, it is necessary to analyze the open loop poles in order to place the closed loop poles, which will settle the response of the system when controlled.

Like in the PID identification method, a step can be applied to trigger a response from the circuit, however, instead of frequency, the H-Bridge Converter, illustrated in figure 4.10, is controlled by a PWM signal.

In order to get the step response of the circuit, the control signals $S5$ and $S8$ must carry the logical level "1" in order to turn "on" the transistors $Q5$ and $Q6$, and the control signals $S6$ and $S7$ must carry the logical level "0" in order to turn "off" the transistors $Q6$ and $Q7$.

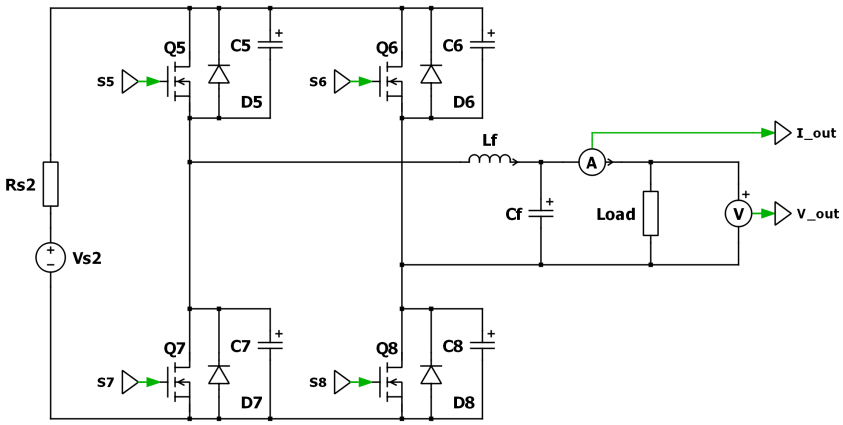

Figure 4.10: H-Bridge Converter Electrical Circuit

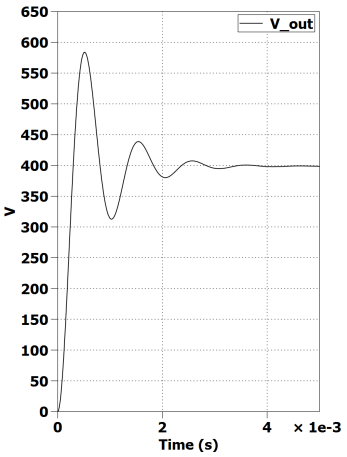

Figure 4.11: H-Bridge Converter Step Response

The circuit was simulated using the following parameters:

$V_{s2} = 400\ V$	V_{BUS} Voltage
$Load = \frac{230^2}{20000}$	Load Resistor

As it is possible to see in figure 4.11, the circuit has a second order system behavior with a measured rise time (t_r) of 0.000301 seconds, and a Percentage Overshoot (PO) of 46%, approximately.

Being the expression of a second order system given by:

$$G(s) = \frac{A\omega_n^2}{s^2 + 2\xi\omega_n s + \omega_n^2} \tag{4.39}$$

Where [46]:

A	Gain of the System	(4.40)
s	Laplace Variable	(4.41)
$\omega_n = \frac{0.8 + 2.5\xi}{t_r}$	Natural Frequency of the System in rad/s	(4.42)
$\xi = \sqrt{\frac{(\ln(PO))^2}{(\ln(PO))^2 + \pi^2}}$	Damping Coefficient	(4.43)

Matching the equation 4.39 to the simulated circuit, makes it possible to extract the following parameters:

$$\omega_n = 4650.8\ rad/s$$

Where:

$$\xi = 0.24$$

For the auxiliary observer polynomial (A_{obs}), which has to be faster than the physical system, a frequency two times greater is considered a good choice:

$$\omega_{obs} = 2 \cdot \omega_n = 9301.6\ rad/s \tag{4.44}$$

To choose the sample frequency the Astrom and Wittenmark method can be applied again, dividing the rise time by 10 samples:

$$T_s = \frac{t_r}{10} = 0.0301\ ms \tag{4.45}$$

When called in every control loop, the RLS identification function returns 4 parameters based on the expected system response and the actual system response: $\hat{\theta_1}$, $\hat{\theta_2}$, $\hat{\theta_3}$, $\hat{\theta_4}$. These estimation parameters, can then be introduced in the control function of the RST controller, which can be done by replacing in equations 4.20 to 4.23 the following variables:

$$a_1 = \hat{\theta_1} \qquad a_2 = \hat{\theta_2} \qquad b_1 = \hat{\theta_3} \qquad b_2 = \hat{\theta_4}$$

At this point, the control signal can be calculated by the following RST control function:

$$\begin{aligned} u(k) = blm \cdot (r(k) + a_{obs1} \cdot r(k-1) + a_{obs2} \cdot r(k-2)) - s0 \cdot y(k) \\ - s1y(k-1) - s2 \cdot y(k-2) - (r_1 - 1) \cdot u(k-1) + r_1 \cdot u(k-2) \end{aligned} \quad (4.46)$$

Where:

$$blm = \frac{1 + a_{m1} + a_{m2}}{\hat{\theta_3} + \hat{\theta_4}} \quad (4.47)$$

This equation is based on the output of the system y, the reference value r and the parameters calculated earlier.

The value of $u(k)$ can now be used to determine the duty cycle of the PWM control signal that will drive the transistors from the H-Bridge Controller, whose switching frequency was established on section 3.3.

In the next chapter, the different modes of operation will be discussed. Unlike the LLC Converter that must keep V_{BUS} constant at all times, the H-Bridge Converter can have multiple behaviors depending on the reference variable of the RST controller (voltage or current) as well as the output/feedback variable (also voltage or current). This will be established by the operation mode selected by the user, as explained next.

Chapter 5

Inverter Operation Modes

5.1 Introduction

As seen in subsection 2.4, even the most advanced commercial inverters available today have separate models for off-grid and on-grid applications, however, the inverter proposed in this dissertation is capable of working in any configuration, while using the same hardware. This is possible due to the adaptive control algorithm implemented, which adds flexibility to the system while delivering the accuracy and performance expected in an equipment like this.

In figure 5.1 are illustrated the three scenarios, or operation modes, tolerated by the proposed inverter. This will allow the user to sell power to the grid, disconnect itself from it, or have a self-consuming system in an on-grid, off-grid and hybrid topology respectively.

In this chapter all the above possibilities will be discussed, linking the scenarios to the legislation in Portugal at the moment [48].

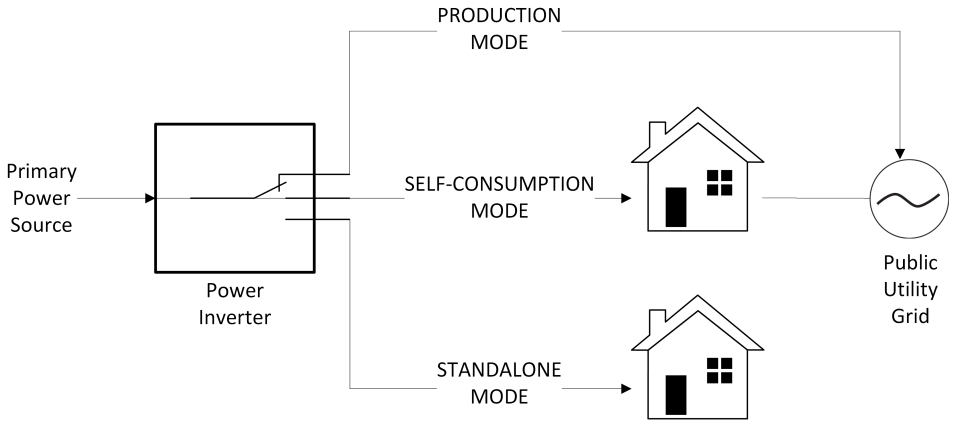

Figure 5.1: Inverter Modes Diagram

5.2 Production Mode

Production Mode suits the users that want to produce energy, using renewable energy sources, and sell it to the public utility company at a certain rate. In Portugal this regime is currently named as "Pequena Produção" which can be translated to "Small Production".

Previously named as "Mini-Production" and "Micro-Production", at the present time these former solutions were merged in order to simplify the legislation in force.

Small Production is accessible up to 250kW, however, it is limited to 100% of the contracted power from the utility company, plus, the facility that produces that energy must consume at least 50% of the total generated power. In 2015 the selling rate can go up to €0,11/kWh for solar energy, depending on the regime chosen, and a 15 year contract is required [49]. It is worth mentioning that the selling rate for solar systems in 2008 was fixed at €0,65/kWh and in 2012 at €0,32/kWh.

The typical electrical connection of this solution is illustrated in figure 5.2, where the utility company installs a second power meter in the facility, which measures the power produced by the inverter.

To make the proposed inverter capable of operating in this on-grid topology, its output waveform has to be synchronized with the public utility grid, which establishes the output voltage of the system. Thus, the H-Bridge Controller designed in section 4.3.3.2 must use the output current of the inverter as its feedback parameter to control the output power of the device.

Since the user will sell the energy produced by the system, it is necessary to maximize it using the MPPT Controller, as designed in section 4.3.1.1, which will be responsible for creating a control signal that will instruct the H-Bridge Controller to increase or decrease the RMS output current of the inverter while tracking MPP of the energy source where it is connected.

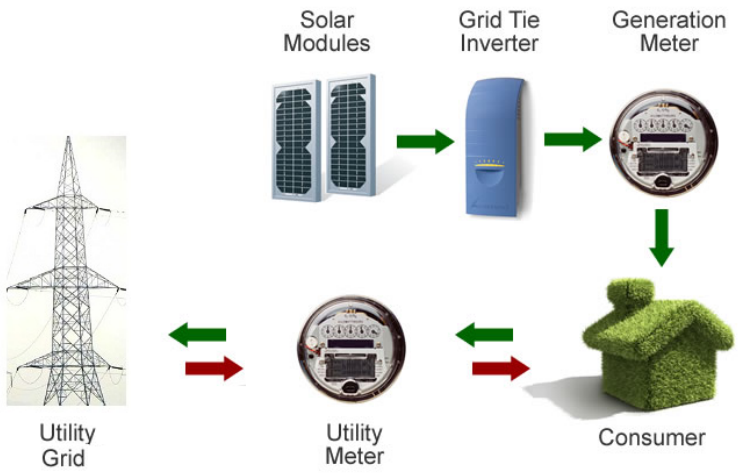

Figure 5.2: Grid Tie Mode Diagram

5.3 Standalone Mode

Mostly used by backup systems, off-grid or standalone systems have a very limited use in a typical household, since a power source is already available. However, in remote locations, where there is not a public utility grid available, it can be an extremely good option in terms of cost and practicality.

In Portugal, electrical companies charge a minimum of €7,4 per meter to connect a distant household to the grid. Therefore, the installation of an off-grid solar system capable to power a domestic circuit might be an interesting option.

For a complete isolated system, a battery bank should always be installed, even with systems that support solar and wind, preventing power outages in cases where the power source may fail for a certain period of time.

The use of battery banks to power an average house is still considered very expensive. Looking at figure 5.3 it is possible to see that an household in Europe consumes around 4000 kWh/year. If a third of that amount of power is consumed when there is no sun, the amount of stored energy per day would be:

$$\frac{4000}{365} \cdot 0.33 = 3.65 \text{ kWh/day}$$

This amount of power would require 6 deep cycle batteries of 12v 140Ah each, as calculated with the Trojan Battery Renewable Energy Sizing Calculator tool, illustrated in figure 5.4. Costing each battery around €500 and having a lifetime of 1135 cycles/days,

the price per stored kWh can be calculated by:

$$\frac{500 \cdot 6}{4000 \cdot 0.33 \cdot 3} = €0.76/\text{kWh}$$

This value can be acceptable or not depending on the situation but the use of batteries should be always avoided in order to reduce the overall price of the system.

Since no output synchronization is needed, this operation mode can be implemented on the proposed inverter simply by using the output voltage of the inverter as the feedback variable of the H-Bridge Controller. For the reference signal, a 50Hz $230V_{RMS}$ sinewave can be calculated by the control algorithm using its sample period and a sine function.

The MPPT Controller has no use here since the goal of this operation mode is to generate a stable output voltage waveform, instead of maximizing the output power of the inverter.

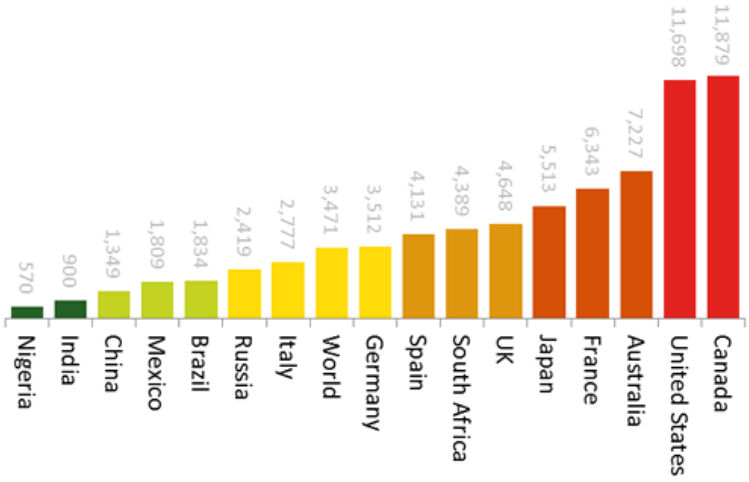

Figure 5.3: Household Electricity Consumption in kWh/year [50]

Individual Battery				System Design						
Battery	Trojan Model Number / Product Line / Warranty	Individual Battery Voltage	Ah Capacity @ 20 Hour Rate	Number of Batteries in Series	Number of Strings in Parallel	Total Number of Batteries	System Voltage	Ah Capacity @ 20 Hour Rate	Calculated DOD	Calculated Cycle Life
	12-AGM/ AGM/ 2 years	12	140	2	3	6	24	420	44.1%	1135
	6V-GEL/ Gel/ 2 years	6	189	4	2	8	24	378	49.0%	991

Figure 5.4: Trojan Battery Bank Simulator [51]

5.4 Self-Consumption Mode

This operation mode was introduced on the proposed inverter in order to provide a less expensive solution, compared to mini/micro-productions (now called "small productions") or even off-grid systems.

On the 20th of October 2014, the Government of Portugal approved the Decree-Law 153/2014, which allows the domestic energy production up to 1500Wh without any contracts or licenses required.

Using an example of a 1kWh PV kit, formed by 4 solar panels of 250W each and 1 inverter, costing around €2000, producing proximately 1800 kWh/year and having a 20 year equipment life spawn, the price per kilowatt during those 20 year can be calculated by the following expression:

$$\frac{Equipment\ Cost}{Production\ per\ year \cdot Equipment\ Lifetime} = €0.055/\text{kWh}$$

This value represents around 58% less compared to the current cost rate in Portugal: €0,1317/kWh.

The main goal of this operation mode is to minimize the power consumed by a household from the public utility grid where it is connected. While there is sunlight, the inverter can sense the power consumption of the household and produce that exact amount of power, which will result in a neutral current coming from the utility grid.

As an example and looking at figure 5.5 it is possible to see that:

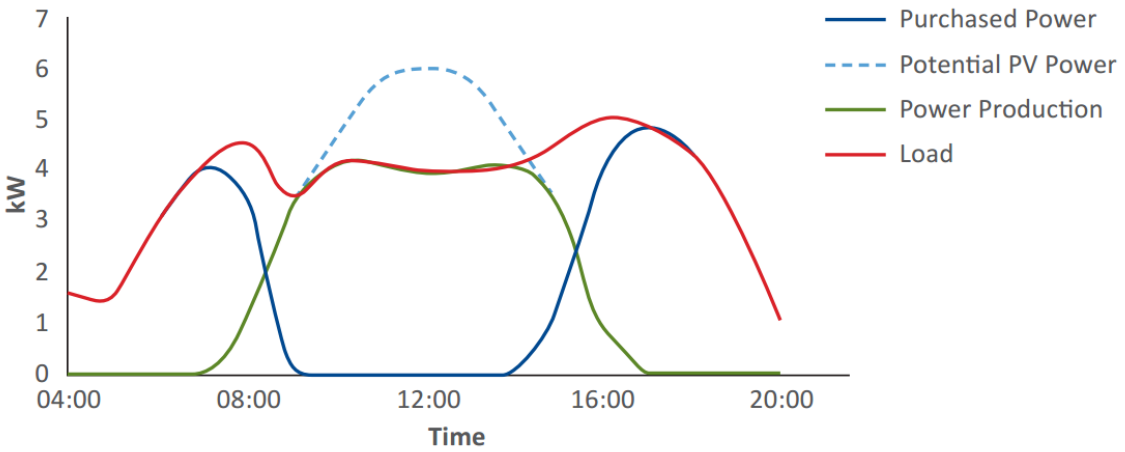

Figure 5.5: Domestic Power Consumption vs PV Array Power Production [27]

- Before 8am the "Power Production", or output power of the inverter, is not enough to cover the power consumed by the load. Therefore, the "Purchased Power" (from the utility grid) is greater than zero and the user is paying for each purchased watt.
- Between 8am and 4pm all the energy consumed by the load is coming from the inverter, which must adjust its output power in order not to produce more than needed by the circuit. At this point, the "Purchased Power" is zero.
- After 4pm the behaviour of the system is the same as before 8am.

This operation mode can be implemented in the proposed inverter by, just like in Production Mode, synchronizing its output waveform with the utility grid, since both power sources will be powering the same circuit.

If the power consumed by the load exceeds the maximum output power of the inverter, the H-Bridge Controller must truncate its output current in order to prevent damaging the electronic components of the circuit. On the other hand, since the goal of this operation mode is to match the output current of the inverter with the current being delivered to the load, instead of maximizing the output power of the inverter, the MPPT Controller becomes useless.

Due to the need of knowing the power consumed by the load, an extra sensor must be placed in the circuit. Its purpose is to instruct the H-Bridge Converter to increase or decrease the output current of the inverter, in order to achieve the zero "Purchased Power" point. This takes place when the output current of the inverter is greater than zero and when the current sensed by this sensor is zero.

As discussed in this chapter, three operation modes were designed for the proposed inverter: Production Mode, Standalone Mode and Self-Consumption Mode. These are possible due to the on-grid, off-grid and self-consumption topologies, as well as, the use of an adaptive RST Controller to control the H-Bridge Converter, all designed in previous chapters of this dissertation.

All the operation modes discussed in this chapter are legal in Portugal since October 20th 2014 and for that reason were implemented on the proposed inverter.

Due to the specificity of each mode, each one will be simulated in the next chapter using a simulation software in order to evaluate:

- Its the correct implementation in terms of control signals.
- The stability of the RST Controller when operating at each mode.
- The energy yield of the hardware designed to support all these topologies.

Chapter 6

Simulation

6.1 Introduction

When developing electronic circuits, the features provided by simulation software save precious time and money sometimes wasted in prototyping. This practice is growing in education and enterprises, representing now a crucial step in almost every project that designs electronic devices.

In this chapter, a simulation software will be used to evaluate the behavior of the LLC Converter and H-Bridge Converter, both composed by circuits and control algorithms designed in previous chapters. This will evaluate each design separately and ease debugging if necessary.

Both circuits will then be put together, creating the circuit of the resonant inverter proposed in this dissertation, which will also be simulated when working at all the operation modes described in chapter 5. This will evaluate its interoperability, adaptability, power efficiency and stability.

The organization of this chapter is as follows:

- **Section 6.2** presents the simulation software used.
- **Section 6.3** presents the simulation of the LLC Converter circuit.
- **Section 6.4** presents the simulation of the the H-Bridge Converter circuit.
- **Section 6.5** presents the simulation of the power inverter while working at the three operation modes proposed in chapter 5.

6.2 Plexim® PLECS

Piecewise Linear Electrical Circuit Simulation (PLECS), developed by Plexim, started in 1999 as a Simulink® toolbox for modeling large power electronic systems containing both electrical circuits and controllers [52]. Using the numerical engine of MATLAB®, this toolbox achieved high benchmarks when simulating switching circuits by modeling switches as ideal, instead of nonlinear elements that generate transient voltages and currents, usually both of little interest. In a later version, PLECS was released as a standalone version, using a high-level interpreted language - GNU Octave - as its numerical engine.

The software covers the electrical, the magnetic, thermal, and mechanical aspects of power conversion systems and their controls [53].

When working on a project in PLECS, Standalone version in this case, a simple Graphical User Interface (GUI) is presented with 3 main windows providing interaction with the user as figure 6.1 illustrates.

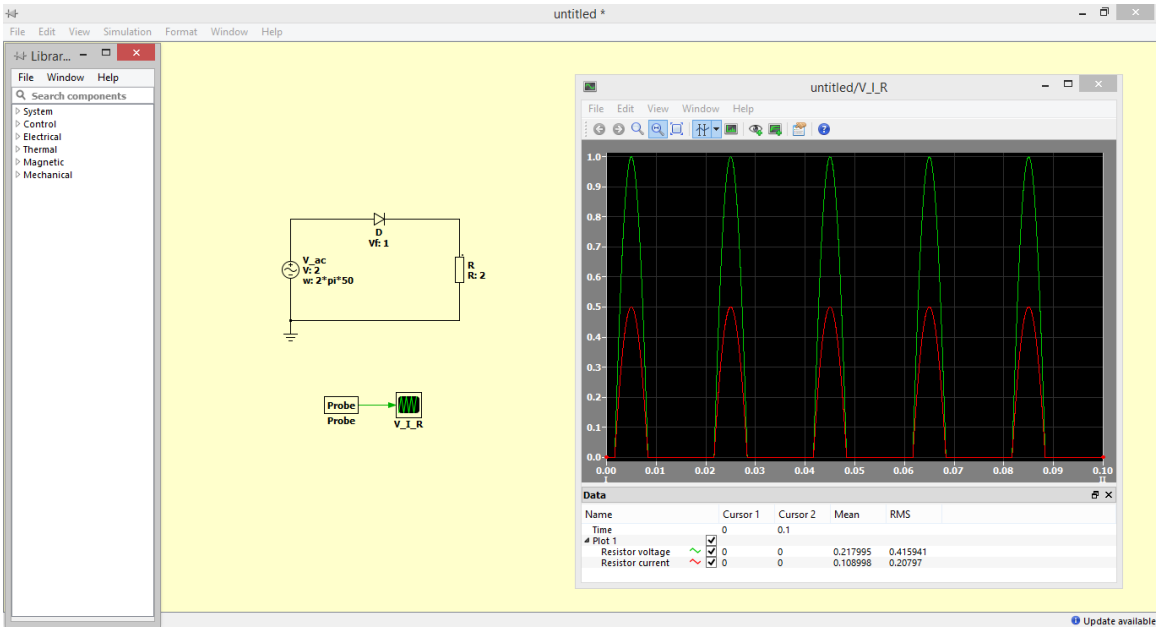

Figure 6.1: PLECS User Interface

The **"Library Browser"** window lets the user navigate through the components library or alternative search for a particular component. To use a component in the "Schematic Editor" window, a simple drag and drop is needed. In terms of component categories:

- "System" has a collection of common system components such as: Scopes, Probes, Signal From, Signal Goto, etc.
- "Control", has all the control components such as: sources, mathematical operations, logic operations, continuous functions, discrete functions and C-Scripts that allows the user to enter its own code, just like in a regular microprocessor.

- "Electrical" is the section where electric sources, passive components, transformers or power semiconductors can be found.
- "Thermal" section provides tools for a thermal evaluation of the circuit.
- "Magnetic" offers the components needed to simulate inductors or transformers with ideal or non ideal behaviors.
- "Mechanical" offers sources, sensors and components in order to simulate mechanical behavior.

In the **"Schematic Editor"** window it is possible to place the components picked from the library and build a circuit. The simulation of this circuit can evaluate electrical, control, thermal, magnetic or mechanical signals, all placed in the same circuit and interacting with each other. PLECS separates these different components by colors, as in figure 6.2, being black for electrical, green for control, blue for thermal, red for magnetics and purple for mechanical.

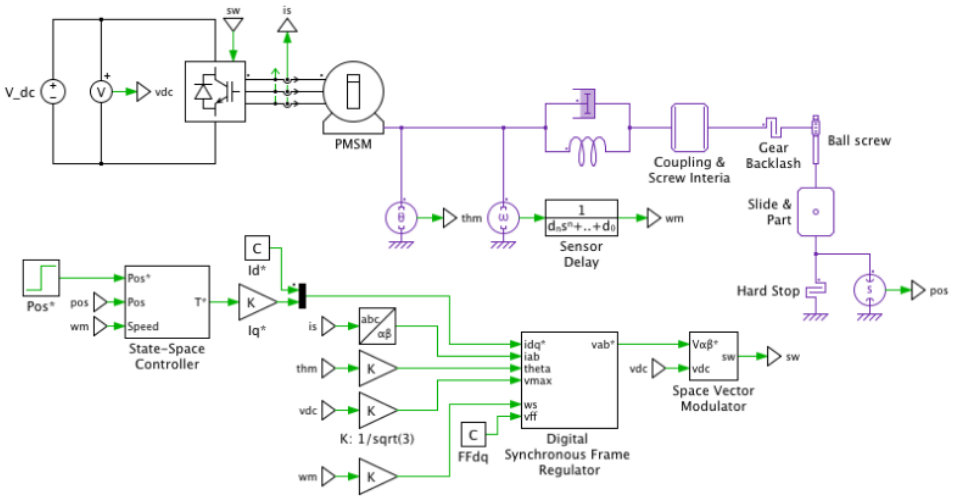

Figure 6.2: PLECS Servo Drive Demo [54]

"Scopes" are used to display simulation results offering many powerful tools to evaluate the data. Zooming, cursors placement, mathematical operations with cursors, and Fourier analysis can be implemented to a single or multiple signals while being simulated. After finishing the simulation it is possible save the displayed data as a PLECS trace file or export it as a Portable Document Format (PDF), Bitmap or Comma Separated Values (CSV) file.

PLECS can be used to simulate power electronics that use complex control algorithms since the component libraries available make possible to signals from one categories interact with components of other categories. As an example, the "C-Script" is a component from the "Control" category that allows the user to have a number of input signals, a section of code in C language to interact with those signals, export the result back into the simulation and control a transistor state, the voltage of a voltage source, or any other component that has a control input signal.

Multiple "C-Scripts" can run multiple control algorithms, each with its own sample frequency and code. This will be used in the simulation of the proposed inverter in order to simulate a RTOS where multiple threads run at the same time, as seen in subsection 4.2.

6.3 LLC Converter

In this section, PLECS will be used to evaluate the hardware architecture of the LLC Converter designed in section 3.2, as well as its PID control algorithm designed in section 4.3.2.1.

6.3.1 PLECS Schematic

In order to build the schematic of the LLC Converter, the following PLECS components were used:

- A **Voltage Source(Controlled)** was chosen to simulate the primary power source of the circuit. This component has an input which allows the user to change its output voltage using components from the "Control" category. Thus, using a C-Script, component described later, it is possible to set different output voltages at certain time instants.

Figure 6.3: Voltage Source Controlled - PLECS Component

- A **Signal From** was connected to the input control signal of the Voltage Source (Controlled) placed earlier. This component must be used with a "Signal Goto" and its purpose is to virtually connect the components with the same "tag"/name and simplify the schematic. Thus, whenever a "Signal Goto" and a "Signal Goto" are placed in the schematic with the same tag, these represent the same control signal.

Figure 6.4: Signal From - PLECS Component

Figure 6.5: Signal Goto - PLECS Component

- Four **Mosfets with Limited di/dt** (with no diode), each with a **Diode with Reverse Recovery** in an anti-parallel topology and a **Capacitor** in a parallel topology, were added to the schematic. This combination simulates the transistors of the h-bridge of the LLC Converter. Due to the simple components available is PLECS library, a more complex transistor model had to be implemented.

  The "Mosfet with Limited di/dv" allows the user to set the rise/fall time, on-state resistance, continuous drain current and breakdown voltage of the transistor.

  The "Diode with Reverse Recovery" was introduced to simulate the reverse recovery time of the internal diode of the transistor. This will give the simulation a much accurate result in terms of switching losses.

  The "Capacitor" component was added to the circuit in order to replicate the capacity of the transistor, which will also affect its losses.

  The parameters of these three components were configured based on the CREE® C2M0025120D Silicon Carbide Power MOSFET, which characteristic are presented in table 6.1 and 6.2.

  To the gate of each transistor was connected a **Signal From** in order to establish the connection between the electrical components and the control components (explained later in this section).

Figure 6.6: Mosfet with Limited di/dt - PLECS Component

Figure 6.7: Diode - PLECS Component

Figure 6.8: Capacitor - PLECS Component

Drain-Source Breakdown Voltage	1200	(V)
Continuous Drain Current	90	(A)
Drain-Source On-State Resistance	0.025	(Ω)
Rise Time	31.6	(ns)
Fall Time	28.4	(ns)

Table 6.1: CREE® C2M0025120D Electrical Characteristics

Diode Forward Voltage	3.3	(V)
Reverse Recover Time	45	(ns)
Reverse Recovery Charge	406	(nC)
Peak Reverse Recovery Current	31.6	(A)
Drain-Source Capacitance	205	(pF)

Table 6.2: CREE® C2M0025120D Built-in SiC Body Diode Characteristics

- Two **Inductors** and one **Capacitor** were used to build to resonant tank. The electrical values of these components were calculated in section 3.2.2.

Figure 6.9: Inductor - PLECS Component

- An **Ideal Transformer** with a 1:1+1 topology was used to simulate the HF transformer present in the LLC Converter circuit. The transformer turn ration was calculated in section 3.2.2.

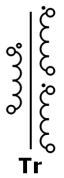

Figure 6.10: Ideal Transformer - PLECS Component

- Two **Diodes with Reverse Recovery** were used to simulate the rectification of converter. The electrical characteristics of the GeneSiC® GB50SLT12-247 Silicon Carbide Power Schottky Diode, chosen in section 3.2.4, are illustrated in table 6.3.

Figure 6.11: Diode with Reverse Recovery - PLECS Component

Diode Forward Voltage	3.0	(V)
Reverse Recover Time	50	(ns)
Reverse Recovery Charge	247	(nC)
Reverse Current	3000	(μA)
Total Capacitance	142	(pF)

Table 6.3: GeneSiC® GB50SLT12-247 Silicon Carbide Power Schottky Diode [38]

- A **Capacitor** in series with a **Resistor** was used to simulate a filtering capacitor and its respectively ESR.

Figure 6.12: Resistor - PLECS Component

- A **Resistor** was placed to simulate the load of the LLC Converter. Its electrical value can be calculated using the following expression:

$$R_{load} = \frac{V_{BUS}^2}{P_{inverter}} = \frac{400^2}{20\ kW} = 8\ \Omega \tag{6.1}$$

The accomplished circuit is illustrated in figure 6.13.

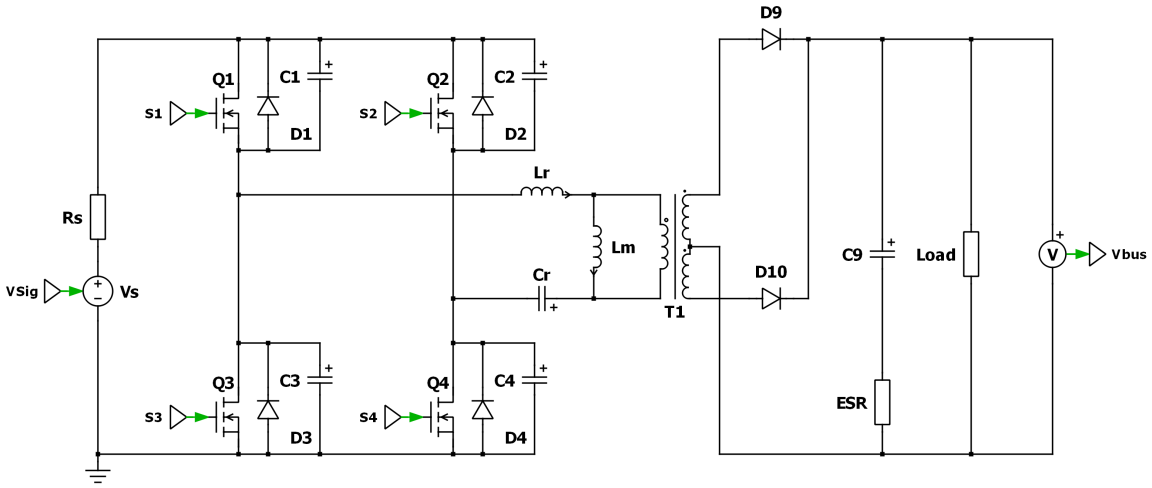

Figure 6.13: LLC Converter - PLECS Schematic

At this point it is necessary to build a **Control Circuit** in PLECS, which will be responsible for generating the control signals $VSig$, $S1$, $S2$, $S3$, and $S4$. This control

circuit, or schematic, can be built using the components present in the "Control" section of PLECS Library Browser.

- The **C-Script** is the most important component of the control circuit. This component simulates a microcontroller, where an algorithm in C can be executed at a certain frequency, as illustrated in figure 6.15. It also allows multiple inputs and outputs (all from the "control" library).

  In order to implement the PID Control algorithm designed in section 4.3.2, this "C-Script" must have one input signal, the voltage across the load or V_{BUS}, and one output, the operation frequency of the LLC Converter.

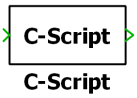

Figure 6.14: C-Script - PLECS Component

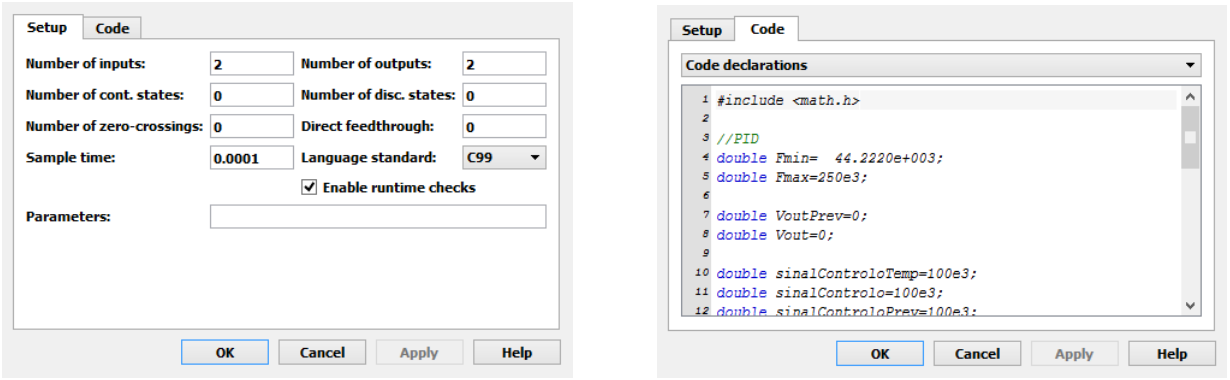

(a) Setup Tab

(b) Code Tab

Figure 6.15: C-Script Window - PLECS Component

- A second **C-Script** must be implement into this control circuit, not simulating a microcontroller but this time simulating a timer. Since the PLECS library does not have a component which generates a controlled frequency square wave, one was implemented this way. This "C-Script" uses the LLC Converter operation frequency, generated by the first "C-Script" as its input signal and generates a square wave with that exact frequency.

- A **Logical Operator** with the "Not" function was also added into the control circuit. Since all mosfets available in PLECS become "on" when connected to a control signal greater than zero, when using an h-bridge it is necessary to turn "off" Q1 and Q4 while Q2 and Q3 are turned "on" and vice-versa. In order to generate a complementary signal of the control signal generated by the second "C-Script", or timer, this component was added to the circuit.

Figure 6.16: Logical Operator - PLECS Component

- A **Turn-On-Delay** was also added to prevent short circuiting the h-bridge during the rise or fall time of the transistors.

Figure 6.17: Turn On Delay - PLECS Component

- A **Relay**, providing a Schmitt-Trigger behavior, was implemented to disable the bridge if the voltage V_{bus} reaches alarming levels, due to faulty control. Since this fault signal shutdowns the h-bridge, this control signal must be connected to the microcontroller so it can know when this happens.

Figure 6.18: Relay - PLECS Component

- A second **Logical Operator**, now with the logical function "And" was placed just before the "Signal-Gotos" in order to turn "off" all transistors, and therefore shutdown the h-bridge, when the control signal generated by the "Relay" assumes the logical level "1".
- A third **C-Script** was placed into the control circuit in order to change the input voltage of the LLC Controller.
- At least, four **Signal Goto's** were added to connect the mosfets that compose the h-bridge to their control signals.

The accomplished control circuit is illustrated in figure 6.19.

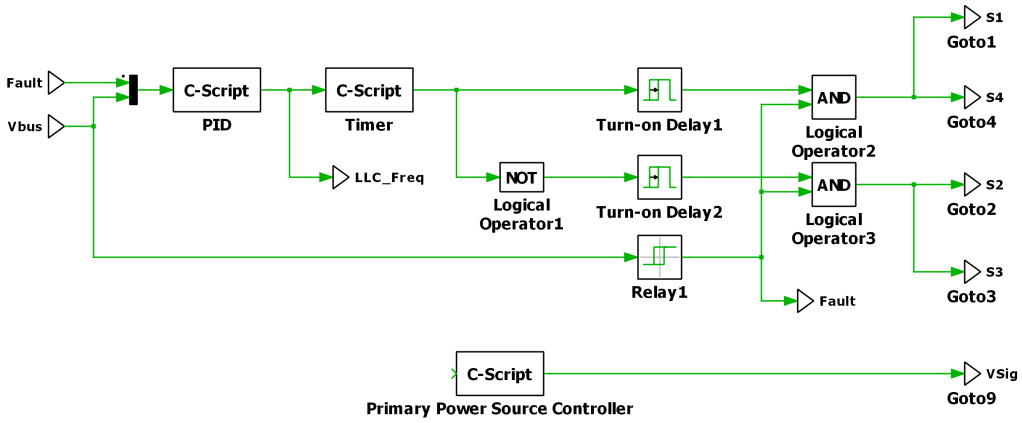

Figure 6.19: LLC Controller - PLECS Schematic

6.3.2 Simulation Results

Since the objective of the PID Controller is to keep V_{BUS} stable, it is expected for it to be very close to $400V$ (value established in section 3.2) at all times, even after an input voltage variation. Due to the design of the resonant tank (described in section 3.2.2), the controller must allow input voltages between $950V$ and $200V$, and when the input voltage of the LLC Converter is $600V$, the circuit must operate at its nominal switching frequency (100 kHz) having V_{BUS} a voltage value of $400V$.

In terms of the energy efficiency of the circuit, an average value greater than 80% is expected due to the resonant architecture of the converter, maximized when the tank is working at its resonant frequency, and when the converter is working with a 20kW load due to the reasons described in section 3.2.2.

In order to determine the energy efficiency of the LLC Converter circuit, the PLECS Components "Voltmeter" and "Ammeter" were used to sense the voltages and currents at the primary power source and load of the circuit. The difference of the average value of these two parameters multiplied defines the losses (conduction losses plus switching losses) of the circuit.

Figure 6.20: Ammeter - PLECS Component

Figure 6.21: Voltmeter - PLECS Component

As it is possible to see in figure 6.23, the LLC Converter manages to keep a stable voltage across its output/load while its input voltage variates from $1000V$ to $200V$.

Usually, the input voltage of an inverter does not change instantaneously as $VSig$ does, however, this approach makes possible to acquire more information about the response of the controller, evaluating its stability even in extreme situations.

At first, due to the charge time of the resonant tank, the control signal fluctuates more than expected, introducing a 15% overshoot on the output voltage of the converter. At the following transitions of $VSig$, it is possible to notice some undershooting, which is quickly corrected by the control system.

The voltage gain of the converter it is also presented as expected, operating at its resonant frequency (100kHz) when its input voltage level is $600V$.

In terms of power performance, the converter was simulated working at $200V$, $400V$, $600V$, $800V$ and $1000V$. In each situation its overall efficiency was measured for an output power of 5kW, 10kW, 15kW and 20kW. These multiple tests resulted in the graphic illustrated in 6.22.

As expected, the converter achieved a maximum yield when working at its maximum load and with an input voltage around $600V$. A peak of 97.79% was measured, having the converter a power efficiency greater than 90% at almost its entire operating region.

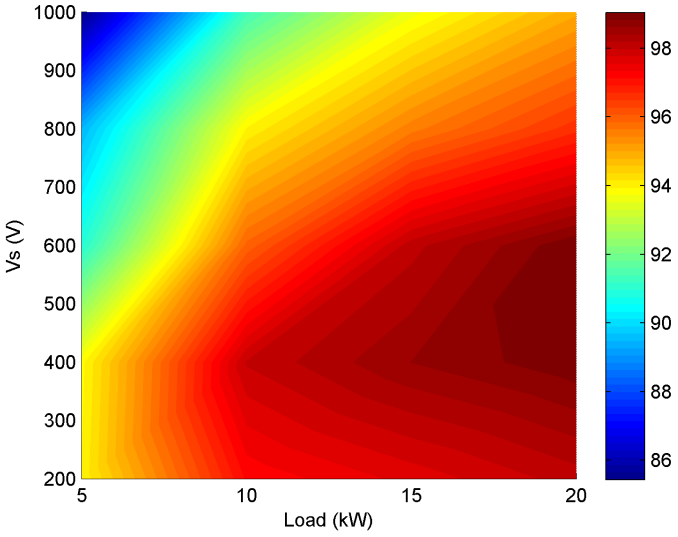

Figure 6.22: LLC Converter Energy Efficiency

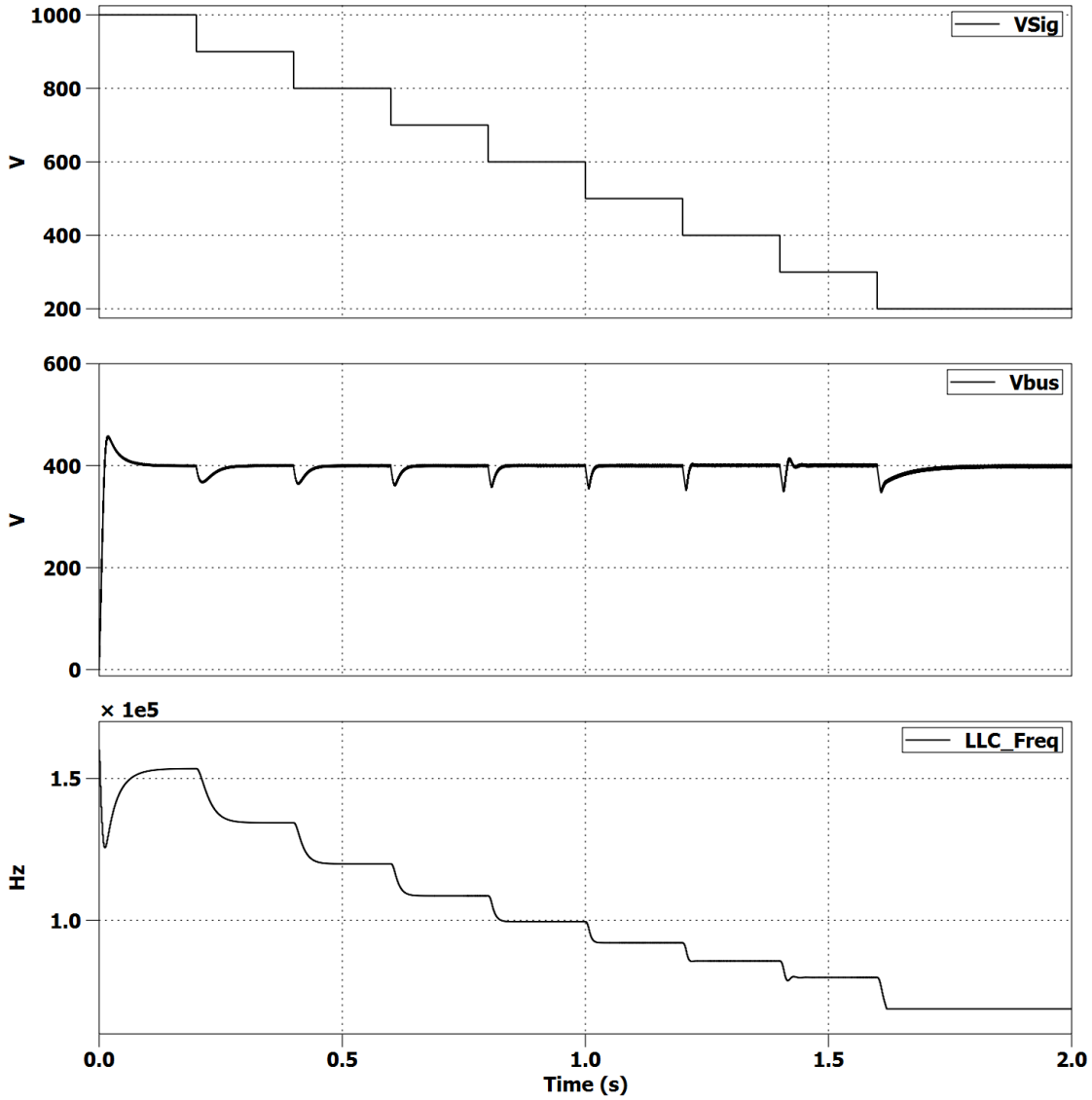

Figure 6.23: LLC Converter Simulation Results

6.4 H-Bridge Converter

The architecture of the proposed inverter creates a dependency between the LLC Converter, which generates a stable output voltage, V_{BUS}, and the H-Bridge Converter, which uses that voltage level to create an AC waveform.

When simulating the H-Bridge Converter, this dependency must not influence the results in order to facilitate the debug process in case of unexpected results. Thus, this circuit was simulated using a standard voltage source from PLECS.

6.4.1 PLECS Schematic

In order to simulate the H-Bridge Converter, the following PLECS components were used:

- A **Voltage Source DC**, in series with a **Resistor**, was used to simulate a non ideal voltage source.

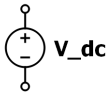

Figure 6.24: Voltage Source DC - PLECS Component

- Four **Mosfet with Limited di/dt** (with no diode), each with a **Diode with Reverse Recovery** in an anti-parallel topology and a **Capacitor** in a parallel topology were used to simulate the transistors of the h-bridge of the H-Bridge Converter. Since the components used here are exactly the same as the components used to build the h-bridge of the LLC Converter, its electrical characteristics were already described in section 6.3. Four **Signal From's** were also used to connect the electrical components to the control components (described later).

- An **Inductor** and a **Capacitor** were added to build the output filter of the proposed inverter. The electrical specification of these components can be found on section 3.4.

- A **Voltmeter** and an **Ammeter** were added in order to generate the feedback signals needed by the RST Controller. Two **Signal Goto's** were used to route the signals.

Using the components described above, the following circuit was assembled using PLECS:

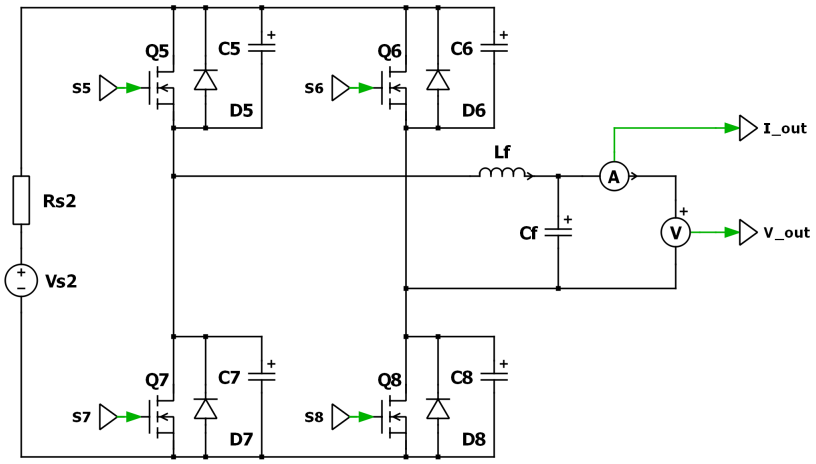

Figure 6.25: H-Bridge Converter - PLECS Schematic

As for the control circuit, its design is very similar to the control circuit designed for the LLC Converter in section 6.3. The following PLECS components were used:

- A **C-Script** was placed in order to simulate the MPPT Controller designed in section 4.3.1. As it was defined earlier in this dissertation, this algorithm will only by used when applied the Production Mode described in section 5.2.

- A second **C-Script** was used to simulate a microcontroller running the RST control algorithm designed in section 4.3.3, which generates the duty cycle of the PWM control signal used to drive the mosfets of the H-Bridge Converter. This control signal has a value between -100 and 100 (where -100 permanently closes the transistors S6 and S7 opening S5 and S8, 100 permanently closes the transistors S5 and S8 opening S6 and S7, and 0 permanently opens S5, S6, S7, and S8.) As it was described in chapter 5, this control algorithm can use different feedback signals in order to apply the different operation modes described earlier. Due to that, multiple signals such as: the output voltage of the inverter, the output current of the inverter, the signal of an external current sensor (whose placement will be discussed later) used in the self-consuption mode, and the output of the MPPT Controller will be the input signals of this "C-Script". Each will be connected using a "Signal From".

- A **Symmetrical PWM** was used to generate a control signal with a constant switching frequency, whose value was established in section 3.3, and a variable duty cycle which will be controlled by the output of the second "C-Script". Thus, the output signal of this component will have two values, zero (representing the logical level "0") and a positive value (representing the logical level "1").

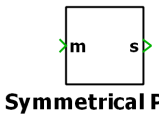

Figure 6.26: Symmetrical PWM - PLECS Component

- A **Relay** was also added to the circuit in order to shut down the bridge if the absolute value of the output current of the inverter (mathematical operation performed by the PLECS component **Abs**) exceeds the following level:

$$I_{out\ max} = \frac{P_{max\ inverter}}{V_{output}} = \frac{20\ kW}{230\ V_{RMS}} = 86.96\ A \tag{6.2}$$

- The **Turn-on Delays**, **Logical Operators** and **Signal Goto's** that drive the mosfets have the exact same behavior as described in section 6.3.

The accomplished control circuit is illustrated in figure 6.27.

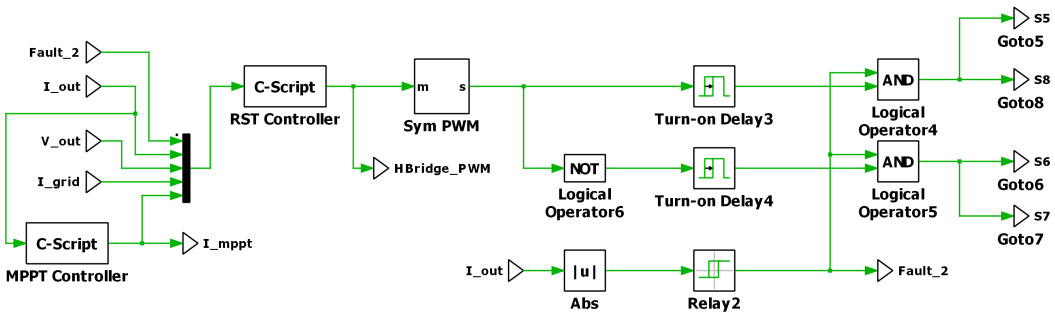

Figure 6.27: H-Bridge Controller - PLECS Schematic

6.4.2 Simulation Results

In order to simulate the H-Bridge Converter, it is necessary to choose an operation mode for the proposed inverter. Since two of the three operation modes designed for the proposed inverter are grid-connected, the Production Mode (a grid-connected topology) was chosen.

Thus, a **Voltage Source AC** was connected to the output of proposed inverter the in order to simulate the utility grid (230 V_{RMS} at 50Hz - in Portugal). Since this simulation will try evaluate the behavior of the RST Controller, the MPPT controller was modified to force the implementation of multiple load steps. This will stress the controller, creating multiple load discontinuities that will evaluate the adaptability and stability of the controller.

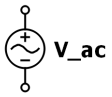

Figure 6.28: Voltage Source AC - PLECS Component

As illustrated in figure 6.29, the H-Bridge Controller presents a flexible and accurate behavior during the entire simulation. The output current of the inverter is synchronized with the grid and has the expected amplitude and frequency.

When the load changes, the control signal oscillates very gently, achieving stability moments later. This flexibility keep the controller stable at all output powers tested: 5kW, 10kW, 15kW and 20kW.

Looking at figure 6.30, it is possible to see the estimated parameters of the RLS identification method. It is clear that the system changes its parameters during this simulation, however, the RLS keeps track of those changes.

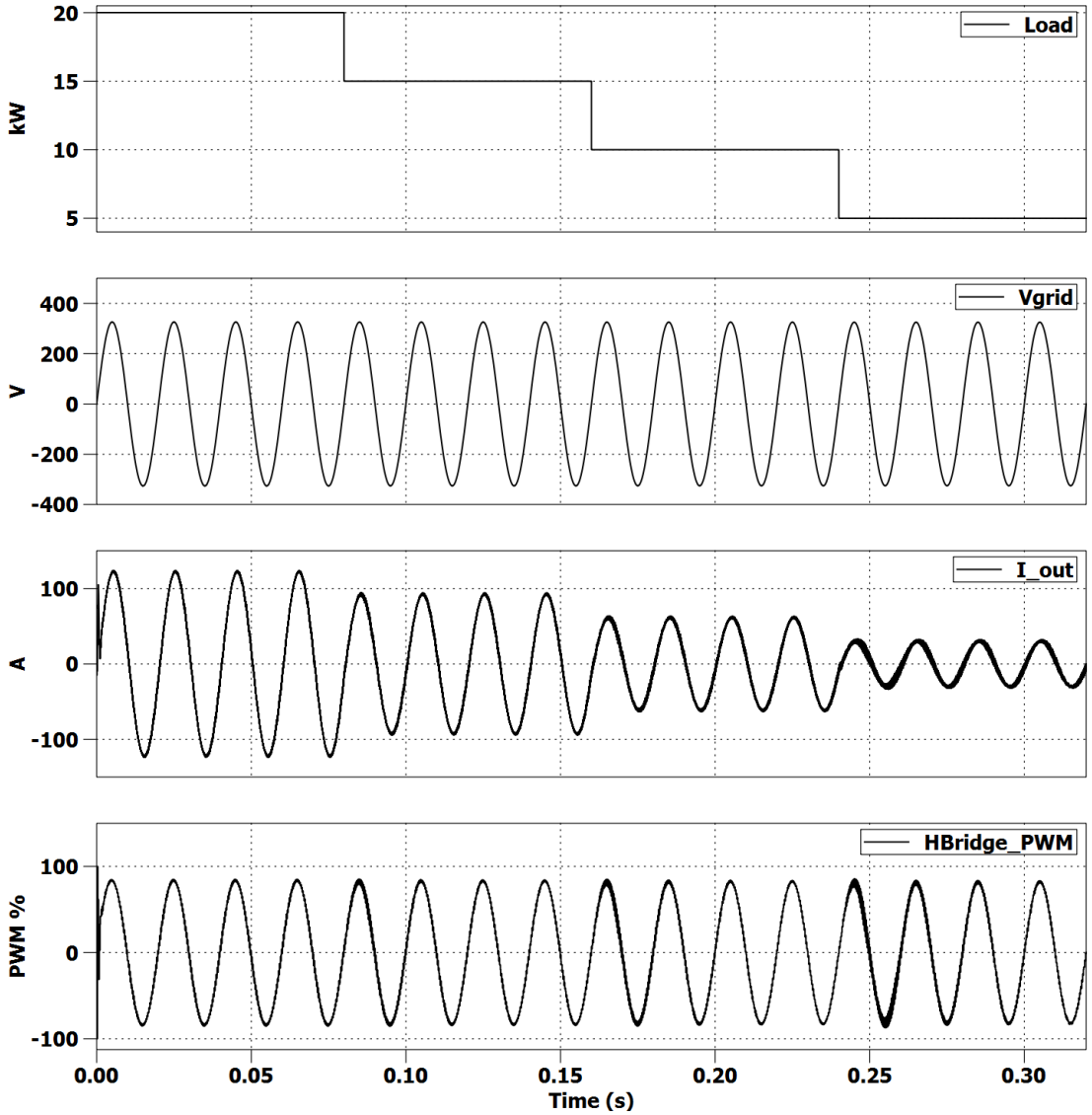

Figure 6.29: H-Bridge Converter Simulation Results

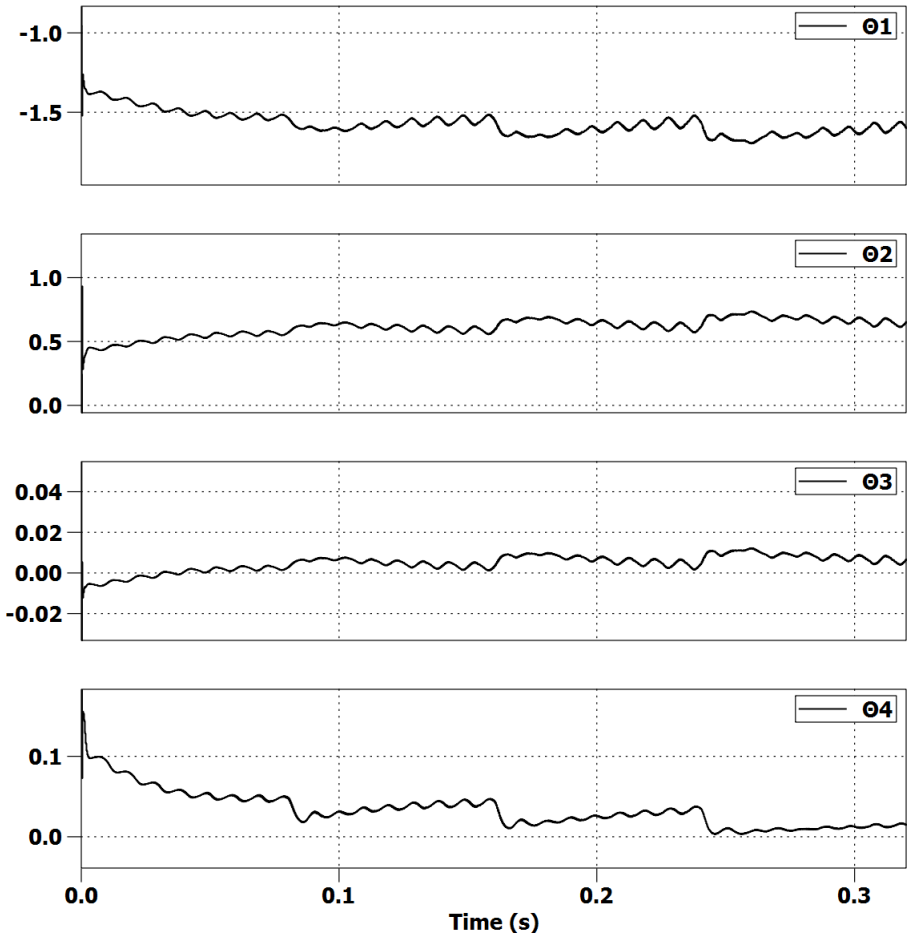

Figure 6.30: H-Brigbe - RLS Identification Method Estimated Parameters

6.5 Proposed Inverter

Having, at this point, verified the correct behavior of the control systems and converters that will incorporate the proposed inverter, whose electrical circuit designed in PLECS is illustrated in figure 6.31, the final simulations can now take place. This circuit was achieved simply by connecting the output of the LLC Converter to the input of the H-Bridge Converter.

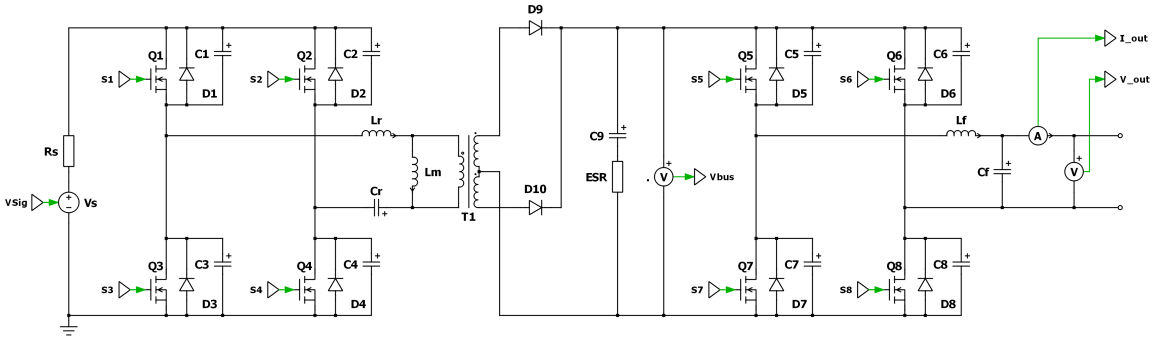

Figure 6.31: Inverter Electrical Schematic in PLECS®

Since a "Voltage Source (Controlled)" was used in section 6.3.1 to simulate the primary voltage source of the LLC Converter, the electrical specifications of the 20kW PV array described in table 3.2 can now be simulated. This will provide a more realistic simulation. The V/I curve for this power source is illustrated in figure 6.32.

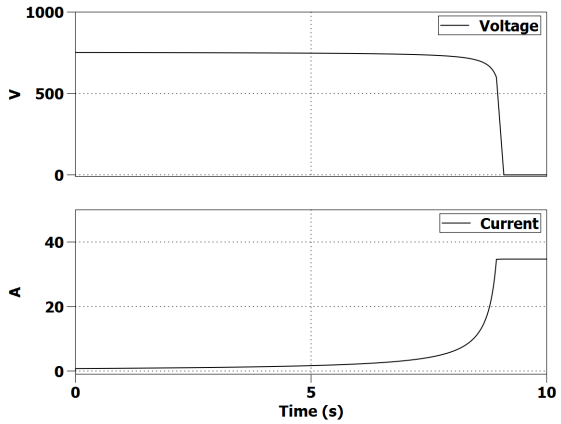

Figure 6.32: Primary Power Source V/I Curves

In figure 6.33, the possible output topologies for the proposed inverter, depending on the selected operation mode, are illustrated. These circuits will be connected to the output of the proposed inverter, ie, connected to the output filter of the circuit.

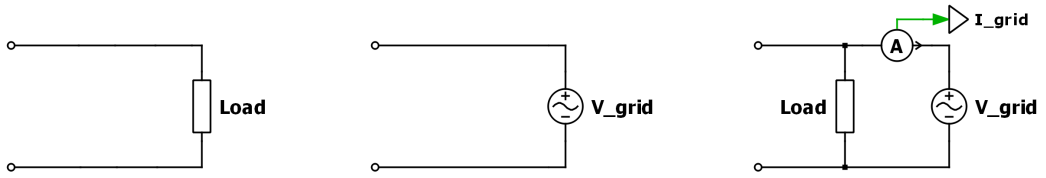

(a) Standalone Mode (b) Production Mode (c) Self-Production Mode

Figure 6.33: Possible Loads for the Proposed Inverter

The following sections will evaluate the results obtain for each operation mode.

6.5.1 Standalone Mode

Due to the lack of synchronization with the grid this operation mode can be defined as the simplest in terms of control. Even so, the system was simulated with a variable load, making its output power change between $20kW$, $15kW$, $10kW$ and $5kW$. In order to test the stability of the controller, the transitions between this values were instantaneous (only resistive loads have been considered).

As previously discussed in section 5.3, the output voltage of the proposed inverter will have a sinewave waveform, an amplitude of $230V_{RMS}$ and a frequency of 50Hz.

During the simulation period, and as a consequence of the PID Controller designed for the LLC Converter in section 4.3.2.1, a constant V_{BUS} voltage of $400V$ is expected.

It is also expected to have a stable output voltage, even with load variations, due to the implementation of the RST Controller, designed for the H-Bridge Converter in section 4.3.3.2.

As it is possible to see, in figures 6.34, 6.35 and 6.36:

- Vs, the voltage level of the primary power source (controlled by the control signal $VSig$), has an expected behavior. As visible in figure 6.32, the higher the output current, the lower the output voltage. Thus, it is expected to have a higher and more stable Vs when the inverter operated at lighter loads, and a lower Vs (affected by some ripple) at heavier loads.

- Even with a fluctuating input voltage, Vs, the PID controller manages to accomplish a stable V_{BUS} voltage. Due to the sinusoidal output voltage and current of the inverter, this voltage level presents some ripple, whose magnitude can be considered as acceptable.

- Due to the abrupt load changes, the output voltage waveform is affected by a short period of time. However, when the RLS starts identifying the new parameters of the

system, as illustrated in figure 6.36, the RST controller rapidly adjusts its output. As expected, a sinewave with an amplitude of $230V_{RMS}$ and a frequency of 50Hz is presented.

- The control signal generated by the PID controller (denominated as LLC_Freq) does not get saturated at any time and despite presenting some noise due to the ripple present in V_{BUS}, it shows a good control behavior.
- The control signal generated by the RST controller (denominated as HBridge_PWM) starts at saturated levels, but when the RLS estimation methods starts adjusting the parameters of the system, the signal achieves stability. This behavior can also be observed when the output power of the inverter changes abruptly.
- The RLS estimation parameters also have an expected behavior, starting at incorrect levels but constantly adjusting over time.

During the time simulated, the circuit presented energy efficiency of 92.8%.

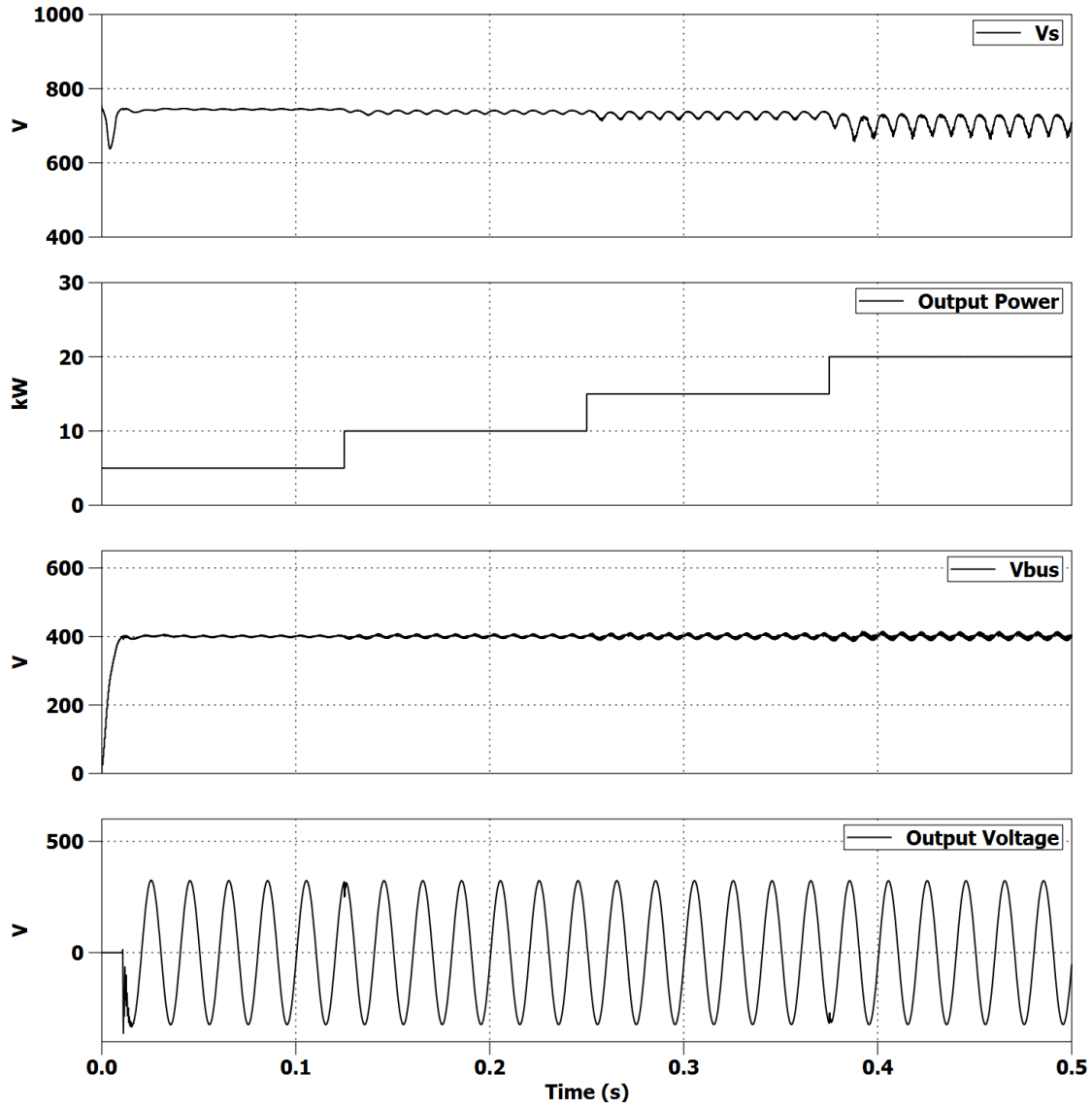

Figure 6.34: Standalone Mode - Variables over time

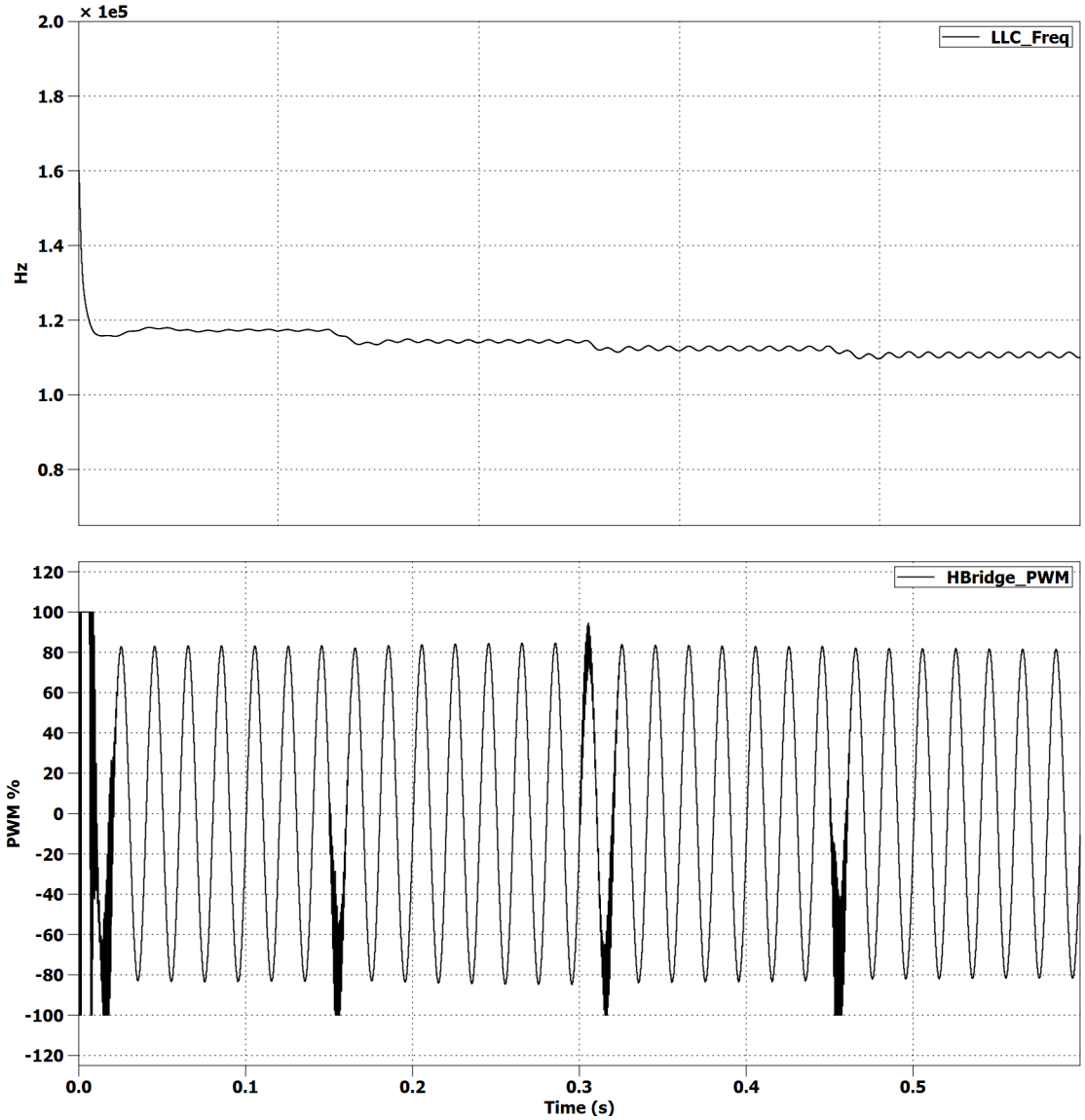

Figure 6.35: Standalone Mode - Variables over time (2)

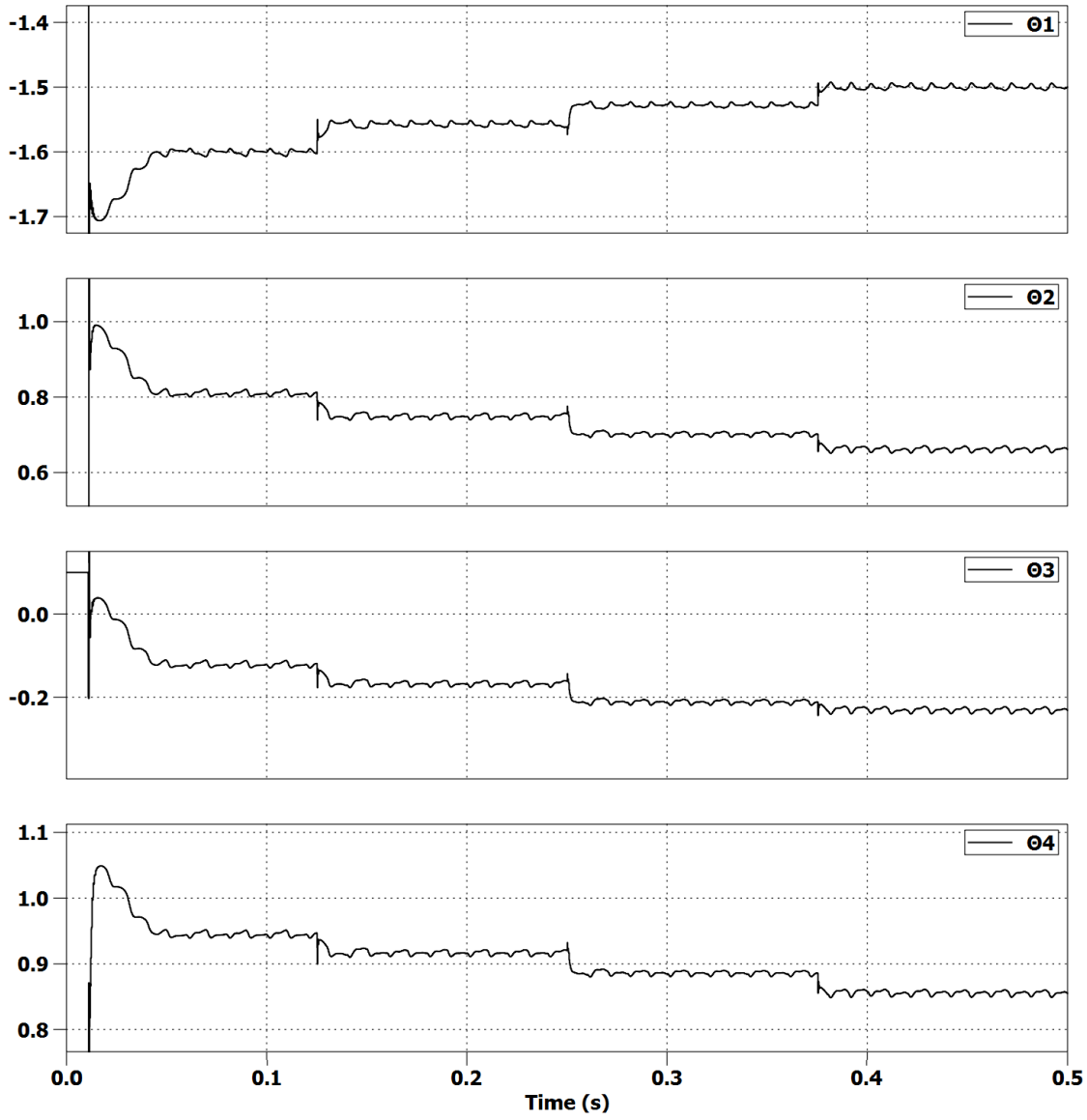

Figure 6.36: Standalone Mode - RLS Estimated Parameters

6.5.2 Production Mode

In this mode the proposed inverter will operate as described in section 5.2. Since its output voltage is the same as the utility grid voltage, the inverter will inject power into the grid when its output current is greater than zero.

Thus, in order to maximize the amount of power injected into the utility, and therefore, capitalize the investment of the user, the MPPT controller designed in section 4.3.1 will be used.

Due to this, it is expected to have a stable V_{BUS} voltage, an output current synchronized with the waveform of the utility grid and that tracks the MPP of the source where the inverter is connected.

As it is possible to see, in figures 6.37, 6.38 and 6.39:

- Vs has an expected behavior, achieving lower levels at heavier loads.
- The output power of the proposed inverter, which is controlled by the MPPT controller, starts at a lower value and keeps increasing until surpassing the MPP of the renewable energy source. When that happens, the controller goes back one iteration and lowers the output current of the inverter in order to minimize the distance to that same MPP and maximize the output power of the device.
- V_{BUS} has a stable voltage level during all the simulation time, even with the fluctuations present at the input power source.
- The output current of the inverter is synchronized with the utility grid, whose voltage is also denominated as the output voltage of the inverter due to the paralleled topology between the circuit and the grid. It is also noticeable that the magnitude of the output current presented has a direct relation with the output power demanded by the MPPT controller.
- As seen previously, the control signal generated by the PID controller (denominated as LLC_Freq) has some noise associated to it, however, it never gets saturated, showing a good control design.
- In this operation mode, the control signal generated by the RST controller (denominated as HBridge_PWM) gets saturated more often, however, due to the RLS identification method implemented, it achieves stability immediately after.
- Due to the constant change of the output power of the circuit during this simulation, the RLS estimation parameters achieved present some oscillation, ensuring the correct behavior of the identification method.

The average energy yield achieved while working at this operation mode was 93.9%.

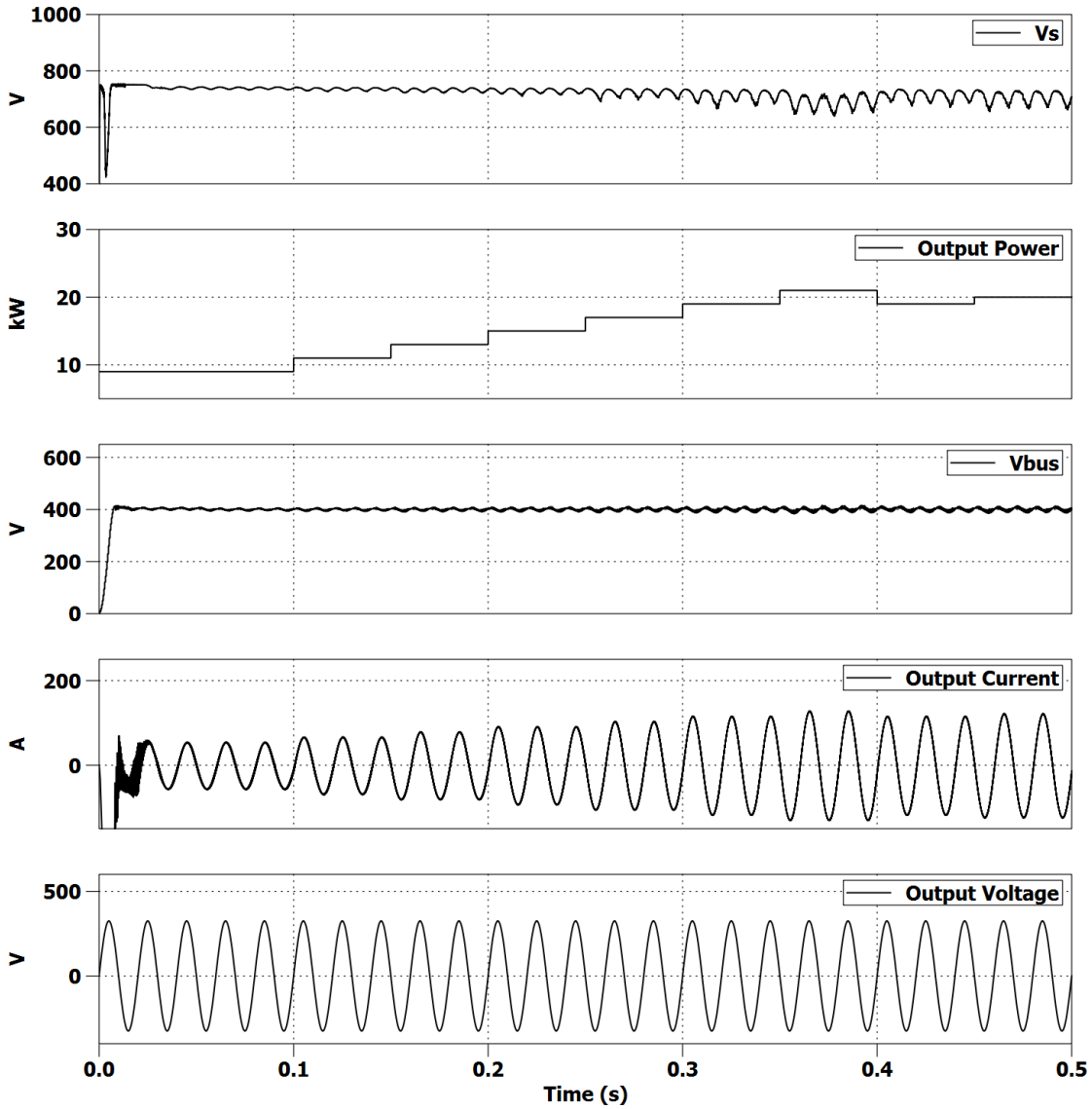

Figure 6.37: Production Mode - Variables over time

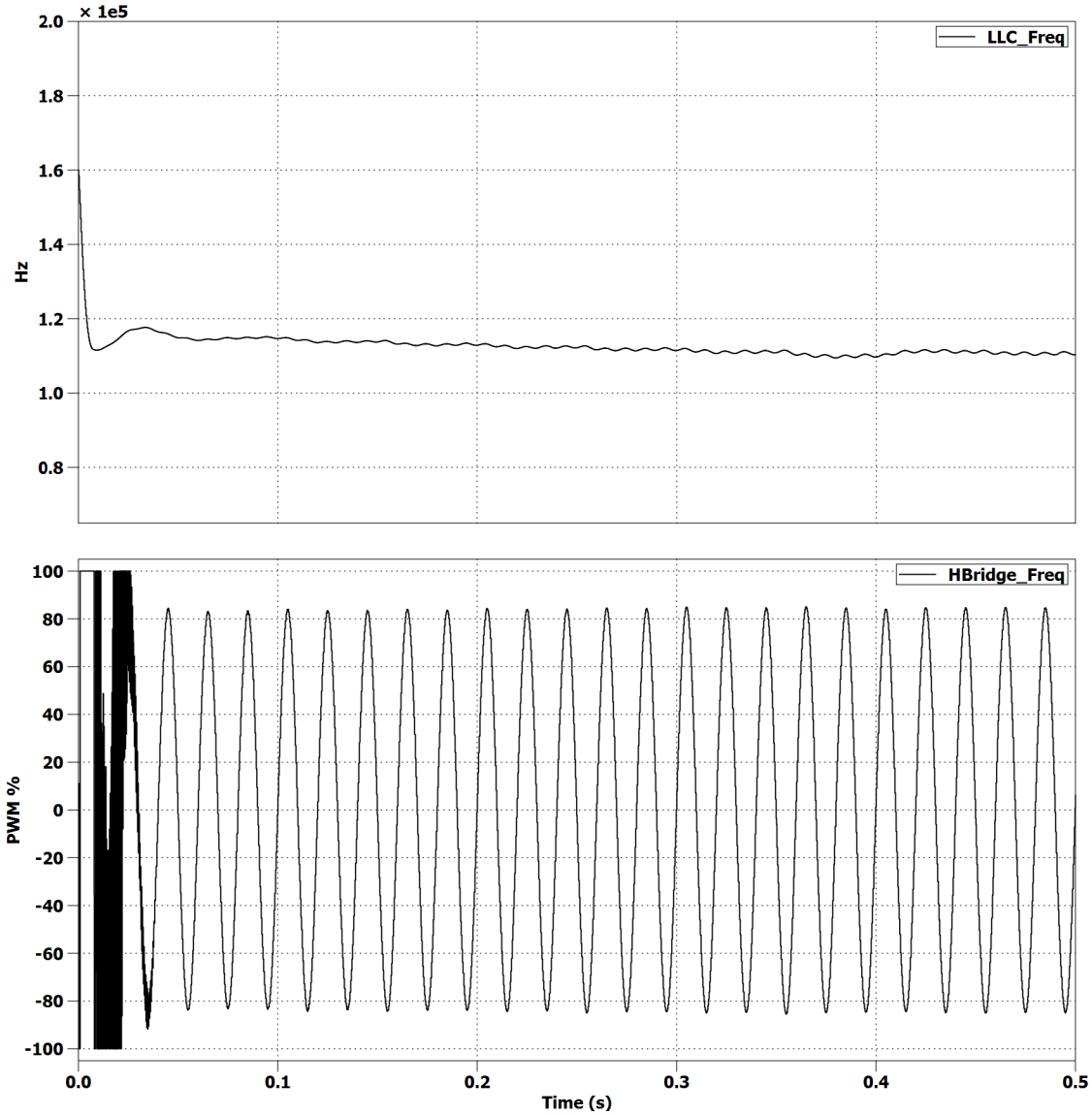

Figure 6.38: Production Mode - Variables over time (2)

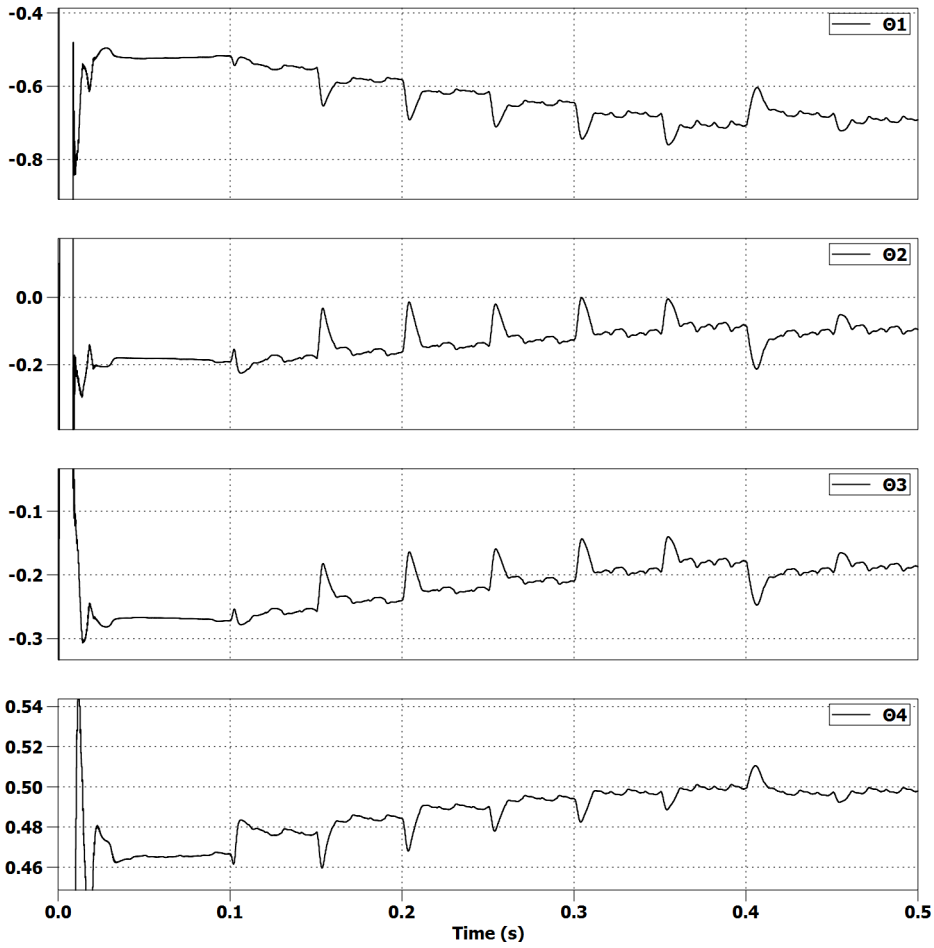

Figure 6.39: Production Mode - RLS Estimated Parameters

6.5.3 Self-Consumption Mode

When working in this mode, the inverter is placed in a parallel topology with a load and public utility grid, however, due to the introduction of a second power meter (or current sensor), it is possible to know the power injected into the grid.

The difference between the power being consumed from the grid, and the power injected into the grid, was denominated "power balance". If this value gets positive, it means that the power delivered to the load is coming from the grid. If negative it means that the inverter is producing an amount of power greater than the power absorbed by the load, being the rest delivered to the grid. If zero, it means that the load is being powered at 100% by the inverter, and that there is no power delivered/consumed to/from the grid.

As in the previous simulation, it is expected to have an stable V_{BUS} voltage level and in this case, an output current that creates a power balance near zero. In order to test the correct behavior of the inverter, a variable load was connected to the circuit, having values from 5kW to 30kW. At load levels greater than 20kW, the controller of the proposed inverter must truncate its output current/power in order not to damage the electronic components.

As it is possible to see, in figures 6.40, 6.41 and 6.42:

- Vs the same correct behavior as before.
- V_{BUS} also has the same correct behavior, having its voltage level around 400V during the entire simulation.
- At the first instants, turning on the equipment creates a power balance peak that immediately disappears. Then, the inverter measures the power that is being delivered by the grid to the load and adjusts its production to match that value. As soon as the inverter starts delivering power to the load, the power balance reaches a value very close to zero.

  When the load increases to $10kW$, $15kW$ or $20kW$, the inverter takes half of a sine wave to measure the power needed by the load and updates its output power, matching that value. In these cases the power balance is almost zero.

  At a certain point the load starts demanding more power than the power that the inverter can deliver. To prevent the equipment from a catastrophic event, the control system sets a limit for the output power, and the power balance becomes positive. This means that from the 30kW demanded by the load, 20kW are being delivered by the inverter and the rest, 10kW, are being delivered by the grid.
- The RST controller manages to keep the output current of the inverter stable during most of the power balance transitions. Synchronized with the grid, it presents the expected magnitude (demanded by the second sensor in order to keep the power balance zero) and frequency.

- Due to the output power variation, the RST estimation parameters present some oscillation, expected due to the behavior the circuit.

While performing this simulation, the inverter presented a power efficiency of 93.7%.

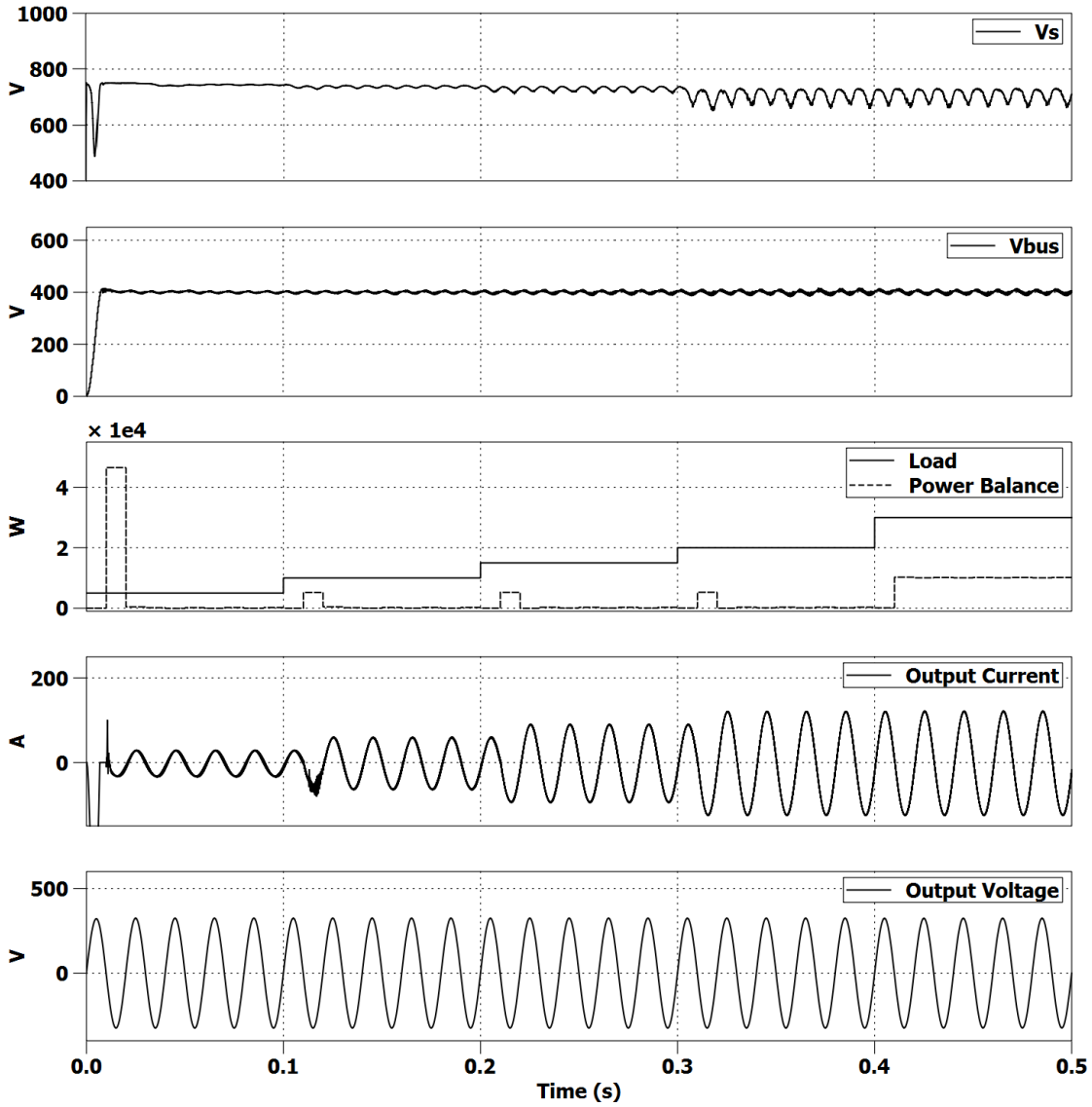

Figure 6.40: Self-Consumption Mode - Variables over time

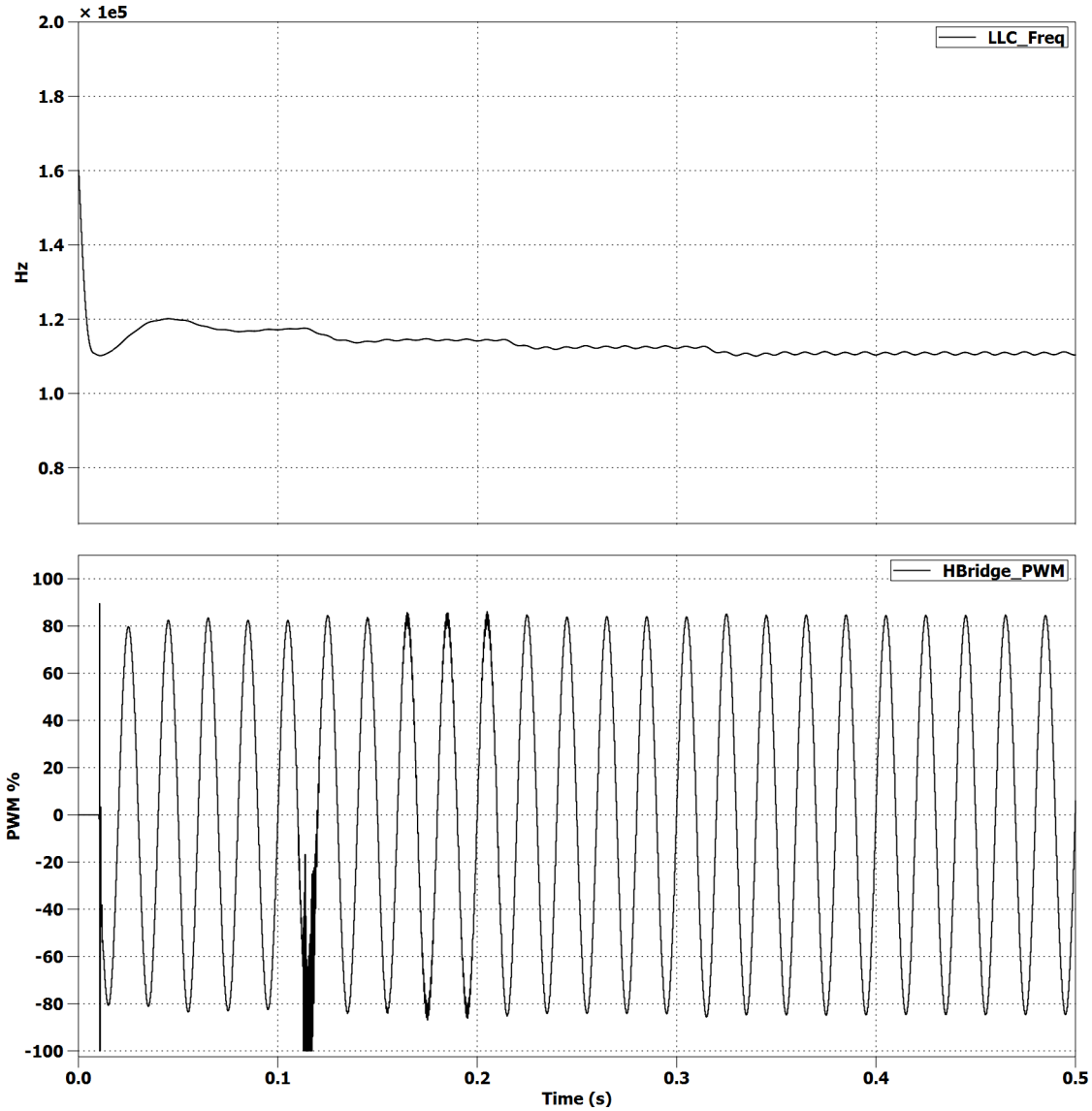

Figure 6.41: Self-Consumption Mode - Variables over time (2)

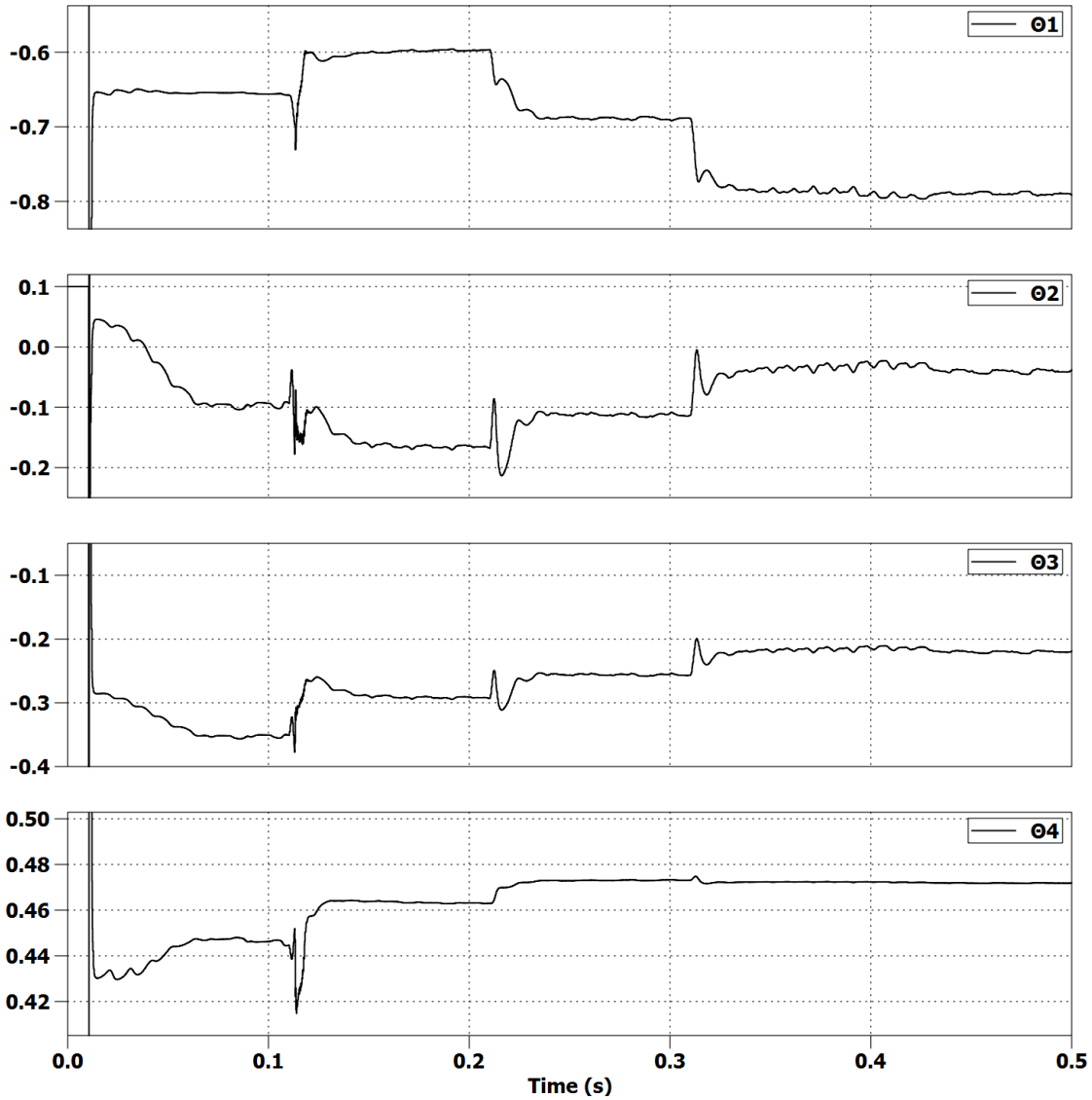

Figure 6.42: Self-Consumption Mode - RLS Estimated Parameters

Chapter 7

Conclusions and Future Work

7.1 Conclusions

This dissertation aimed to design an adaptable yet energy efficient power inverter. For this purpose, several technologies and architectures were taken into account.

In order to design the electronic circuit of the equipment, a LLC Converter, an H-Bridge Converter and a LC output filter were projected. The circuit was designed to have an input voltage range from 200V to 950V and an output of $230V_{rms}$ at 50Hz, allowing a synchronization with the public utility grid.

For the DC-DC conversion of the inverter a PID controller was designed. For the DC-AC converter, an adaptive RST controller with a RLS identification method was implemented. Both control systems were developed to keep the output voltage of the inverter stable, even with input voltage variations or load variations.

Due to the adaptive control system of the inverter, various modes of operation were implemented in the equipment. These modes allowed an off-grid, on-grid, and auto-consuming topology, always using the same circuit.

To evaluate the performance of the hardware, and the stability of the controllers, while working in every operation mode, the simulation software PLECS was used.

In these simulations, the hardware achieved an average energy yield of 93%, approximately, while having its peak when working with an input voltage of 600V and a 20kW load, as it was expected. In terms of control, flawless stability and performance were accomplished by every control algorithm, while operating at every operation mode. During some abrupt load variations, it was possible to verify some minor oscillation, however, in a few iterations the controller successfully corrected the output waveform.

Due to the complexity and magnitude of the project embraced, certain aspects can surely be improved, however the results achieved can be considered very good. Hopefully from now on, equipments like this will enter the domestic environment, generating clean energy without any fees or contracts.

7.2 Future Work

During the development of this dissertation, it was possible to find some aspects that can be improved::

- Due to the short lifetime of large electrolytic capacitors, when working with large currents, the use of this type of components must be avoided. However, the proposed inverter makes use of a component of this type, limiting its life time to a couple thousand hours. To avoid this, a different type of capacitor or circuit architecture must be implemented.
- The LLC Converter reduces the power losses of the circuit due to its soft-switching method. However, the H-Bridge Converter still uses hard-switching to generate the AC output wave form of the inverter. This not only causes the equipment to be less energy efficient but also leaves no margin to increase the operation frequency of this circuit. In order to get lighter and smaller inverters, these operation frequencies must increase what can be done using resonant circuits in both converters.
- When using the Self-Consumption method an external power meter has to be placed between the load and the public utility grid. To avoid connecting the sensor to the inverter using long cables, a powerline system could be developed.

Appendices

Appendix A

Circuit Assembly

A.1 Introduction

Having designed the hardware and software of the resonant power inverter, followed by the simulation of the system in every operation mode, it is now proposed a hardware implementation of the project.

Due to the cost of the components needed to build a 20kW power inverter, associated to the fact that a power of this magnitude can be fatal in case of a catastrophic event, it was decided do downscale the whole system. This means that the hardware implementation presented in the following chapter tries to build a resonant power inverter, with the same operation modes, hardware architecture and control system, however, with a maximum output power of 100W.

Having successfully proved the concept in a simulated environment, it will now be attempted in a real scenario.

The organization of this chapter is as follows:

- **Section A.2** presents the electronic components chosen to build the prototype.
- **Section A.3** describes de PCB designed for the downscaled inverter.
- **Section A.4** analyzes the results obtained.

A.2 Components

The downscaled resonant inverter has now a input voltage range from 20V to 100V, and the LLC Converter an output voltage, V_{BUS}, of 40V. The H-Bridge Converter will have an output voltage of $23V_{RMS}$ and a 50Hz transformer between the LC filter and the utility grid will amplify this value to get a system with an output voltage of $230V_{RMS}$.

A.2.1 LLC Converter

Having the inverter proposed in this chapter, a maximum input voltage of 100V, much cheaper transistors can be used to build the h-bridge of the LLC Converter. Due to its fast switching speed and low R_{DS} the Fairchild FDP054N10 N-Channel MOSFET was chosen.

Drain-Source Breakdown Voltage	100	(V)
Continuous Drain Current	144	(A)
Drain-Source On-State Resistance	0.0046	(Ω)
Rise Time	92	(ns)
Fall Time	39	(ns)
Reverse Recovery Time	57	(ns)

Table A.1: Fairchild FDP054N10 Electrical Characteristics

Due to the different voltages and currents, a new resonant tank must be calculated. When adjusting its output power of 100W, the following values were obtained:

$$f_{sw-min} = 38.2370e + 003\ (Hz)$$
$$L_m = 2.5144e - 006\ (H)$$
$$L_r = 359.2015e - 009\ (H)$$
$$C_r = 7.0518e - 006\ (F)$$

As stated before, the L_m and L_r can be build from the leakages inductances present in the windings of the HF transformer. On the other hand, the capacitor C_r can be purchased, having the VISHAY MKP1848S57070JP2C 7UF Film Capacitor the perfect specifications for it. With a capacitance tolerance of 5% and an almost inexistent ESR, it is an extremely good capacitor for high currents and low losses.

For the HF transformer an ETD29 core is capable to handle 100W of power while working at the operating frequencies of the LLC converter. The winding section and number of turns can be calculated exactly the same way as before.

To the rectifiers the IXYS DPG10I300PA High Performance Fast Recovery Diode was selected, not only for the fast recovery time but also for the low forward voltage:

Max. Repetitive Reverse Voltage	300	(V)
Average Forward Current	10	(A)
Forward Voltage	1.27	(V)
Reverse Recovery Time	35	(ns)

Table A.2: IXYS DPG10I300PA Electrical Characteristics

To the electrolytic filtering capacitor a 4.7mF Multicomp with a tolerance of 20% was chosen.

A.2.2 H-Bridge Converter

This part of the inverter, composed by an h-bridge and a LC output filter, can be build using only three different components.

The transistors used in this bridge, due to the performance reported in switching activities, are the same used in the bridge of the LLC Converter.

When calculating the LC filter, the following values were obtained:

$$L = 0.0013\ (H)$$
$$C = 19.535e - 06\ (F)$$

The capacitor chosen for this filter was the VISHAY MKP1848S62070JP2F, 20UF, 700V film capacitor. The inductor has to be manufactured due to its high value.

A.2.3 Control System

In an early approach an adaptive control algorithm was uploaded to the DETPI32 development board, however, the complexity of the algorithm, associated to the emulation of a floating point unit in this microprocessor, made it impossible to use.

In an implementation of control algorithms using the ARM-Cortex M4 microcontroller, FreeRTOS was used. Three tasks were created: the RST controller; the PID controller ; and a MPPT controller.

To power the microcontroller a 2W 5V isolated DC-DC converter was implemented in the circuit, protecting the digital logic circuit from the switching noise around the power components. Also powered by this converter is the LEM current transducer, responsible to generate a feedback signal for the controller, that was placed in series with the output of the inverter. The Avago optocouplers, responsible for isolating the control signals connected to the microcontroller, were also powered by this isolated power source.

These isolated control signals, either generated by the RST or the PID control algorithms, were connected to two Intersil 4081 full-bridge drivers, one for the DC-DC h-bridge and another for the DC-AC h-bridge converter.

A signal transformer was also placed in the circuit providing voltage feedback from the output of the inverter to the microcontroller.

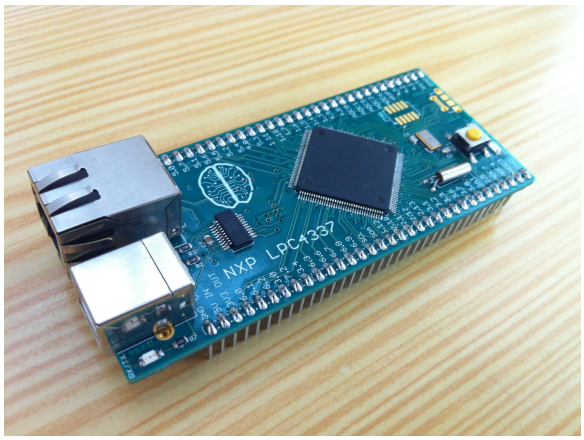

Figure A.1: ARM-Cortex Development Board

A.3 PCB

Using the CadSoft® Eagle PCB Design Software, a Printed Circuit Board (PCB) for the resonant inverter was created. In figure A.2 it is possible to see the electrical schematic of the circuit. The components on the top represent power electronics, such as the LLC Converter, the H-Bridge Converter, and the LC output filter. On the bottom is it possible to see the microcontroller and the Integrated Circuit (IC)'s responsible for driving the bridges. In the middle part of the schematic are the voltage regulators, and on the right, the sensors.

Looking at figure A.3 it is possible to see the actual PCB as it would look when fabricated. Its dimensions are 273mm x 175mm, and the component placement is very similar to the schematic presented in figure A.2. Due to the large currents needed in this circuit, much larger traces had to be placed between the power components in order to add more copper to the connections and therefore, achieve less conduction losses in the circuit.

A.4 Results

As it is possible to see in figure A.4 the assembly of the PCB for the proposed inverter was not completed. Due to that it was not possible to evaluate the inverter in real conditions.

However, having configured the ARM-Cortex microcontroller, designed the electronic circuit of the control system, designed the PCB and build part of it, makes it a relevant factor in this dissertation.

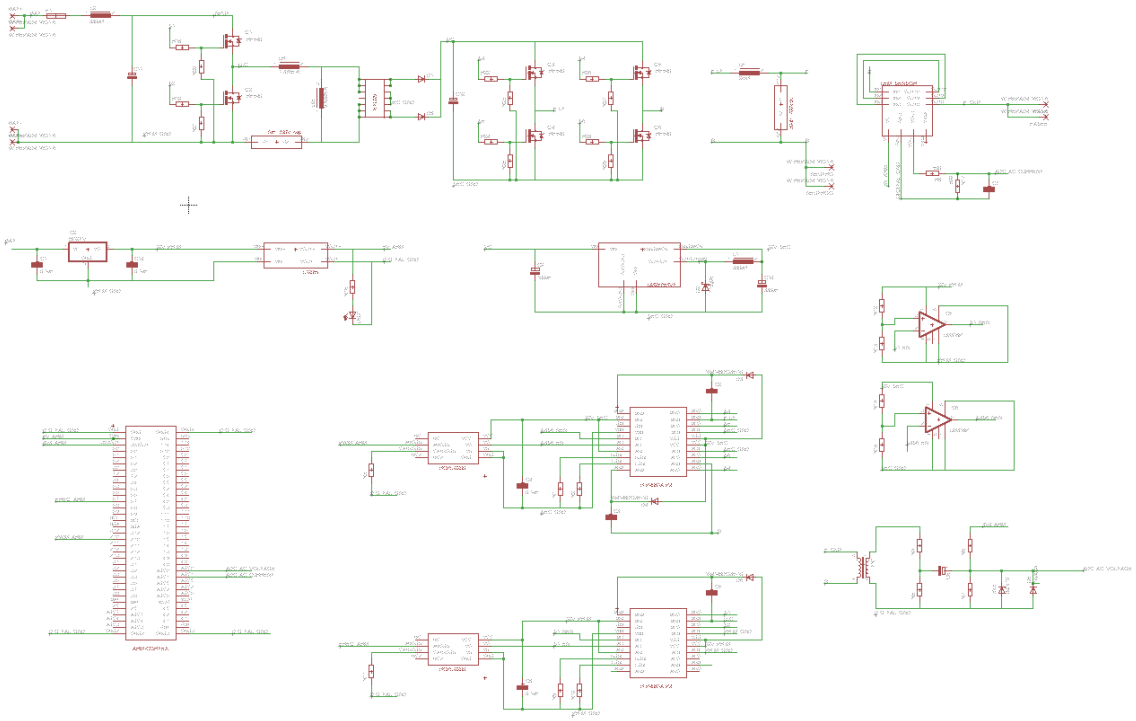

Figure A.2: Schematic View - CadSoft® Eagle

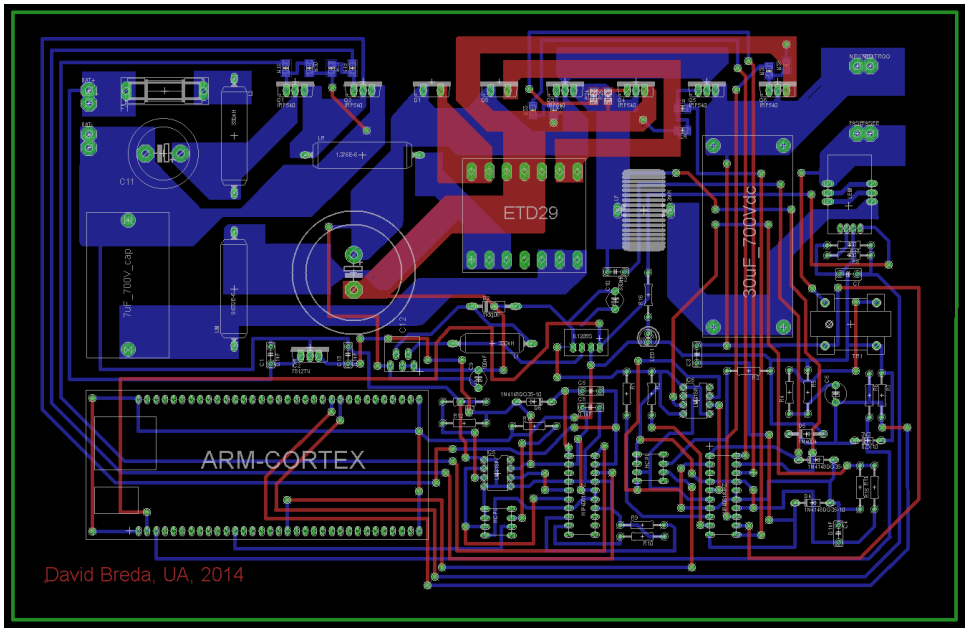

Figure A.3: Board View - CadSoft® Eagle

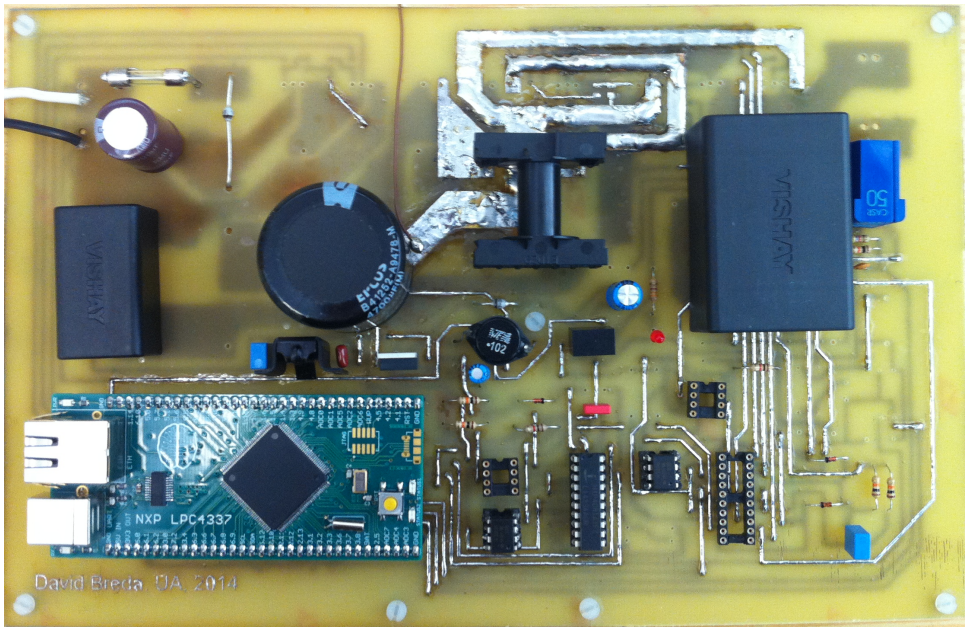

Figure A.4: Resonant Inverter Fabricated PCB

Bibliography

[1] Observ'ER. Worldwide electricity production from renewable energy sources. http://www.energies-renouvelables.org/observ-er/html/inventaire/pdf/15e-inventaire-Chap01-Eng.pdf. [Online; accessed 25-Nov-2015].

[2] David F. Morehouse John H. Wood, Gary R. Long. Long-term world oil supply scenarios. http://www.eia.gov/pub/oil_gas/petroleum/feature_articles/2004/worldoilsupply/oilsupply04.html. [Online; accessed 25-Nov-2015].

[3] ExxonMobil. Exxonmobil's outlook for energy sees global increase in future demand. http://news.exxonmobil.com/press-release/exxonmobils-outlook-energy-sees-global-increase-future-demand. [Online; accessed 25-Nov-2015].

[4] Frankfurt School-UNEP Centre. Global trends in renewable energy investment 2015. http://fs-unep-centre.org/publications/global-trends-renewable-energy-investment-2015. [Online; accessed 25-Nov-2015].

[5] Ordenamente Do Território e Energia Ministério Do Ambiente. Decreto-lei n.º 153/2014, de 20 de outubro. https://info.portaldasfinancas.gov.pt/NR/rdonlyres/7C8B4709-4E30-4ABF-B58B-97616A0E33B1/0/Decreto_Lei_153_2014.pdf. [Online; accessed 25-Nov-2015].

[6] PhD Bill Kovarik. History of sustainable energy. https://sustainablehistory.wordpress.com/2011/03/29/the-surprising-history-of-sustainable-energy. [Online; accessed 25-Nov-2015].

[7] NREL. Silicon materials and devices. http://www.nrel.gov/pv/silicon_materials_devices.html. [Online; accessed 25-Nov-2015].

[8] Fraunhofer Institute for Solar Energy Systems ISE. Photovoltaics report. https://www.ise.fraunhofer.de/de/downloads/pdf-files/aktuelles/photovoltaics-report-in-englischer-sprache.pdf. [Online; accessed 25-Nov-2015].

[9] Energy Informative. The homeowner's guide to solar panels. http://www.energyinformative.org/best-solar-panel-monocrystalline-polycrystalline-thin-film. [Online; accessed 25-Nov-2015].

[10] Sunny Ray. Monocrystalline vs polycrystalline solar panels. http://www.sunnyray.org/Monocrystalline-vs-polycrystalline-solar-panels.htm. [Online; accessed 25-Nov-2015].

[11] Alternative Energy. Common types of solar cells. http://www.altenergy.org/renewables/solar/common-types-of-solar-cells.html. [Online; accessed 25-Nov-2015].

[12] Wind power's beginnings. http://ww.telosnet.com/wind/early.html. [Online; accessed 25-Nov-2015].

[13] Windustry. How much do wind turbines cost? http://www.windustry.org/how_much_do_wind_turbines_cost. [Online; accessed 25-Nov-2015].

[14] www.solarpanelscostguide.com. Complete solar panel cost guide. http://www.solarpanelscostguide.com/. [Online; accessed 25-Nov-2015].

[15] Dimension Engineering. A beginner's guide to switching regulators. https://www.dimensionengineering.com/info/switching-regulators. [Online; accessed 25-Nov-2015].

[16] On Semiconductor. Effects of high switching frequency on buck regulators. http://www.onsemi.com/pub_link/Collateral/TND388-D.PDF. [Online; accessed 25-Nov-2015].

[17] FairchildSemi. Understanding diode reverse recovery and its effect on switching losses. https://www.fairchildsemi.com/technical-articles/Understanding-Diode-Reverse-Recovery-and-Its-Effect-on-Switching-Losses.pdf. [Online; accessed 25-Nov-2015].

[18] Erno Temesi. Advantages of sic schottky diodes. http://www.vincotech.com/fileadmin/user_upload/articles/Bodo'sPowerSystems_May2008_.pdf, 2008. [Online; accessed 25-Nov-2015].

[19] ROHM Semiconductor. Silicon carbide schottky barrier diodes. http://www.rohm.com/documents/11405/851233/ROHM_SiC+Diodes_wp.pdf. [Online; accessed 25-Nov-2015].

[20] STMicroelectronics. Silicon carbide diodes. http://www.st.com/web/en/catalog/sense_power/FM64/SC489?sc=sicdiodes. [Online; accessed 25-Nov-2015].

[21] EECatalog. Microcontrollers make waves in automotive and internet of things. http://eecatalog.com/8bit/2014/01/31/microcontrollers-make-waves-in-automotive-and-internet-of-things/. [Online; accessed 25-Nov-2015].

[22] umich.edu. Introduction: Digital controller design. http://ctms.engin.umich.edu/CTMS/index.php?example=Introduction&section=ControlDigital. [Online; accessed 25-Nov-2015].

[23] SMA. Sunny boy 3000tl / 3600tl / 4000tl / 5000tl. http://files.sma.de/dl/15330/SB5000TL-21-DEN134924W.pdf. [Online; accessed 25-Nov-2015].

[24] SMA. Sunny island 6.0h / 8.0h. http://files.sma.de/dl/2485/SI_6H8H-AEN131411W.pdf. [Online; accessed 25-Nov-2015].

[25] SMA Solar Technology AG. Sma flexible solution. http://files.sma.de/dl/2485/FSSMAPPE-DEN1510-V10web.pdf. [Online; accessed 25-Nov-2015].

[26] SolarEdge. About us. http://www.solaredge.com/groups/corporate/about. [Online; accessed 25-Nov-2015].

[27] SolarEdge. Smart energy management for reduced electricity bills. http://www.solaredge.com/files/pdfs/products/se_feed_in_limitation_flyer.pdf. [Online; accessed 25-Nov-2015].

[28] Infineon Technologies. Resonant llc converter: Operation and design. http://www.infineon.com/dgdl/Infineon+-+Application+Note+-+PowerMOSFETs+-+OptiMOS%E2%84%A2+-+Resonant+LLC+Converter+Operation+and+Design.pdf?folderId=db3a3043156fd5730115939eb6b506db&fileId=db3a30433acf32c9013ad11cddde01b6, 2012. [Online; accessed 25-Nov-2015].

[29] MPRIME. Pv modules m 230 -255 — 3r. http://www.mprimesolar.com/Documents/Mprime_Solar_M_SERIES_3R_PLUS_EN.pdf. [Online; accessed 25-Nov-2015].

[30] Advanced Energy. Transformerless inverters. http://solarenergy.advanced-energy.com/upload/File/White_Papers/ENG-TransformerlessInverters-270-02.pdf. [Online; accessed 25-Nov-2015].

[31] Magnetics. Transformer design with magnetics ferrite cores. http://www.mag-inc.com/design/design-guides/Transformer-Design-with-Magnetics-Ferrite-Cores. [Online; accessed 25-Nov-2015].

[32] Magnetics. Typical power handling chart. http://www.mag-inc.com/File%20Library/Products/Ferrite/MagneticsTypicalPowerHandlingChart2012.pdf. [Online; accessed 25-Nov-2015].

[33] Magnetics. Learn more about ferrite shapes. http://www.mag-inc.com/products/ferrite-cores/ferrite-shapes/learn-more-shapes. [Online; accessed 25-Nov-2015].

[34] Magnetics. Design application notes, section 4. power design. http://www.lodestonepacific.com/distrib/pdfs/Magnetics/Design_Application_Notes.pdf. [Online; accessed 25-Nov-2015].

[35] Awg table. http://www.powerstream.com/Wire_Size.htm. [Online; accessed 25-Nov-2015].

[36] Wolfram. Skin effects in straight wires. http://demonstrations.wolfram.com/SkinEffectsInStraightWires/. [Online; accessed 25-Nov-2015].

[37] New England Wire. Litz wire theory. http://www.newenglandwire.com/products/litz-wire-and-formed-cables/theory.aspx. [Online; accessed 25-Nov-2015].

[38] GeneSIC. Gb50slt12-247 datasheet. http://www.farnell.com/datasheets/1917000.pdf. [Online; accessed 25-Nov-2015].

[39] Hyosung Kim and Seung-Ki Sul. A novel filter design for output lc filters of pwm inverters. http://manuscript.jpe.or.kr/ltkPSWeb/pub/pubfpfile.aspx?ppseq=484, 2011. [Online; accessed 25-Nov-2015].

[40] Ray Marston. Lc filters. http://www.n5dux.com/ham/files/pdf/LC%20Filters.pdf. [Online; accessed 25-Nov-2015].

[41] Nicolas Melot. Study of an operating system: Freertos. http://wiki.csie.ncku.edu.tw/embedded/FreeRTOS_Melot.pdf. [Online; accessed 25-Nov-2015].

[42] Building Automation Consultants. Automation history. http://www.building-automation-consultants.com/building-automation-history.html. [Online; accessed 25-Nov-2015].

[43] Sujay Parekh Joseph L. Hellerstein, Yixin Diao and Dawn M. Tilbury. Pid control. http://www.globalspec.com/reference/51987/160210/chapter-9-4-pid-control. [Online; accessed 25-Nov-2015].

[44] Jinghua Zhong. Pid controller tuning: A short tutorial. http://saba.kntu.ac.ir/eecd/pcl/download/PIDtutorial.pdf, 2006. [Online; accessed 25-Nov-2015].

[45] Cheng-Liang Chen. Tuning pid controllers. http://www.hobbielektronika.hu/forum/getfile.php?id=217496. [Online; accessed 25-Nov-2015].

[46] Alexandre Mota. Sistemas de controlo ii - texto de apoio, 2013.

[47] MathWorks. Pid tuning algorithm for linear plant model. http://www.mathworks.com/help/control/ref/pidtune.html. [Online; accessed 25-Nov-2015].

[48] Governo de Portugal. Legislaçao. http://www.renovaveisnahora.pt/web/srm/legislacao. [Online; accessed 25-Nov-2015].

[49] FFSolar. Pequena produção (antiga microprodução e miniprodução). http://www.ffsolar.com/index.php?lang=PT&page=pequena-producao. [Online; accessed 25-Nov-2015].

[50] Shrink That Footprint. Average household electricity use around the world). http://shrinkthatfootprint.com/wp-content/uploads/2013/02/household1.gif. [Online; accessed 25-Nov-2015].

[51] Trojan. Trojan battery renewable energy sizing calculator. http://www.batterysizingcalculator.com/. [Online; accessed 25-Nov-2015].

[52] Plexim. Piece-wise linear electrical circuit simulation for simulink. https://www.hitpages.com/doc/4541684310343680/1#pageTop. [Online; accessed 25-Nov-2015].

[53] Plexim. Plecs. http://www.plexim.com/plecs. [Online; accessed 25-Nov-2015].

[54] Plexim. Servo drive with optimum braking. http://www.plexim.com/de/node/543. [Online; accessed 25-Nov-2015].